University of Southampton Research Repository

UNIVERSITY OF SOUTHAMPTON

FACULTY OF PHYSICAL SCIENCES AND ENGINEERING

OPTOELECTRONICS RESEARCH CENTRE

MULTI-WAVELENGTH PUMPING of HIGH POWER FIBRE RAMAN LASERS

by

Soonki Hong

Thesis for the degree of Doctor of Philosophy

Dec 2020

UNIVERSITY OF SOUTHAMPTON

ABSTRACT

FACULTY OF PHYSICAL SCIENCES AND ENGINEERING

OPTOELECTRONICS RESEARCH CENTRE

Doctor of Philosophy

MULTI-WAVELENGTH PUMPING of HIGH POWER FIBRE RAMAN LASERS

Soonki Hong

Fibre Raman lasers are an alternative to high power rare-earth-doped fibre lasers with benefits such as wavelength versatility and resilience to photodarkening. However, stimulated Raman scattering is a weak nonlinear process that requires high pump intensities, which are difficult to reach with high-power multimode diode lasers, which are favoured for pumping. Nevertheless, research has shown that power-scaling of fibre Raman lasers pumped directly by such diode laser is possible. Whereas high-power diode-laser-pumped fibre Raman lasers have been investigated with only a single-wavelength (narrow-bandwidth) pumping thus far, this study aims to further power-scale diode-laser-pumped fibre Raman laser by using wide-span multi-wavelength pumping.

First, I examined two-wavelength (976 and 950 nm) pumped fibre Raman laser. Two high-power diode lasers are spectrally combined and launched into graded-index fibre. Although the separation between the two wavelengths was far from ideal (neither smaller than the Raman linewidth nor comparable to the Raman shift), the laser emitted 23 W at a single wavelength. This indicates that the separation among pump wavelengths is not so critical. Next, another three high power diode lasers at 969, 940, and 915 nm were spectrally added to the pump, expanding the total pump bandwidth to 683 cm^{-1} (915 – 976 nm). Three different fibres (silica-core step-index fibre, graded-index fibre with high germanium-doping, and step-index fibre with high germanium-doping) were tested. All three cases led to high-power single-wavelength output, reaching 32, 67, and 101 W, respectively. Also, this showed the advantages of germanium-doping. (*e.g.*, higher Raman gain and pump launching efficiency) Lastly, numerical simulations showed that a pump bandwidth of up to ~1000 cm^{-1} can be used to pump a fibre Raman laser with an efficiency of more than 70%, for a clad-to-core area ratio up to ~7.

Overall, the results show that multi-wavelength pumping of fibre Raman laser allow for efficient high power lasers. Thus, the basic concept of a multi-wavelength-pumped fibre Raman laser that may evolve into a new type of kW-laser is established in this thesis.

Table of Contents

List of Tables

List of Figures

List of symbols

Beam quality	M^2
Germanium concentration	$x_{\mathrm{GeO_2}}$
Cladding area	A_{clad}
Core area	A_{core}
Critical pump power	P_0^{cr}
Effective area	A_{eff}
Effective bandwidth of the Stokes near the peak shift	B_{eff}
Effective length	L_{eff}
Generalised coordinate	ζ
Raman shift	Ω
Launched power	P
Loss of fibre	α
Numerical aperture	NA
Optical frequency	ν
Optical Intensity	I
Optical power	P
Photon flux	N
Photon flux (fraction)	n
Photon flux (total)	$\mathbb{N}$
Propagation coordinate	z
Pump indicator	ϵ_{ij}
Raman gain coefficient	g_R
wavelength	λ

Definitions and Abbreviations

Angle of incidence	AOI
Area ratio	AR
Brightness enhancement	BE
Beam product parameter	BPP
Continuous wave	CW
Carbon dioxide	CO_2
Charge-coupled device	CCD
Cladding-mode stripper	CMS
Double-clad fibre	DCF
Erbium	Er
Fibre Bragg grating	FBG
Fibre Raman amplifier	FRA
Fibre Raman Laser	FRL
Figure of merit	FoM
Four wave mixing	FWM
Full width at half maximum	FWHM
Germania	GeO_2
Graded-index	GRIN
Helium-Neon	HeNe
Nitrogen	N
Numerical aperture	NA
Ordinary differential equation	ODE
Optical time domain reflectometer	OTDR
Pump multiplier	PM

• Phosphorus Oxide	P_2O_5
• Quasi-continuous wave	QCW
• Right hand side	RHS
• Raman gain fibre	RGF
• Self-phase modulation	SPM
• Silica	SiO_2
• Stimulated Raman scattering	SRS
• Thulium	Tm
• Volume Bragg grating	VBG
• Ytterbium	Yb
• Ytterbium-doped fibre laser	YDFL

Research Thesis: Declaration of Authorship

Soonki Hong

Title of thesis: Multi-wavelength pumping of high power fibre Raman lasers

I declare that this thesis and the work presented in it are my own and has been generated by me as the result of my own original research.

I confirm that:

1. This work was done wholly or mainly while in candidature for a research degree at this University;
2. Where any part of this thesis has previously been submitted for a degree or any other qualification at this University or any other institution, this has been clearly stated;
3. Where I have consulted the published work of others, this is always clearly attributed;
4. Where I have quoted from the work of others, the source is always given. With the exception of such quotations, this thesis is entirely my own work;
5. I have acknowledged all main sources of help;
6. Where the thesis is based on work done by myself jointly with others, I have made clear exactly what was done by others and what I have contributed myself;
7. Parts of this work have been published as:

[1] S. Hong, Y. Feng, and J. Nilsson, "Wide-Span Multi-Wavelength High-Power Diode-Laser Pumping of Fiber Raman Laser," *IEEE Photonics Technol. Lett.*, vol. 31, no. 24, pp. 1995–1998, 2019, doi: 10.1109/LPT.2019.2953195.

[2] S. Hong, Y. Feng, and J. Nilsson, "Off-Peak Dual-Wavelength Multimode Diode-Laser- Pumped Fiber Raman Laser," *IEEE Photonics Technol. Lett.*, vol. 30, no. 18, pp. 1625–1628, 2018, doi: 10.1109/LPT.2018.2863559.

[3] N. Zhao, S. Hong, A. V. Harish, Y. Feng, and J. Nilsson, "Simulations of multiwavelength cladding pumping of high-power fiber Raman amplifiers," *Opt. Eng.*, vol. 58, no. 10, p. 1, 2019, doi: 10.1117/1.oe.58.10.102701.

Signature: ....

Date: 03/DEC/2020

Acknowledgements

Firstly, I would like to express deep gratitude and respect to my supervisor, *Prof.* Johan Nilsson, for guiding me in every step of my PhD with his prestigious knowledge, as well as for funding me.

Secondly, I would like to thank Dr. Jaesun Kim and Dr. Pranabesh Barua who fabricated the custom-made fibres which took a very important role in this thesis. The completion of this thesis would not have been possible without their professional expertise.

I am also very grateful to my lab members. I thank Dr. Nan Zhao for introducing me the labs and setup when I started my course, Dr. Yutong Feng for never hesitating to help me and do the experiments together, Sheng Zhu for always providing quality discussions, Dr. Huaiqin Lin for knowing the whereabouts of everything in the chaotic labs and sharing tea leaves, and Pablo for going to Unikebab together on hungry days.

And I thank the Koreans, Dr. Joonyoung Kim and Dr. Goo Yu, who were always there when I needed to vent out in my mother tongue when I am tired of speaking English. (정말 감사합니다! 곧 한국에서 뵈어요!) A special thanks goes to Ellie for enduring all of my thesis-grumpiness in the middle of this pandemic. And I thank my immigrant friends, Fernando, Norberto, Andrea, and Krzysztof, who showed a crude and childish friendship and presented me the endless laughter and cries that coloured the unforgettable moments.

Lastly, I gratefully acknowledge the help of Dr. Jonathan Price, *Prof.* Andy Clarkson, and *Prof.* Michalis Zervas for thoroughly examining on my progress reports, the help of Tim Hoad for processing many aluminium plates and blocks for me, and the funding of AFOSR.

Chapter 1: Introduction

This thesis introduces high power fibre Raman lasers (FRLs) and amplifiers that are pumped by multi-wavelength high power diode lasers. The potential of multi-wavelength pumping for FRL as a high power laser scheme is examined through a series of experiments and numerical simulations.

The benefits of FRL partly derive from the elimination of doping with rare-earth (RE) ions. As stimulated Raman scattering (SRS) happens in “passive” fibres, FRL has no restriction for selecting the output wavelength as long as the background loss is acceptable and the pump wavelength that gives the desired signal wavelength is available. This, also, means that high-quality, low-loss, and readily-available commercial fibres, which have been advanced to meet the needs of long-distance telecommunication, can be used as gain fibre.

However, SRS is a weaker process than rare-earth-ion-based absorption and stimulated emission. Therefore, FRL requires a brighter pump source to be as efficient as the conventional RE-doped fibre lasers. Pumping with diode lasers is often preferred. As shown in this thesis, this can be achieved by spectrally combining several pumps as the state-of-art brightness of a conventional high-power diode laser at a single wavelength is not enough to make FRLs as efficient as RE-doped fibre lasers. Note that this approach is less amenable to pumping of rare-earth ions due to their atomic energy-level structure.

In this chapter, I outline the history of fibre lasers and the state-of-art of high power lasers. In regard to that, the motivation and the significance of multi-wavelength pumped high power FRLs are explained. Lastly, I outline the thesis.

1.1 Overview of fibre lasers

Since the demonstration of the first laser by Theodore Maiman in 1960 [1], it took only one year to see the first fibre laser (it was more like a thin-rod laser than a “fibre” laser but the essential science has many commonalities) [2], [3] among other inventions that followed within half a decade such as gas lasers (*e.g.*, HeNe, CO_2, N), diode lasers, organic dye lasers, and many types of solid state lasers. Theoretical proposals for modelocking and excimer lasers were also made around that time [4]. However, it was not until the 1980s that fibre lasers (including amplifiers) became realistic for the commercial and industrial needs of telecommunications, including for the intercontinental telecommunication plans such as the first transatlantic fibre-optic cable (TAT-8) by Bell. This need was soon answered by the first erbium fibre amplifier, demonstrated by L. Reekie, R. J. Mears, S. B. Poole, I. M. Jauncey and D. N. Payne in 1986 [5], [6].

Since then, other industrial needs such as material processing arose, nudging the development of high power lasers. Therefore, fibre lasers of various rare earth ions (*e.g.*, Yb, Er, Tm) were intensively pursued for high power. The geometrical advantage of fibre gives a long interaction length with large surface-to-active-volume ratio and thus excellent thermal dissipation. Another key development was the double-clad-fibre, which in addition to power-scaling made many orders of magnitude of brightness enhancement possible [7]. This led fibre lasers to break the record of high power consequently. As a result, today, ytterbium-doped fibre lasers (YDFLs) of 20-kW single mode output power is commercially available from IPG Photonics, having passed the milestone of 1 kW output power in 2004 [8]. Also recently, 656 W is achieved with erbium [9] (although it is not diffraction limited power) and 1 kW is achieved with thulium [10].

While absorption and-stimulated-emission processes in rare-earth ions thus became a common way to build a laser, stimulated Raman scattering (SRS) is another physical phenomenon that can provide optical gain, and can be used for lasers or amplifiers. Soon after the first laser demonstration, SRS was reported and observed for the first time in 1962 [11], [12]. Ten years later, Raman gain in silica fibre was measured by R. H. Stolen and E. P. Ippen [13]. In the 80's, Raman amplifiers were studied for compensating the attenuation of telecommunication signal in long distance optical fibre [14], [15].

The quantum defect of SRS in silica is lower than that of most other lasers. (One of the well-known exception is the tandem-pumped lasers [16].) This raises the potential of FRL as a method to build an efficient high power laser. In addition, wavelength-versatility makes it possible to adopt any other high power laser (*e.g.*, YDFL), as a pump source [17]. For this reason, many high-power FRLs were pumped by a YDFL. 1.28 kW at 1120 nm was reached with a single Raman conversion step from an YDFL emitting at 1080 nm [18] and 301 W at 1480 nm was reached by a cascaded Raman fibre laser which in five steps converted the output from a high power YDFL at 1117 nm [19].

1.2 Diode laser direct pumping and the potential of multi-wavelength pumping

Although kW-level FRLs have already been demonstrated [18], [19], they all depend on the excellence of YDFLas pump sources. This brings in limitations and doubts. Firstly, the output wavelength cannot be shorter than the emission-wavelength of the pump-YDFL (1030 - 1100 nm). Secondly, the brightness of the pump-YDFL is already very high. Enhancing it further is impossible or almost impossible because YDFLs are usually near-diffraction-limited. In other words, a Raman laser is likely to degrade the brightness of the pump lasers, whereas brightness-enhancement is the raison d'être of many optically pumped lasers.

To address this shortcoming, pumping FRLs directly with diode lasers, i.e., without a YDFL, was suggested. One of the earliest tests was done by Yao [20] reaching 20 W at 1019 nm with 80% of slope efficiency. Since then, the highest power reached by a diode laser pumped FRL is 154 W [21]. Also, ~50 W with an excellent beam quality ($M^2 \sim 2$) at 976 nm was reached with an all-fibre configuration [22], [23]. Another all-fibre FRL reached 1.2 kW of output power [24]. Although it was pumped by four 350-W single-mode YDFLs, the authors claim that the YDFLs are incoherently combined through the combiner into the cladding, degrading the beam quality factor (M^2) to 14.7, which is as bad as a diode laser. A similar setup but a graded-index (GRIN) fibre Raman amplifier reached 2 kW in a demonstration by another group [25].

Even though the progress described above is impressive, it does not fully utilise the wavelength versatility of SRS. A FRL can accept spectrally much broader pump without losing too much of efficiency and that is what this thesis is presenting. FRLs pumped with several wavelengths over a span as wide as, or wider than, the Raman peak of silica (~ 440 cm^{-1}) have not been reported except the work presented in this thesis to my knowledge.

I started with several diode lasers at wavelengths (976, 969, 950, 940, and 915 nm) that are commercially available to experimentally show that multi-wavelength pumping works for FRLs. Numerical simulations were used in order to assess the potential significance of it.

Accompanied with the recent development on spectrally combined bright diode laser for material processing [26], this might become another new standard way to build multi-kW lasers in the future.

1.3 Thesis outline

Chapter 2 contains the theory and background knowledge that are essential to understand this thesis. It includes the coupled differential equation of SRS, the Raman gain coefficients for different glass formers, initial Stokes power and the Raman threshold, as well as the limit on the clad-to-core area ratio for cladding-pumped FRAs.

Chapter 3 and **4** present experimental results. **Chapter 3** contains two experiments that use two diode lasers at 976 and 950 nm. Firstly, a fibre Raman amplifier (FRA) made of GRIN fibre is presented. Amplification of a 976-nm signal seed from a diode laser was pumped by a 950-nm diode laser. Thus, this is not multi-wavelength-pumping but simply conventional single-wavelength pumping of an amplifier at 976 nm. Fibre lengths of 1.5 km and 500 m were tested. Then, turning to pumping with multiple (i.e., two) wavelengths, a FRL that is pumped with both 976 and 950 nm and emits a signal at 1020 nm is presented. 23 W of a signal output power was generated with a slope of 0.5. This shows that even a separation between two pump wavelengths of 250 cm^{-1}, which is awkward for SRS in silica, can pump a FRL with reasonable efficiency.

In **Chapter 4**, the wavelength span and the number of pump lasers are expanded. Three more diode lasers at different wavelengths (969, 940, and 915 nm) are added to the pump, making the total pump span as wide as 683 cm^{-1}. Now, the pump is composed of five wavelengths (976, 969, 950, 940, and 915 nm). Three different fibres (50-µm silica-core, germanosilicate GRIN 62.5- µm diameter core, and germanosilicate quasi-step-index, 40-µm diameter core) are tested and the signal output power reached 31.5, 67, and 100 W, respectively. Temporal traces and the comparison to the numerical simulations of each experiments are also presented and discussed.

Chapter 5 presents numerical simulations of multi-wavelength-pumped FRAs. The first part presents a FRA with an area ratio of eight pumped by discrete multiple wavelengths of fixed and optimised spacings for realistic fibre parameters (e.g., diameter of core and clad and background loss). The second part focuses more on the total span rather than the number of pump wavelengths. A theoretical lossless fibre is analysed and the simulation model was modified so that it can be applied to any equally-spaced multi-wavelength-pumped FRA. The simulation results outline the efficient amplification regime for equally-spaced multi-wavelength-pumped FRA in terms of the total span and area ratio.

Lastly, **Chapter 6** concludes the thesis and suggests the possible next steps.

1.4 References

[1] T. H. MAIMAN, "Stimulated Optical Radiation in Ruby," *Nature*, vol. 187, no. 4736, pp. 493–494, Aug. 1960, doi: 10.1038/187493a0.

[2] E. Snitzer, "Optical maser action of Nd+3 in a barium crown glass," *Phys. Rev. Lett.*, vol. 7, no. 12, pp. 444–446, 1961, doi: 10.1103/PhysRevLett.7.444.

[3] C. J. Koester and E. Snitzer, "Amplification in a Fiber Laser," *Appl. Opt.*, vol. 3, no. 10, p. 1182, 1964, doi: 10.1364/AO.3.001182.

[4] J. Hecht, "Short history of laser development," *SPIE Rev.*, vol. 1, no. 1, pp. 1–23, 2010, doi: 10.1364/ao.49.000f99.

[5] L. Reekie, R. J. Mears, S. B. Poole, and D. N. Payne, "Tunable Sinele-Mode Fiber Lasers," vol. L, no. I, pp. 956–960, 1986.

[6] R. J. MEARS, L. REEKIE, I. M. JAUNCEY, and D. N. PAYNE, "High-gain rare-earth-doped fiber amplifier at 1.54 μm," in *Optical Fiber Communication*, 1987, p. WI2, doi: 10.1364/OFC.1987.WI2.

[7] D. J. Richardson, J. Nilsson, and W. a. Clarkson, "High power fiber lasers: current status and future perspectives [Invited]," *J. Opt. Soc. Am. B*, vol. 27, no. 11, p. B63, 2010, doi: 10.1364/JOSAB.27.000B63.

[8] Y. Jeong, J. K. Sahu, D. N. Payne, and J. Nilsson, "Ytterbium-doped large-core fiber laser with 1.36 kW continuous-wave output power," *Opt. Express*, vol. 12, no. 25, p. 6088, 2004, doi: 10.1364/OPEX.12.006088.

[9] H. Lin, Y. Feng, Y. Feng, P. Barua, J. K. Sahu, and J. Nilsson, “656 W Er-doped, Yb-free large-core fiber laser,” *Opt. Lett.*, vol. 43, no. 13, p. 3080, 2018, doi: 10.1364/ol.43.003080.

[10] T. Ehrenreich, R. Leveille, I. Majid, K. Tankala, G. Rines, and P. Moulton, “1-kW, all-glass Tm: fiber laser,” *Proc. SPIE*, vol. 7580, p. 758016, 2010.

[11] E. J. Woodbury and W. K. Ng, “Ruby Laser Operation in Near IR,” *Proc Inst Radio Eng.*, vol. 50, p. 2367, 1962.

[12] G. Eckhardt, R. W. Hellwarth, F. J. McClung, S. E. Schwarz, D. Weiner, and E. J. Woodbury, “Stimulated Raman Scattering From Organic Liquids,” *Phys. Rev. Lett.*, vol. 9, no. 11, pp. 455–457, Dec. 1962, doi: 10.1103/PhysRevLett.9.455.

[13] R. H. Stolen and E. P. Ippen, “Raman gain in glass optical waveguides,” *Appl. Phys. Lett.*, vol. 22, no. 6, pp. 276–278, 1973, doi: 10.1063/1.1654637.

[14] J. Hegarty, N. A. Olsson, and L. Goldner, “Cw pumped raman preamplifier in a 45 Km-long fibre transmission system operating at 1.5 μm and 1 Gbit/s,” *Electron. Lett.*, vol. 21, no. 7, pp. 290–292, 1985, doi: 10.1049/el:19850208.

[15] E. Desurvire, M. Papuchon, J. P. Pocholle, J. Raffy, and D. B. Ostrowsky, “High-gain optical amplification of laser diode signal by Raman scattering in single-mode fibres,” *Electron. Lett.*, vol. 19, no. 19, pp. 751–753, 1983, doi: 10.1049/el:19830512.

[16] T. Yao, “Fibre Laser Sources With Low Quantum Defect,” University of Southampton, 2014.

[17] V. R. Supradeepa *et al.*, “Raman fiber lasers,” *J. Opt.*, vol. 19, no. 2 (art. no. 023001), 2017, doi: 10.1088/2040-8986/19/2/023001.

[18] L. Zhang *et al.*, “Kilowatt Ytterbium-Raman fiber laser,” *Opt. Express*, vol. 22, no. 15, pp. 18483–18489, 2014, doi: 10.1364/OE.22.018483.

[19] V. R. Supradeepa and J. W. Nicholson, “Power scaling of high-efficiency 1.5 μm cascaded Raman fiber lasers,” vol. 38, no. 14, pp. 2538–2541, 2013, doi: 10.1088/2040-8986/19/2/023001.

[20] T. Yao, A. Harish, J. Sahu, and J. Nilsson, “High-Power Continuous-Wave Directly-Diode-Pumped Fiber Raman Lasers,” *Appl. Sci.*, vol. 5, no. 4, pp. 1323–1336, 2015, doi: 10.3390/app5041323.

[21] Y. Glick, V. Fromzel, J. Zhang, N. Ter-Gabrielyan, and M. Dubinskii, “High-efficiency, 154 W CW, diode-pumped Raman fiber laser with brightness enhancement,” *Appl. Opt.*, vol. 56, no. 3, pp. B97–B102, 2017, doi: 10.1364/AO.56.000B97.

[22] A. G. Kuznetsov *et al.*, “976 nm all-fiber Raman laser with high beam quality at multimode laser diode pumping,” *Laser Phys. Lett.*, vol. 16, no. 10, pp. 2–7, 2019, doi: 10.1088/1612-202X/ab4281.

[23] A. G. Kuznetsov, S. I. Kablukov, E. V. Podivilov, and S. A. Babin, “Brightness enhancement and beam profiles in an LD-pumped graded-index fiber Raman laser,” *OSA Contin.*, vol. 4, no. 3, p. 1034, 2021, doi: 10.1364/osac.421985.

[24] Y. Glick *et al.*, “12 kW clad pumped Raman all-passive-fiber laser with brightness enhancement,” *Opt. Lett.*, vol. 43, no. 19, p. 4755, 2018, doi: 10.1364/ol.43.004755.

[25] Y. Chen, T. Yao, H. Xiao, J. Leng, and P. Zhou, “Greater than 2 kW all-passive fiber Raman amplifier with good beam quality,” *High Power Laser Sci. Eng.*, vol. 8, pp. 1–6, 2020, doi: 10.1017/hpl.2020.33.

[26] J. Malchus, V. Krause, G. Rehmann, M. Leers, A. Koesters, and D. G. Matthews, “A 40kW fiber-coupled diode laser for material processing and pumping applications,” in *Proc. SPIE, High-Power Diode Laser Technology and Applications XIII*, 2015, p. 934803, doi: 10.1117/12.2083909.

Chapter 2: Background

The most important knowledge that is needed to understand this thesis is that of stimulated Raman scattering (SRS). Luckily, the experiments in this thesis are in either the continuous wave (CW) or quasi-continuous wave (QCW) regime. Thus, SRS in the pulse-propagation (or amplitude) regime, with its rather complicated equations, can be avoided. Instead, I simply focus on the equations for steady-state power transfer between waves via SRS in this chapter. Note however that in some experiments, the FRLs self-pulsed, the modelling of which requires time-dependent equations.

This chapter starts with a basic differential equation that is written in terms of intensity and length coordinate, introducing the Raman gain spectrum of fused silica and common dopants of fibres. After that, the equation is transformed to describe multi-wavelength cases. Then, the intensity terms in the equation are replaced by the power and the effective area terms to be able to describe cladding pumping cases. Lastly, the limit on core-to-cladding area ratio for the SRS amplification in the double-clad fibre (DCF) is discussed.

2.1 Stimulated Raman scattering

2.1.1 Raman gain and its spectrum

Under CW and QCW (i.e., quasi-steady-state) conditions, the growth of the Stokes wave is described by [1]

$$\frac{dI_s}{dz} = g_R I_p I_s, \tag{2.1}$$

where I_s is the Stokes intensity, I_p is the intensity of the pump, and g_R is the Raman gain coefficient. The Raman gain coefficient governs the strength of the SRS. It is a function of the frequency difference between the Stokes wave and the pump. For that reason, it is also called the Raman gain spectrum.

The Raman gain spectrum and strength depends on the material. Fundamental in-depth explanations for this can be found in ref. [2]–[4]. Measured Raman gain spectra of fused silica glass, some other glasses made of oxides of commonly used fibre dopants, and of germanosilicate with different Ge-concentrations, are shown in **Figure 2.1** and **2.2**.

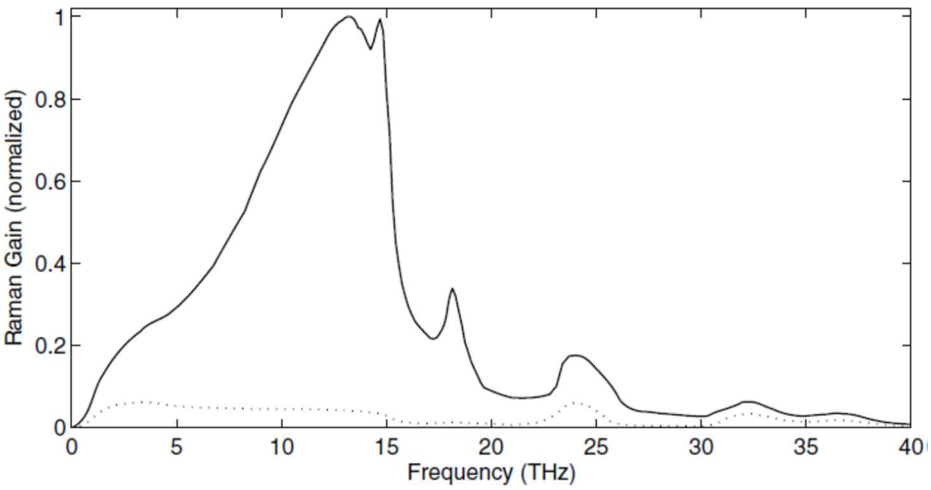

Figure 2.1 Normalised Raman gain for fused silica when the pump and the Stokes waves have the same **(solid curve)** and orthogonal **(dashed cure)** direction of linear polarisation. (*after ref.* [1])

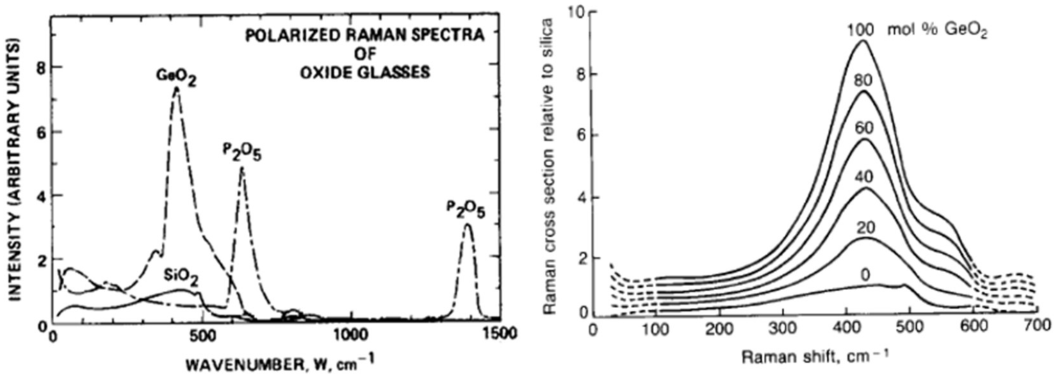

(a) **(b)**

Figure 2.2 Raman gain spectra of various glass formers. **(a)** The relative Raman spectra of SiO_2, GeO_2, and P_2O_5 with SiO_2 normalised to one (*figure extracted from* [5]). **(b)** Raman cross-section of Ge-doped silica relative to the peak value for undoped silica (*figure extracted from* [6]).

For silica, the peak is located at 13.2 THz (440 cm^{-1}), with a secondary peak at 490 cm^{-1} of similar value. The peak value for a 1-μm pump wavelength is $g_R = 1 \times 10^{-13}$ m/W for linearly co-polarised waves. This peak value changes inversely proportionally to the pump wavelength [1], ideally, and also in practice to a good approximation. The orthogonal polarisation has a much smaller gain than the co-linear polarisation near the peak. Therefore, for the unpolarised cases, half of the co-polarised value is taken as the effective Raman gain coefficient. However, the Raman gain in a specific point does not depend on the direction of propagation of the pump and signal, be they co-directional, counter-directional, orthogonal, or at some other angle. Note however that in the presence of pump depletion, the total gain as integrated along the fibre will depend on the relative propagation direction of the pump and Stokes wave.

The peak of pure germania (GeO_2) is at 420 cm^{-1}, which is close to that of SiO_2, and the peak value is 9.2 times bigger than that of the silica [5]. Mixing leads to a Raman gain somewhere in the middle, according to the ratio of two (**Figure 2.2(b)**). More precisely, The Raman gain of the mixture, $g_R(x_{GeO2}, \Omega)$ is formulated as [6]

$$g_R(x_{\mathrm{GeO_2}}, \Omega) = \left[1 + C(\Omega) \cdot x_{\mathrm{GeO_2}}\right] \cdot g_R(\mathrm{SiO_2}, \Omega), \tag{2.2}$$

where $x_{\mathrm{GeO_2}}$ is the concentration of GeO_2 in mol%, $g_R(SiO_2, \Omega)$ is the Raman gain coefficients of pure SiO_2, and $C(\Omega)$ is the slope which depends on the Raman shift Ω as depicted in the graph below (**Figure 2.3**).

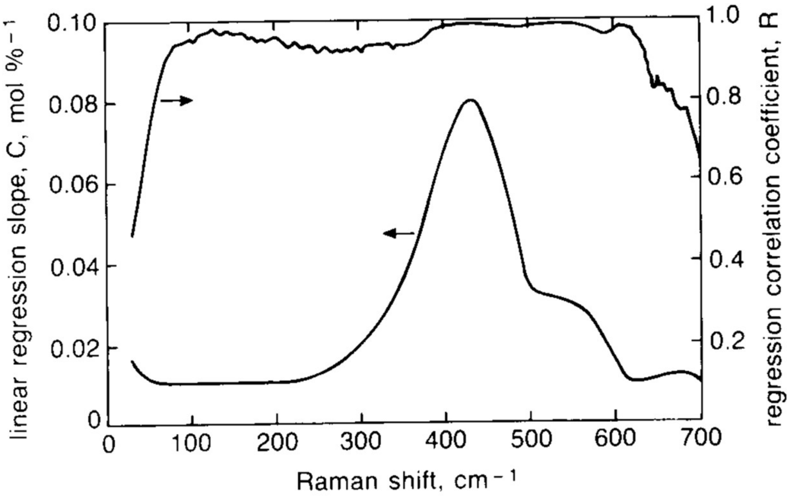

Figure 2.3 $C(\Omega)$ *vs.* Raman shift (*after ref.* [6]). (R is the accuracy of the linear regression.)

This linear regression is valid within the range of 100 - 600 cm^{-1}. The peak value of $C(\Omega)$ equals to 0.08 at 430 cm^{-1}. Therefore, the Raman gain of the 100 mol% GeO_2 is nine times that of silica at their respective peak. This well agrees with the result in ref. [5].

2.1.2 Coupled equations for the intensity and power of an *n*-wavelength FRA

Eq. (2.1) can be extended to include the loss and, explicitly, the change of pump power along the propagation coordinate z. When this is done, the governing equation of SRS for the pump and the Stokes wave becomes a set of two coupled equations [1],

$$\frac{dI_s}{dz} = -\alpha_s I_s + g_R I_p I_s, \tag{2.3}$$

$$\frac{dI_p}{dz} = -\alpha_p I_p - \frac{\nu_p}{\nu_s} g_R I_p I_s, \tag{2.4}$$

where ν_i, α_i, and I_i ($i = s, p$) denote the optical frequency, the background loss and the intensity, respectively, while the subscripts, s and p denote the Stokes wave and the pump.

The finite width of the Raman gain spectra means that SRS can occur between waves with different separation. Consider therefore the case of SRS between more than two wavelengths. The SRS process of n wavelengths can be described by n coupled equations as,

$$\frac{dI_i}{dz} = -\alpha_i I_i + \sum_j \epsilon_{ij} g_{Rij} I_i I_j \qquad with\ i, j = 1, \ldots, n \tag{2.5}$$

where ν_i, α_i, and I_i denote the frequency, the background loss and the intensity of the i^{th} wave, respectively. $g_{Rij} = g_{Rji}$ is the Raman gain coefficient between the i^{th} and j^{th} wave and ϵ_{ij} is an indicator which changes its value depending on whether wave i is pumping or pumped by wave j. If wave i is being pumped, the value of ϵ_{ij} is 1 and if it is pumping, the value becomes $-\nu_i/\nu_j$, as shown below.

$$\epsilon_{ij} = \begin{cases} 1 & if\ \nu_i < \nu_j \\ -\nu_i/\nu_j & if\ \nu_i > \nu_j \end{cases} \tag{2.6}$$

Note that **Eq. (2.5)** describes **Eq. (2.3)** and **(2.4)** when n=2.

Although **Eq. (2.5)** correctly describe the SRS process of many wavelengths, it is written in terms of intensity. However, often the power is of primary interest. It would be straightforward to substitute the intensity with the power divided by the effective area [7] if all waves have identical intensity profiles (*e.g.*, core-pumped single-mode cases and core-pumped well-scrambled multi-mode cases) However, in order to describe the evolution of power in other cases such as cladding-pumped fibres, both sides of **Eq. (2.5)** can be integrated over an infinite cross-sectional area that is normal to z. This becomes

$$\frac{dP_i}{dz} = -\alpha_i P_i + \sum_j \epsilon_{ij} \int_S g_{Rij} I_i I_j \, dS\,, \quad with\, i, j = 1, \dots, n, \tag{2.7}$$

where $P_i = \int_S I_i dS$ is the power of the i^{th} wave. The integral term in the right hand side (RHS) is decided by how much the two intensity profiles overlap. **Eq. (2.7)** can describe the Raman interaction between two waves with different intensity profiles. (*e.g.*, it can describe SRS between a mode in a clad and a mode in a core or between different modes within a core.)

Consider a case of a highly multi-mode, step-index DCF. Also, assume that the modes are scrambled enough for the intensity profile to follow the index profile of fibre (*i.e.*, flat-top profile). This is often true for high power cases. Then, the integral term in the RHS of **Eq. (2.7)** evaluates to

$$\int_S g_{Rij} I_i I_j \, dS = \begin{cases} \dfrac{g_{Rij}}{A_{core}} P_i P_j & if \text{ both } i\text{-th and } j\text{-th waves are guided in the core} \\ \dfrac{g_{Rij}}{A_{clad}} P_i P_j & otherwise \end{cases} \tag{2.8}$$

where A_{core} is the area of the core and A_{clad} is the area of the cladding. This is the model used in ref. [8] and in **Sect. 5.2**.

These equations are equally valid for counter-propagating waves, if dz is replaced by $-dz$. This case is further discussed in the next section, albeit with different notation. However, the equations become significantly more complicated to solve, both analytically (when possible) and through numerical integration.

2.1.3 Coupled equations for the power of an *n*-wavelength FRL

The equations for a FRA in the previous section can also be used for a FRL. However, as lasers come with a cavity, boundary conditions have to be considered. Furthermore, at least with a linear cavity, there will be counter-propagating waves. A case of three waves (a pump wave travelling in one direction and a bi-directional signal) is found in ref. [9]. The uniqueness and the existence of the solution for multi-wavelength FRL was proved in ref. [10] and a numerical model and a comparison to experimental results is presented in ref. [11].

Eq. (2.7) is modified to include counter-propagating waves and it becomes,

$$\frac{dP_i^{\pm}}{dz} = \mp\alpha_i P_i^{\pm} \pm \frac{1}{A_{co}} \sum_j \epsilon_{ij} g_{Rij} P_i^{\pm} \left(P_j^{+} + P_j^{-}\right) \qquad with\ i,j = 1,\dots,n \tag{2.9}$$

where the superscripts on the power term indicate the direction of travel. "+" sign means that the waves are travelling in the direction of increasing z and "–" means the opposite. The Stokes waves are pumped by waves traveling in either, or both, directions at the corresponding pump wavelength (or wavelengths) and, likewise, the pump waves transfer their power to Stokes waves propagating in either, or both, directions. For simplicity, I here assume core-pumping but extension to cladding-pumping is straightforward.

For a simple linear (Fabry-Perot) cavity, the boundary conditions are given at $z = 0$ and $z = L$ (L; the length of fibre). If the pump is injected at $z = 0$, then the boundary conditions become,

$$P_i^{+}(0) = P_i^{0} + r_i^{0} P_i^{-}(0), \qquad with\ i = 1,\dots,n \tag{2.10}$$

$$P_i^{-}(L) = r_i^{L} P_i^{+}(L), \qquad with\ i = 1,\dots,n \tag{2.11}$$

where P_i^0 is the pump power launched into the fibre, r_i^0 and r_i^L are the reflectivities of mirrors at $z = 0$ and $z = L$ for the i^{th} wave. Since the phase between the launched and reflected pump wave is random at the $z = 0$, phase-dependent interference effects are not considered.

In fact, the system of **Eq. (2.9)** of ordinary differential equations (ODEs) is not always stable. For example, numerical integration of any counter-propagating pair of a Stokes and a pump wave can increase the power of each other, seemingly without limit. Indeed, I have experienced many occasions of divergence in Matlab.

The instabilities may be purely numerical or appear also in the physical system. Nevertheless, for certain boundary conditions and with a good numerical algorithm for iteration, one can solve the equation. I only treat such cases. However, I have not found any conclusive study of the stability of multi-wavelength FRLs. Further discussion on this matter is presented in **Sect.4.7**.

2.1.4 The size of initial Stokes power

An issue with both **Eq. (2.7)** and **(2.9)** is that if the initial power of any wave is zero then it will stay zero for all values of z. However, for sufficiently high gain, SRS will build up from spontaneous Raman scattering even if unseeded. Although this occurs along the fibre, it can be modelled as an equivalent input noise power (so-called quantum fluctuations or vacuum fluctuations). In the absence of excess noise, this corresponds to an input of one photon per unit bandwidth per unit time per mode (including polarisation modes). For SRS, the effective input power (also known as the equivalent noise input power) is given by [1],

$$P_{i0}^{eff} = h\nu_i B_{eff}, \qquad B_{eff} = \left(\frac{2\pi}{I_{p0} L_{eff} g_R}\right)^{\frac{1}{2}} \left|\frac{\partial^2 g_R}{g_R \partial \omega^2}\right|_{\omega=\omega_i}^{-\frac{1}{2}} \tag{2.12}$$

where B_{eff} is the effective bandwidth of the Stokes radiation centred near the Raman gain peak, I_{p0} is the intensity of the pump wave for the i^{th} wave, and L_{eff} is the effective length. The second factor in the expression for B_{eff} can be understand as the relative curvature of the gain peak (i.e., how sharp it is). The first factor contains the inverse of the square root of the Raman gain. Although the effective bandwidth thus changes with the Raman gain, I used a value of 4 THz for all the simulations in this thesis after checking that it barely affects the results as long as the order of magnitude is correct. Then, the effective input power becomes ~ 30 μW for wavelengths around 1 μm. **Eq. (2.12)** typically leads to somewhat lower effective bandwidth and lower equivalent noise input power, but again, the difference is not critical and furthermore, this corresponds to quantum-limited noise whereas factors such as background loss and Rayleigh backscattering will increase the equivalent noise input power.

2.1.5 Raman threshold

The Raman threshold (more properly known as the critical power; P_0^{cr}) is defined as the input pump power that makes the Stokes power when unseeded (except for the vacuum fluctuations) equal to the pump power at the fibre output. Using **Eq. (2.3)**, **(2,4)**, and **(2.12)**, it is calculated to,

$$P_0^{cr} \cong 16 \frac{A_{eff}}{g_R L_{eff}}, \tag{2.13}$$

for the forward SRS. Note that $P_0^{cr} g_R L_{eff}/A_{eff}$ is equal to the Raman gain at the critical power in the absence of pump depletion. This is then equal to 16 Np. The 16 Np on the RHS is replaced by 20 Np for backward SRS. Note that this "threshold" (or more properly, critical power) is not the threshold of FRL. Rather, the pump power is launched into a length of fibre and through externally unseeded SRS, the Stokes wave builds up and depletes the pump. Furthermore, there are assumptions that are unlikely to be fulfilled for a FRL or FRA operating with a high efficiency. Refer to chapter 8 in ref. [1] for a detailed derivation.

2.2 Cladding-pumping of FRA

A theoretical study found that the clad-to-core area ratio should not exceed eight for an efficient cladding-pumped FRA because the build-up of the higher order Stokes then starts to deplete the signal Stokes wave faster than the pump transfers power into it, even though significant pump power remains. As a result, the brightness enhancement factor from pump to amplified-signal or laser output of FRAs and FRLs is smaller than that of their rare-earth-doped counterparts. According to the study, the brightness enhancement (BE) factor of an efficient fibre Raman converter can still be as big as 2000 [12]–[14]. Although this is a substantial value, the brightness enhancement of Yb-doped fibre amplifiers (and lasers) can be more than two orders of magnitude higher. Here, I briefly show how the number eight was derived.

Consider a FRA with three waves – the pump, the 1st Stokes, and the 2nd Stokes. The 1st Stokes is the signal, the power of which is to be maximised. The pump wave is guided in the cladding whereas the other two waves are guided in the core. Then, **Eq. (2.7)** rewrites to a set of three coupled equations. The direct interaction between the pump wave and the 2nd Stokes wave is neglected, but will reduce the power that can be transferred somewhat.

$$\frac{dP_p}{dz} = -\alpha_p P_p - \left(\frac{\nu_p}{\nu_{s1}}\right)\frac{g_{Rp,s1}}{A_{clad}} P_p P_{s1}, \tag{2.14}$$

$$\frac{dP_{s1}}{dz} = -\alpha_{s1} P_{s1} + \frac{g_{Rp,s1}}{A_{cl}} P_p P_{s1} - \left(\frac{\nu_{s1}}{\nu_{s2}}\right)\frac{g_{Rs1,s2}}{A_{core}} P_{s1} P_{s2}, \tag{2.15}$$

$$\frac{dP_{s2}}{dz} = -\alpha_{s2} P_{s2} + \frac{g_{Rs1,s2}}{A_{core}} P_{s1} P_{s2}, \tag{2.16}$$

where the subscripts p, $s1$, and $s2$ indicate the pump, the 1st Stokes, and 2nd Stokes waves, respectively. Disregarding the background loss, **Eq. (2.14)** and **(2.16)** solves to

$$P_p(z) = P_p(0)\exp(-G_1), \qquad G_1 = \left(\frac{\nu_p}{\nu_{s1}}\right)\frac{g_{Rp,s1}}{A_{clad}}\int_0^L P_{s1}\,dz, \tag{2.17}$$

$$P_{s2}(z) = P_{s2}(0)\exp(+G_2), \qquad G_2 = \frac{g_{Rs1,s2}}{A_{core}}\int_0^L P_{s1}\,dz. \tag{2.18}$$

G_1 is the nonlinear attenuation of the pump wave induced by SRS and G_2 is the gain of the 2nd Stokes wave in nepers. Because of the inevitable self-seeding, the build-up of the 2nd Stokes become significant when the gain reaches 16 nepers (~70 dB), as in **Eq. (2.13)**. Meanwhile, one would expect, at most, about 10% of the pump power to remain unconverted for the conversion efficiency into the 1st Stokes to be acceptable in a high-power device. In other words, an acceptable lowest value for G_1 is 2 nepers (corresponding to 13.5% unconverted pump) and an allowable highest value for G_2 is 16 nepers. Therefore, the performance factor can be defined as,

$$\frac{G_1}{G_2} > \frac{2}{16} = \frac{1}{8}, \tag{2.19}$$

and it has to be bigger than one eighth. This can be rewritten using **Eq. (2.17)** and **Eq. (2.18)**,

$$\left(\frac{\nu_{s1}}{\nu_p}\right)\frac{A_{clad}}{A_{core}} \cong \frac{A_{clad}}{A_{core}} < 8. \tag{2.20}$$

In conclusion, the area ratio of cladding to core is recommended to be smaller than 8 for making an efficient FRA. I note that spectral filtering that suppresses the 2nd Stokes along the fibre allows for a higher area ratio, but the loss ratio between the 2nd and 1st Stokes wavelength would have to be very large for the filtering to be useful, which is difficult to achieve in practice.

2.3 References

[1] G. P. Agrawal, *Nonlinear Fiber Optics*, 4th ed. London: Elsevier, 2006.

[2] R. W. Hellwarth, "Third-order optical susceptibilities of liquids and solids," *Prog. Quantum Electron.*, 1977, doi: 10.1016/0079-6727(79)90002-8.

[3] Y. R. Shen, *The Principles of Nonlinear Optics*. Wiley, 1984.

[4] R. W. Boyd, *Nonlinear Optics*, 2ed ed. Academic Press, 2003.

[5] F. L. Galeener, J. C. Mikkelsen, R. H. Geils, and W. J. Mosby, "The relative Raman cross sections of vitreous SiO_2, GeO_2, B_2O_3, and P_2O_5," *Appl. Phys. Lett.*, vol. 32, no. 1, pp. 34–36, 1978, doi: 10.1063/1.89823.

[6] S. T. Davey, D. L. Williams, B. J. Ainslie, W. J. M. Rothwell, and B. Wakefield, "Optical gain spectrum of GeO_2-SiO_2 Raman fibre amplifiers," *IEE Proc. J - Optoelectron.*, vol. 136, no. 6, pp. 301–306, 1989, doi: 10.1049/ip-j.1989.0047.

[7] B. E. A. Saleh and M. C. Teich, "Fundamentals of Photonics , 2nd Edition," *Wiley*. 2007, doi: 10.1002/0471213748.

[8] N. Zhao, S. Hong, A. V. Harish, Y. Feng, and J. Nilsson, "Simulations of multiwavelength cladding pumping of high-power fiber Raman amplifiers," *Opt. Eng.*, vol. 58, no. 10, p. 1, 2019, doi: 10.1117/1.oe.58.10.102701.

[9] J. AuYeung and A. Yariv, "Theory of cw Raman oscillation in optical fibers," *J. Opt. Soc. Am.*, vol. 69, no. 6, pp. 803–807, 1979, doi: 10.1364/JOSA.69.000803.

[10] F. Castella, P. Chartier, E. Faou, D. Bayart, F. Leplingard, and C. Martinelli, "Raman laser: mathematical and numerical analysis of a model," *ESAIM Math. Model. Numer. Anal.*, vol. 38, no. 3, pp. 457–475, May 2004, doi: 10.1051/m2an:2004022.

[11] F. Leplingard *et al.*, "Modeling of multiwavelength Raman fiber lasers using a new and fast algorithm," *IEEE Photonics Technol. Lett.*, vol. 16, no. 12, pp. 2601–2603, 2004, doi: 10.1109/LPT.2004.836355.

[12] J. Ji, C. A. Codemard, M. Ibsen, J. K. Sahu, and J. Nilsson, "Analysis of the conversion to the first stokes in cladding-pumped fiber raman amplifiers," *IEEE J.*

Sel. Top. Quantum Electron., vol. 15, no. 1, pp. 129–139, 2009, doi: 10.1109/JSTQE.2008.2010229.

[13] J. Ji, C. A. Codemard, J. K. Sahu, and J. Nilsson, "Design, performance, and limitations of fibers for cladding-pumped Raman lasers," *Opt. Fiber Technol.*, vol. 16, no. 6, pp. 428–441, Dec. 2010, doi: 10.1016/j.yofte.2010.09.011.

[14] J. Ji, C. A. Codemard, and J. Nilsson, "Brightness enhancement limits in pulsed cladding-pumped fiber Raman amplifiers," in *Proc. SPIE, Fiber Lasers VII: Technology, Systems, and Applications*, 2010, p. 75801L, doi: 10.1117/12.844919.

Chapter 3: Off-Raman-Peak Dual-Wavelength High power Diode Laser Pumped Fibre Raman Laser

3.1 Introduction

This chapter presents two experiments, a fibre Raman amplifier (**Sect. 3.2**) and a fibre Raman laser (**Sect. 3.3**), that use two high-power diode lasers at 976 and 950 nm. In both experiments, two diode laser beams are spectrally combined and launched into a multimode germanosilicate GRIN fibre. In the amplifier experiment, a signal at 976 nm was seeded and amplified by pumping at 950 nm. In the laser experiment, both wavelength pumped a newly generated signal at 1020 nm (1st Stokes of 976 nm). The latter is published in [1].

The separation between 976 and 950 nm corresponds to 270 cm^{-1} in wavenumber domain. This is both substantially larger than the Raman linewidth and substantially smaller than the shift to the Raman peak of germanosilicate (440 cm^{-1}). I expect this separation to be close to the most challenging (thus least efficient) for any value smaller than 440 cm^{-1}. Nevertheless, I saw meaningful results in the laser experiment. This shows that it is possible to transfer the power efficiently with two wavelengths of such adverse wavelength spacing.

Section 3.2 demonstrates the amplifier experiment, which in part served as a stepping stone and formed a basis configuration for subsequent experiments. I tested 1.5 km of GRIN fibre as a Raman gain fibre where I saw a high build-up of the 2nd order Stokes already from relatively low levels of pumping. After that, I used a shorter GRIN fibre (500 m). For further improvement, I have modulated the current of the pumping diode. I reached 46% of pump-to-signal conversion efficiency. Because the input signal was large, the gain was low.

Section 3.3 demonstrates the laser experiment. I reached 23 W of output power at 1020 nm, which is more than twice the 7.8 W reached with 976-nm single-diode pumping.

3.2 Fibre Raman amplifiers seeded by a 976-nm diode laser and pumped by a 950-nm diode laser

3.2.1 Experimental setup

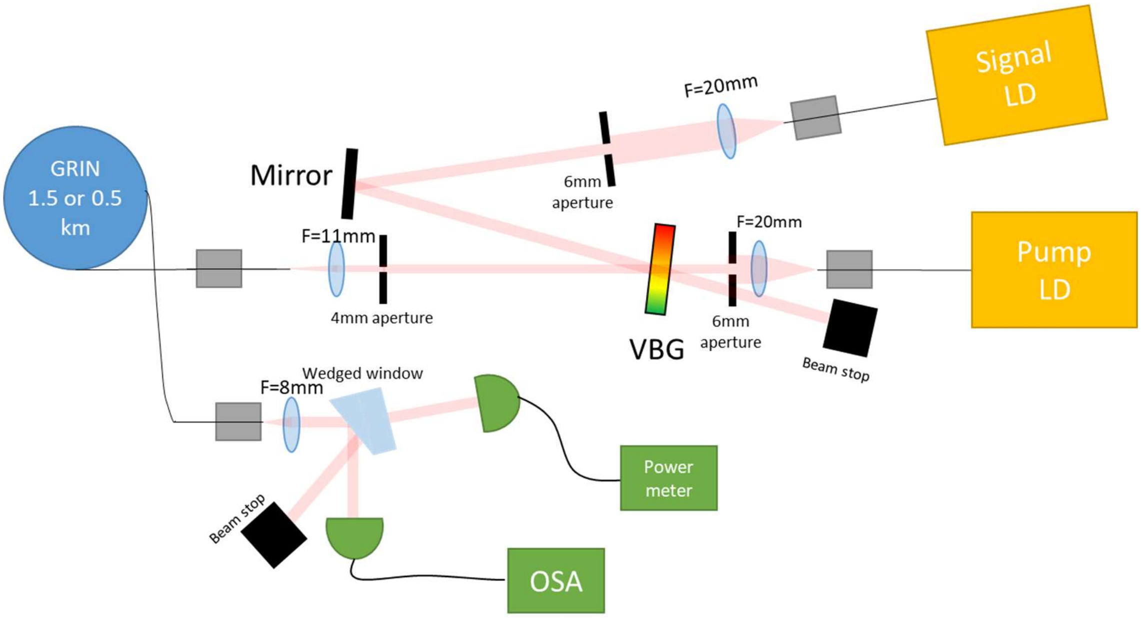

Figure 3.1 Experimental setup for 976-nm amplifier

Figure 3.1 illustrates the experimental setup. The output beams from both the pump and signal diode are collimated with f = 20 mm lenses. The beams are then combined with a volume Bragg grating (VBG) and steered toward the launching f = 11 mm lens that focuses the beams into the 1.5-km-long GRIN fibre where Raman amplification occur. The two ends of the fibre were normally cleaved to avoid complications in the alignment. This means that both ends work also as reflectors with 4 % (–14 dB) retro-reflection. This arrangement means that the fibre lases for 14 dB of single-pass net gain and is therefore often not used for amplifiers, the strong seeding keeps the 1st-Stokes gain low. The output of the amplifier is collimated and split so that the power and spectra can be measured.

3.2.1.1 Diode laser sources

Both the signal diode laser (nLight element e18) and the pump diode laser (JDSU Stingray-140 W) have the same maximum output power of 140 W from similar pigtails. The diameters of the core and clad of the fibre of the signal diode laser are 105 and 125 μm and those of the pump diode lasers are 106.5 and 125 μm. Both fibres have NA of 0.22 and 95% of the power lies within an NA of 0.15 according to specifications.

The signal diode laser is wavelength-locked and has a narrow linewidth of 0.7 nm (full width at half maximum, FWHM). The central wavelength is measured to 975.63 nm (measured in air and recalculated to vacuum) when operated at full power.

The FWHM linewidth and the central wavelength of the pump diode laser are measured to ~3.8 nm and 949.8 nm at full power. The central-wavelength drift from low to maximum power was measured to ~10 nm. This considerable shift is caused by the thermal load in the diode laser.

3.2.1.2 Beam combining

Apertures with 6 mm-diameter were inserted into the beams from the diode lasers, following collimation. These clip power in the edges in the beams to reduce the thermal load on the VBG with only a small reduction of launched power. The reduction in combined power also improves laser safety. The power of the signal and pump beam passed through their respective 6 mm-diameter-aperture was measured to 126 W and 103 W at maximum power. The signal power reflected by the VBG was measured to 104 W (83% of reflectance) and there was no noticeable reduction of the transmitted pump power.

3.2.1.3 Raman gain fibre

The Raman gain fibre is a GRIN fibre with a 62.5-μm diameter, 0.275-NA parabolic-index core and 125-μm diameter cladding (OFS OM-4). It has a perpendicularly cleaved pump launch end. The background loss was measured by filling the core with white light and evaluated from the difference in the transmission through 1.5-km and a short length of the fibre. Especially the values at 950, 976, and 1020 nm are measured to 1.87, 1.70, and 1.45 dB/km. The core is germanium-doped with a concentration that leads to a peak value of the Raman gain coefficient which is more than twice of that of pure silica. It was measured to 1.19×10^{-13} m/W for unpolarised light by Yao *et al.* [2]. Lengths of 1.5 km and 500 m are used in **Sect. 3.2.2** and **3.2.3**, respectively. For the used 270-cm^{-1} pump-signal separation, the Raman gain coefficient is estimated to 0.33×10^{-13} m/W.

3.2.1.4 Launching light into the Raman gain fibre

A 4 mm-diameter-aperture was added before the launch lens in order to reject the portion of the light that exceeds the acceptance angle of the GRIN fibre. The power through this aperture were 60.4 W and 80.5 W for signal and pump. The launched power was calculated by measuring the power through the fibre and compensating for the propagation loss. The power of the coupled signal and pump beam was thus evaluated to 44.1 W and 48.4 W, having 75% and 60% of coupling efficiency.

The peak Raman gain induced by the pump at the launch end becomes approximately 48.4 W × 1.19 × 10^{-13} m/W / (π × (62.5 μm / 2)^2) = 1.88 Np/km = 8.15 dB/km. For the used 270-cm^{-1} pump-signal separation, this reduces to 2.26 dB/km, which is still larger than the background loss.

3.2.2 1.5 km GRIN fibre

3.2.2.1 Main amplification result

During amplification experiments, the seed was kept at maximum power while the pump power was gradually increased. Each power of the pump, signal (1st Stokes) and higher-order Stokes waves was obtained by multiplying the measured total power by their respective power fraction, calculated by integrating the spectrum over their respective wavelength intervals.

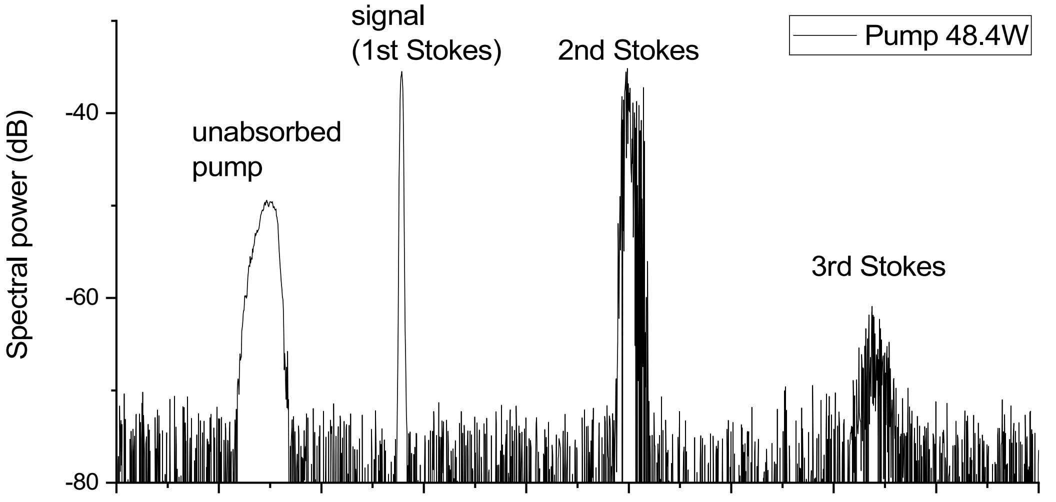

Figure 3.2 Measured output spectrum at 48.4-W pump power . Resolution 0.5 nm.

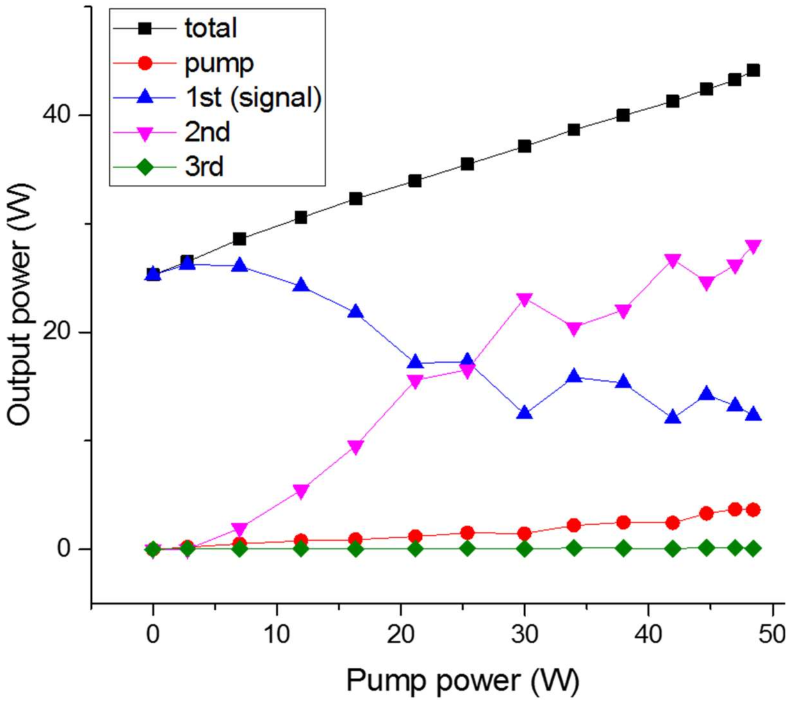

Figure 3.3 Output power of the leaked pump, signal, higher order Stokes, and the summed total *vs*. launched pump power. The irregularities are due to the wavelength drift caused by heat accumulation in the pump diode lasers. (See **Sect.3.2.2.2.2**)

Figure 3.2 shows the measured spectrum at maximum pump power (48.4 W). Four peaks are observed, unabsorbed pump, signal (1st Stokes), 2nd Stokes and 3rd Stokes. The intervals used to integrate the power in each peak are selected as 930 - 960 nm, 960 – 1000 nm, 1000 – 1040 nm and 1040 – 1080 nm.

Figure 3.3 shows how the power in the different Stokes orders as well as unconverted pump changes with increasing pump power. The fraction of power in 1st, 2nd, and 3rd Stokes order, as well as unconverted pump, at maximum pump were 0.280, 0.636, 0.002 and 0.082 (rounded to the third digit after the decimal point). I can see the signal (1st Stokes) has pumped the 2nd Stokes. With the pump off, the signal output power was 25.3 W. However, with increasing pump power, it started to decline already from low pump power, after a marginal growth to 26.5 W. At the same time, the 2nd Stokes started to build up and this trend continued until the maximum pump power, where the power in the 2nd Stokes (28.05 W) is higher than that in the 1st Stokes (12.35 W). The irregularities are due to the wavelength drift caused by heat accumulation in the pump diode lasers. (See **Sect.3.2.2.2.2**)

The amplifier could not produce a positive net gain as the signal's output power did not exceed its input power, 44.1 W. In fact, even if the 2nd order Stokes power is included in the signal power, the total of 43.6 W is still less than the 976-nm seed power due to the background loss. The fibre was clearly too long as the 2nd order Stokes emerged and the total loss was too high.

Meanwhile, if I consider the 2nd Stokes, its growth is quite impressive. Its slope efficiency calculates to 0.6. However, it seems that the 2nd order Stokes was lasing because of the two normally cleaved fibre ends which form a pair of 4% reflectors and thus a laser cavity. From **Eq. (2.13)** Raman threshold, the unseeded Raman threshold power for unidirectional travel (without reflections, i.e., the so-called critical power) calculates to 372 W. On the other hand, the laser threshold power at 976 nm of the laser cavity with a pair of 4% reflectors calculates to only 84.4 W. Seeing the total launched power at 976 and 950 nm of 92.5 W, which is much lower than 372 W, I may conclude that it was lasing, although the threshold is lower than the calculation.

I could have tried an angled cleave at an end to restrain the lasing but at the time of this experiment I did not realise that the 2nd Stokes may have been lasing. By contrast, remember that the strong seeding at the 1st Stokes prevents this from lasing.

3.2.2.2 Additional observations

3.2.2.2.1 Suppression of SRS by injecting nearby seed

An interesting observation was how strong seeding at 976 nm affects the Raman signals. See **Figure 3.4**.

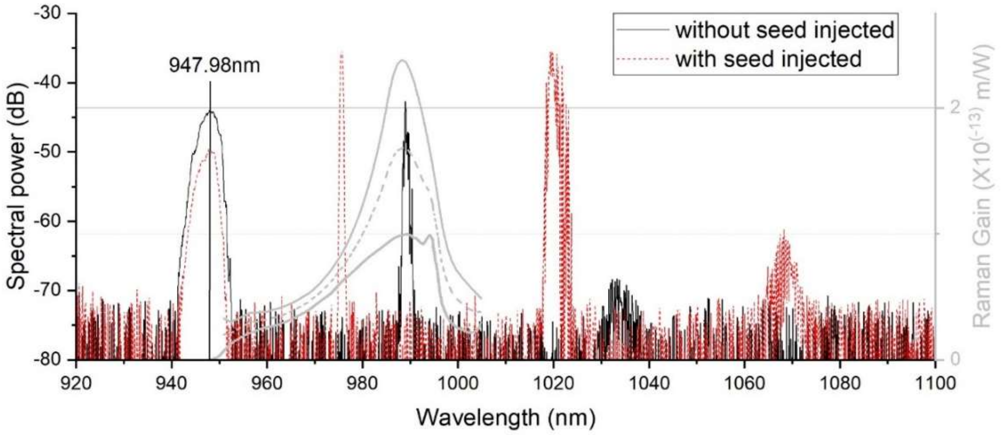

Figure 3.4 Spectra with and without the presence of the seed. The weak grey curves are Raman gain spectra of different glasses; silica and germania.

Figure 3.4 shows that the seeding with full power (44.1 W) at 976 nm suppresses the SRS at 989 nm, which is where the original SRS gain peaks when pumped at 948 nm as shown by the grey curves**.** Although the Raman gain at 976 nm is about a quarter to half of that at 989 nm, the injection of the seed eliminated SRS at 989 nm from the spectral trace. Thus, it was reduced by more than 30 dB, to below the noise level.

3.2.2.2.2 The problem of wavelength-drifts in the diode lasers

The temperature increase of the pump-diode at higher powers increases its wavelength and degrades the amplification due to the reduced Raman gain for wavelength separations smaller than that to the gain peak. Though this is not fundamental (it could be addressed by better thermal control of the diode lasers), it is an important practical effect which persisted in experiments with CW pumping in later chapters.

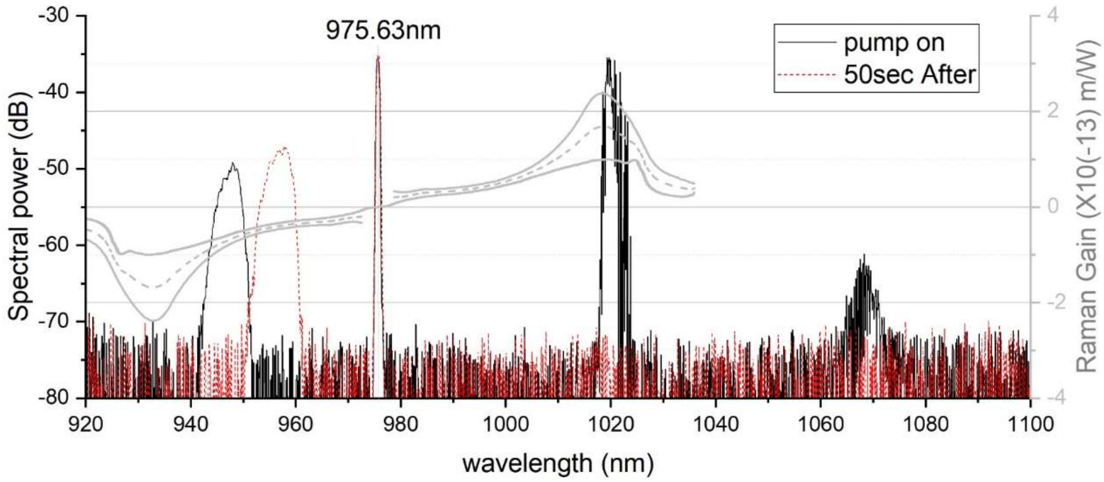

Figure 3.5 Output spectrum before and after the drift of pump-wavelength. The weak grey curves are Raman gain spectra of different glasses; silica and germania.

Figure 3.5 exemplifies how the shift of pump wavelength affected the amplification process. The 2nd and 3rd Stokes disappeared 50 seconds after the pump diode laser was switched on. At the same time, the leaked pump power increased. This means the conversion of the pump to signal decreased as the pump wavelength gradually moved toward the signal, when the diode heated up. The inverted Raman gain spectra, grey curves on the left side of the **Figure 3.5** show how the pump wavelength moves away from the SRS peak. To minimise this effect (when present), the power and spectrum were measured immediately after the pump diode laser was powered up.

3.2.3 0.5 km GRIN fibre

I used a shorter (0.5 km) GRIN fibre as a Raman gain fibre. This length was thought to be close to the optimum according to a numerical simulation result that is not introduced in the thesis.

I do not present this simulation because I will cover other simulations in chapter 5 which corrects this specific simulation, which appears invalid at present. Specifically, a variable of the simulation was adjusted to fit the result of **Sect. 3.2.1** without perceiving that the 2nd Stokes might be lasing. In order to meet the greatly underestimated Raman threshold of the 2nd Stokes wave, the effective core area had to be reduced down to 642 μm^2. This is much smaller than the physical area of the core (3068 μm^2), as well as the 1530 μm^2 arrived at from an estimation that considers the modal distribution of the GRIN fibre [2]. This under-estimates the optimum length (500 m according to simulations) relative to the actual value because of the overestimated Raman gain.

The 2nd Stokes disappeared in the shortened fibre. However, the conversion at high power pump was still unstable and / or low because of the thermal load on the pump-diode. In order to reduce the impact of the thermal load, I also investigated QCW pumping.

The experimental setup is same as for the 1.5-km Raman gain fibre in **Sect. 3.2.1**, except for the shorter length of 500 m. The maximum launched seed and pump power were measured to 45 W and 46.6 W when operated CW.

3.2.3.1 CW pumping

Figure 3.6 depicts the amplified signal output power and leaked pump power *vs.* launched pump power and their spectra. The power fraction of pump and signal was calculated by integrating the spectrum within the corresponding wavelength ranges where they reside (940 nm – 953 nm for the pump and 975 – 977 nm for the signal).

The signal grew linearly from 31 W to 42.9 W with a slope of 0.6 until the pump power reaches 20 W with low unconverted pump. Then, as the unconverted pump started to rise, the signal stopped growing, showing an irregularity. At the maximum pump, the signal reaches 44.6 W. The overall slope in the entire range was 0.29 (**Figure 3.6(a)**).

(a)

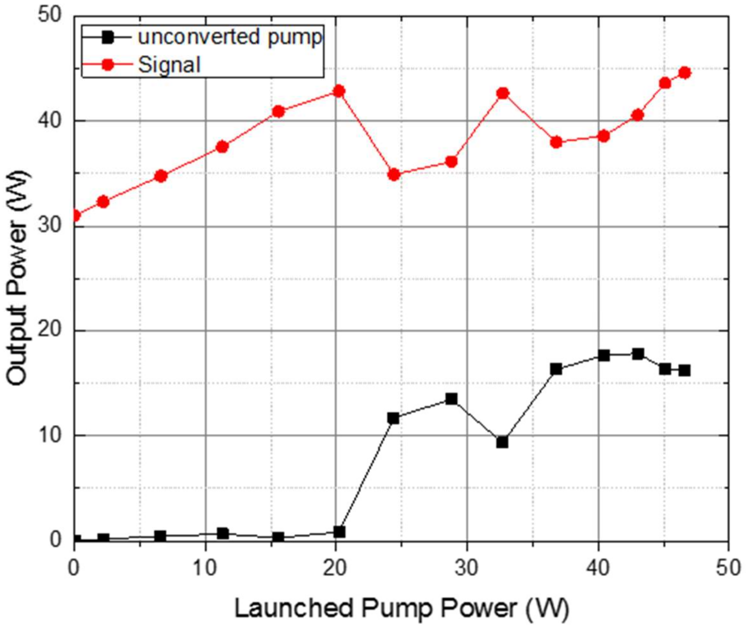

(b)

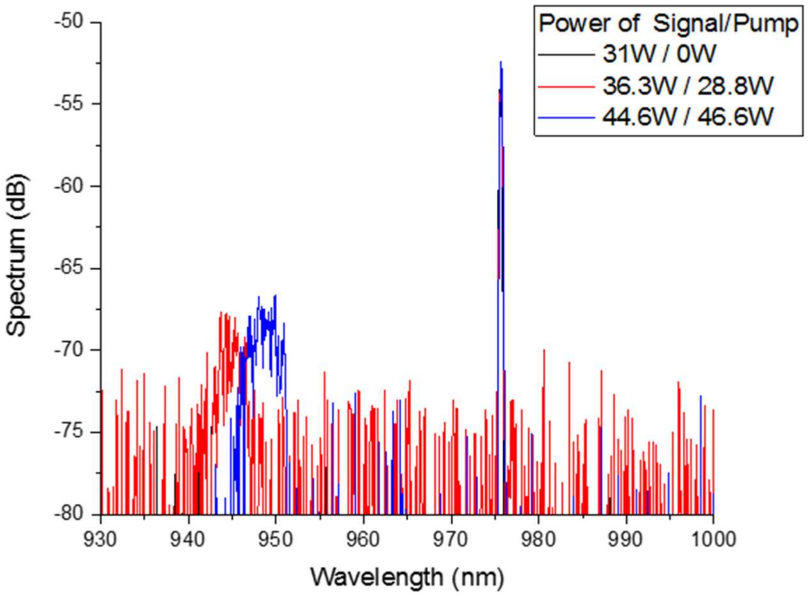

Figure 3.6 (a) Signal output power and leaked pump power *vs*. launched pump power for 0.5-km of GRIN fibre. **(b)** Output spectrum.

The spectrum was presented in **Figure 3.6(b)** only up to 1000 nm because there was no recognisable 2nd Stokes. It is, again, observed that the wavelength of the pump moves towards that of the signal, gradually as the temperature of the pump diode increases. As there was no 2nd Stokes, I conclude that the smaller separation of the two wavelengths and thus the smaller value of the Raman gain coefficient is responsible for the deterioration at higher power. The increased pump leakage also consistent with a reduced value of the Raman gain coefficient.

3.2.3.2 QCW pumping

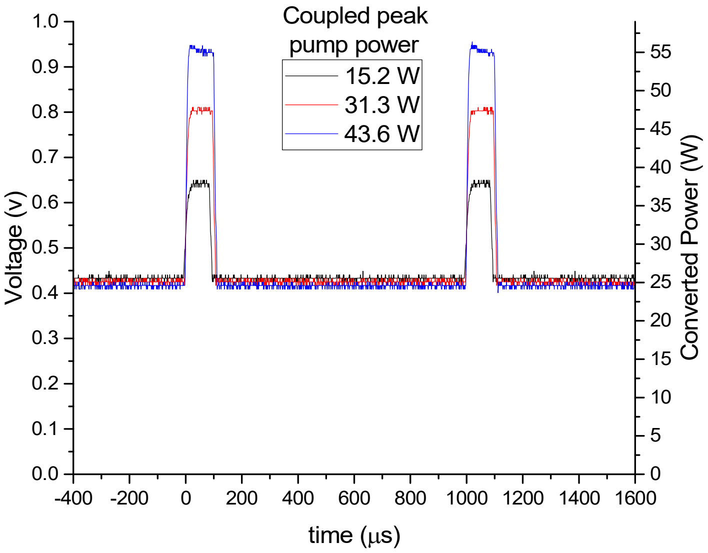

Figure 3.7 Voltage trace measured with a photodetector in the combined signal and pump output beam. The corresponding instantaneous powers (axis on the right) are calculated from the voltage trace with a calibration factor of 59 W/V.

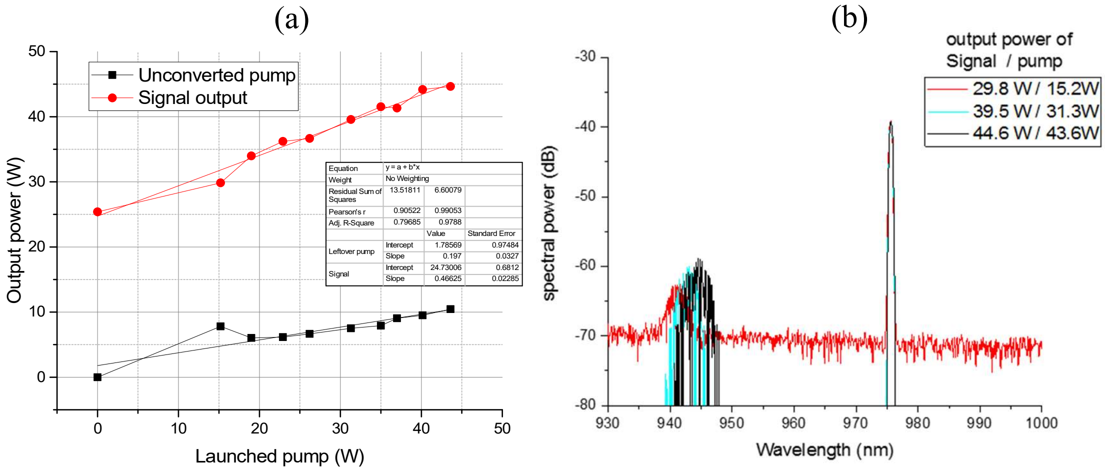

Equation	y = a + b*x		
Weight	No Weighting		
Residual Sum of Squares	13.51811	6.60079	
Pearson's r	0.90522	0.99053	
Adj. R-Square	0.79685	0.9788	
		Value	Standard Error
Leftover pump	Intercept	1.78569	0.97484
	Slope	0.197	0.0327
Signal	Intercept	24.73006	0.6812
	Slope	0.46625	0.02285

Figure 3.8 (a) Launched pump power *vs.* signal and unconverted pump power, **(b)** The spectrum

I changed to QCW pumping to reduce the thermal load and thus the wavelength drift of the pump diode laser. The signal was always on (the wavelength-locking stopped it from drifting), while the pump was modulated by a square signal at 1 kHz with 10% duty cycle from a function generator.

Figure 3.7 shows the voltage trace obtained from a photodetector sampling the combined pump and signal output beam. The base level of 0.43 V shows the output corresponding to the level of the CW signal seed when the pump is not present whereas the square peak shows the signal and the pump together when the pump is switched on for 100 μs.

I converted the voltage axis to optical power assuming that the voltage reading of the photodetector is proportional to the total optical power. I ignored the small responsivity difference (3%) of the biased Ge photodetector (DET50B/M) between the pump and signal. The converted power axis on the right side of the graph in **Figure 3.7** was added, giving the offset line (0.43 V) a value of 25.4 W of signal output power when the pump is off.

The summed peak power of the pump and the signal was retrieved from the **Figure 3.7** and the signal and the pump power are separated from each other by integrating the spectrum (shown at **Figure 3.8(b)**) for different pump power levels. This is shown in **Figure 3.8(a).**

Since, the measured spectrum is averaged on time, an extra calibration was needed to separate out the pump power accurately. As the trace is periodic, I integrated the voltage within one period and then multiply the ratio of the pump to total output power which is obtained from the spectrum analyser. Dividing this by 100 μs (the pump on-time), I can obtain the voltage resulting from the unconverted pump, which can be converted to optical power. Then, the signal output can be found simply by subtracting this from the peak power.

For unknown reasons, the launched maximum seed and pump power was reduced to 36.9 and 43.6 W. The signal grew linearly without any abnormality from the seed power of 25.4 W to 44.6 W with an overall slope of 0.44. Notice that in **Figure 3.8(b)** the wavelength drift is much smaller than for the CW-pumping shown in **Figure 3.6(b)**. Even though the maximum signal output power is same as with the CW experiment (by coincidence), this is a better result because the launched seed power is about 8 W (20%) less. The gain calculates to +0.82 dB. Although it is a small gain, it is the very first positive-gain diode-laser-pumped high power FRA, in which the separation between seed and pump is rather awkward (270 cm^{-1}), in the world to my best knowledge.

3.3 Fibre Raman laser simultaneously pumped at 950 and 976 nm by diode lasers

3.3.1 Experimental setup

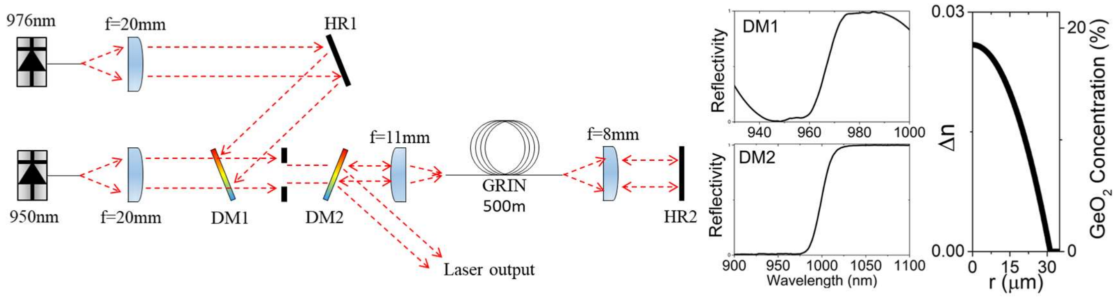

Figure 3.9 Experimental setup. Inset graph depicts the reflectivity of DM1 and DM2 as well as the refractive index and GeO_2 concentration profile of the used GRIN fibre. Both HR1 and HR2 are broadband dielectric high reflectance mirrors (Thorlabs, BB1-E03).

In this section, I describe work on a FRL diode-laser-pumped at 950 and 976 nm simultaneously. **Figure 3.9** shows the experimental setup. The pump beam combining part is almost identical with that of the amplifier setup in **Sect. 3.2.1**, except that the beam is combined by a dichroic mirror (DM1, Layertec) that replaced the VBG.

The combined power now reaches up to 235 W. The beam is then passed through an aperture of 4.5 mm diameter. This reduces the size of the combined beam and, thus, improves its beam quality. The power then drops to 176 W, i.e., by 20%. The purpose of the aperture is to reduce the amount of pump light which is not coupled into the Raman gain fibre and thus instead adds to the thermal load at the fibre launch, which can lead to failure.

The combined pump beam then passes through another dichroic mirror (DM2) with high transmission (98%) for the pump beam and high reflection for the Stokes beam at 1020 nm and is then launched into the Raman gain fibre through an f = 11 mm aspheric lens (Thorlabs, C220 TM-B).

The Raman gain fibre is a 500-m length of the GRIN fibre introduced in **Sect. 3.2.1.3**. It also has perpendicularly cleaved ends at both sides. The maximum incident pump powers were measured before the focusing lens to 103 W for the 976-nm pump and to 72.5 W for the 950-nm pump. The launching efficiency was measured to 47% (976 nm) and 57% (950 nm) at maximum power. This was determined by measuring the power transmitted through the fibre and compensating for the background loss of the fibre. This was measured to 3.44 dB/km (950 nm), 3.3 dB/km (975 nm), and 3.0 dB/km (1020 nm), by filling the core with white light and measuring the transmission through the 500-m length. The fibre was then cut back to a short length whereby the transmission loss was evaluated. These loss values are almost twice of those of the longer fibre (1.5 km) in **Sect. 3.2.1.3**. The difference may at least in part arise from mode-dependent loss, which can cause the attenuation to deviate from Beer-Lambert's law and lead to lower loss per unit length in longer fibres. In both 500-m and 1.5-km GRIN fibre, it is confirmed by a measurement with an optical time-domain reflectometer (OTDR) that the loss differs in different intervals. The loss steeply decreases from 5 dB/km in the 150-250-m interval to 1 dB/km in the 350–450-m interval, then to 0.5 dB/km in the 1350-1450-m interval, at the OTDR's wavelength of 1.3 µm.

In the far end of the fibre, a collimating lens and a high reflecting mirror (HR2; Thorlabs BB1-E03) closed the laser cavity. The mirror also reflected the pump back into the fibre in order to double-pass the pump. At the other end (pump launch end), the perpendicularly cleaved facet served as a 4%-reflecting output coupler of the laser cavity. After being reflected in DM2, the out-coupled beam was characterised with a thermal power meter and an optical spectrum analyser. As before, the powers in different spectral bands were obtained by numerical integration of the optical spectra.

3.3.2 Experimental result

I evaluated the FRL by gradually increasing the power of one pump while the other pump was either off or at full power. To evaluate the launched pump power, I blocked the feedback from the HR mirror and launched one pump at a time. This suppressed SRS, which would otherwise affect the transmitted pump power and thus the determination of the launch. For each pump, I measured the transmitted pump power and compensated for the loss of the fibre and thus determined the launched pump power.

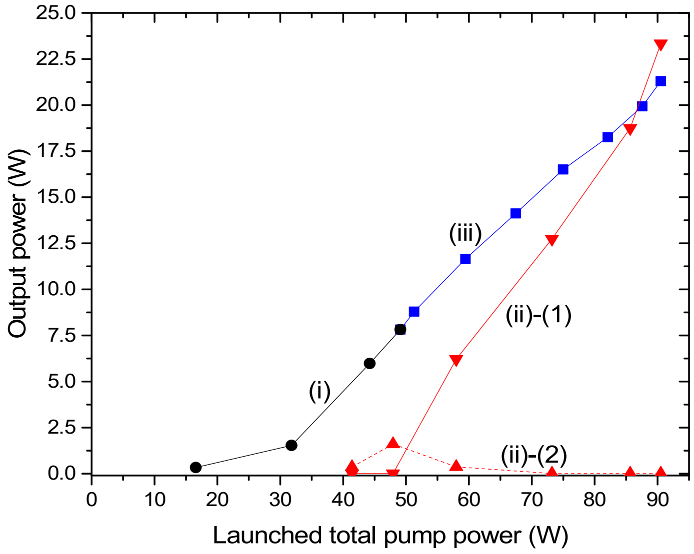

Figure 3.10. Laser output power *vs.* launched total pump power, measured the reflected beam from output mirror (DM2). The parentheses labels on curves and different-coloured segments indicate the results when **(i)** varying the 976-nm pump while the 950-nm pump was switched off, **(ii)** varying the 976-nm pump while the 950-nm pump was set to the maximum (41 W), **(iii)** varying the 950-nm pump while the 976-nm pump was set to the maximum (49 W). Especially, **(ii)-(1)** indicates the power of the signal (1020 nm) while **(ii)-(2)** indicates the power of the 1st Stokes order of the 950-nm pump.

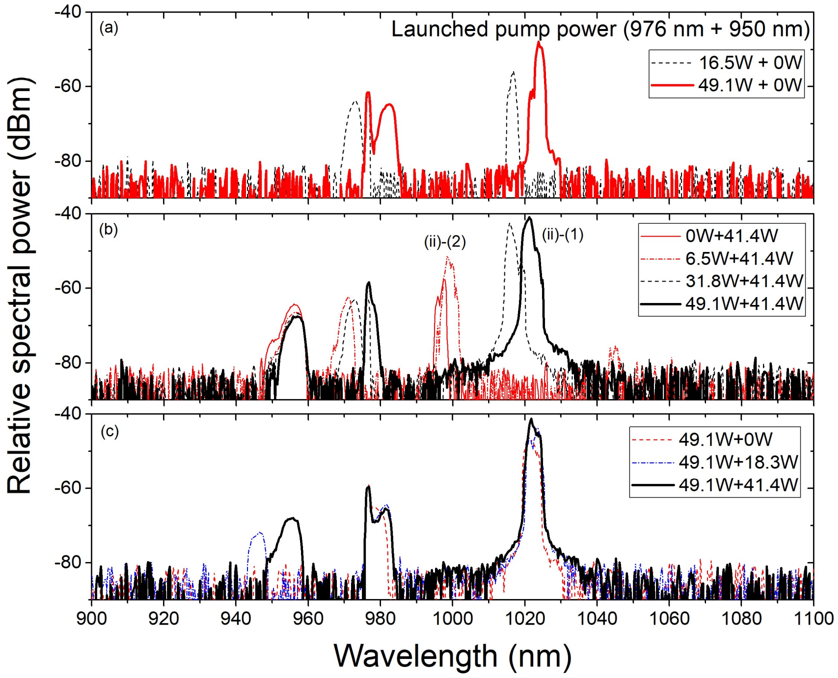

Figure 3.11 Output spectra for combinations of pump power as indicated when **(a)** varying the 976-nm pump while the 950-nm pump was switched off, **(b)** varying the 976-nm pump while the 950-nm pump was set to the maximum (41 W), **(c)** varying the 950-nm pump while the 976-nm pump was set to the maximum (49 W). Especially in **3(b), (ii)-(1)** indicates the signal peak (1020 nm) while **(ii)-(2)** indicates the 1st-Stokes peak of the 950-nm pump.

3.3.2.1 Output power and spectra

First, I varied the 976-nm pump power while the 950-nm pump was switched off. Curve **(i)** in **Figure 3.10** and **Figure 3.11(a)** shows the results. The FRL emits at a wavelength of ~1020 nm. The threshold is approximately 15 W. The slope efficiency increases for higher pump power and reaches 36% in the range 30 W - 50 W of coupled pump power.

The heatsinking of the 976-nm diode laser was inadequate for ensuring wavelength-locking over the full range of pump power, so the spectrum drifts to longer wavelengths as the pump power increases. **Figure 3.11(a)** shows spectra measured at the output of the fibre laser, following reflection in DM2. The unlocked part of the pump spectrum drifts from 973 nm at the threshold of the FRL to 983 nm at maximum power. At the same time, the output wavelength of the FRL drifts from 1017 nm to 1024 nm.

Next, I varied the 950-nm pump power while the 976-nm diode was switched off. In this case, the peak Raman gain occurs around 990 nm, where the reflection of DM2 is small. Thus the output power is negligible when the FRL is pumped only by the 950-nm pump although it was captured in the optical spectra.

I then set the 950-nm pump to maximum power (41 W launched) and gradually increased the 976-nm pump. The curve **(ii)-(1)** and **(ii)-(2)** in **Figure 3.10** show the resulting output power and **Figure 3.11(b)** shows spectra at different pump levels. At low 976-nm pump powers (including when the 976-nm power is off), I see SRS at 990 – 1000 nm although the low reflectivity of DM2 means that the power is low. There is also a small amount of second-order SRS at 1045 nm.

When the 976-nm power is increased beyond 6.5 W of launched power (48 W of total launched pump power), FRL emission appears at ~1020 nm, i.e. the 1st Stokes of 976 nm. The 1020-nm power then grows with a slope of 51% as the launched 976-nm power increases to its maximum value, 49.1 W (90 W of total coupled pump power). At the same time, the Stokes waves at the 1st and 2nd-order Stokes peaks of the 950-nm pump disappear. The reason is that the pumping of the 1st Stokes peak at ~990 nm decreases as the depletion rate of the 950-nm pump increases due to increasing SRS into 976 nm. Although the radiation at 976 nm and 1020 nm adds to the Raman gain at 1045 nm, this is apparently not enough to compensate for the reduction in Raman gain from the 990-nm wave.

Lastly, I set the 976-nm pump to its maximum power (49 W) and gradually increased the 950-nm pump. The curve **(iii)** in **Figure 3.10** shows the output power and **Figure 3.11(c)** shows the spectra at different pump powers. The wavelength of the 950-nm pump drifts from 946 nm to 956 nm by the heat. The output power increased from 7.8 W to 21.3 W with a slope of 31% by adding 41 W of the 950-nm pump. This slope efficiency is comparable to the 36% achieved with 976-nm single-diode pumping. The slight reduction from 23 W achieved previously may be caused by a degraded alignment.

3.3.2.2 Beam quality

TABLE 3.1
BRIGHTNESS ENHANCEMENT
ACHIEVED FOR DIFFERENT COMBINATIONS OF PUMP POWER, UNDER THE ASSUMPTION THAT ALL PUMP MODES ARE EQUALLY EXCITED.

Launched pump power, (976 nm + 950 nm) [W]	Brightness of signal (B_s) [$W \cdot sr^{-1} \cdot \mu m^{-2}$]	BRIGHTNESS OF PUMP (B_P) (976 nm + 950 nm) [$W \cdot sr^{-1} \cdot \mu m^{-2}$]	Brightness Enhancement (B_s / B_p)
49.1 + 0	0.46	0.16 + 0.00	2.8
49.1 + 18.4	0.64	0.16 + 0.06	2.9
49.1 + 41.4	0.76	0.16 + 0.14	2.5

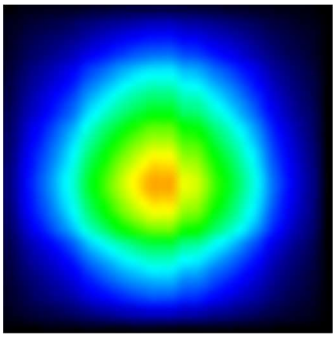

Figure 3.12 2-D power distribution reconstructed from 1-D measurements in orthogonal directions.

The beam quality factors (M^2) averaged for the two orthogonal axes were measured to 4.1, 4.6, and 5.2 for 7.8 W, 14.1 W, and 21.3 W of output power, respectively, for a brightness of 0.76 $W \cdot sr^{-1}$ μm^{-2} at maximum power. The beam quality factors of the launched pump within the GRIN fibre is around 18 with the assumption that all the modes are equally excited. From this, the full-power brightness of the pumps following the launch into the fibre are calculated to 0.16 $W \cdot sr^{-1}$ μm^{-2} (976 nm) and 0.14 $W \cdot sr^{-1}$ μm^{-2} (950 nm). This shows that the enhancement of the signal brightness for the maximum output power (21.3 W) is a factor of ~2.5 relative to the brightness of the combined pumps, and a factor of ~4.76 relative to the 976-nm pump alone. **Table 3.1** summarises the brightness enhancement.

I next consider if it is reasonable to assume that all modes are equally excited. Given a filled NA of 0.15 (containing 95% of the power) from the step-index pigtail, the effective V-value of the 950-nm diode laser becomes $V_{eff} = \pi \times 106.5\ \mu m \times 0.15 / 0.95\ \mu m = 52.8$. Assuming a top-hat intensity distribution, this corresponds to $V_{eff}^2 / 4 = 698$ modes (not counting polarization multiplicity). The total output power of 140 W stems from multimode diode lasers and is therefore expected to be relatively uniformly distributed amongst the modes, so the power per mode becomes 0.181 W. Given that a diffraction-limited single mode corresponds to a beam-parameter product (BPP) of λ / π, this corresponds to 0.20 $\mathrm{W \cdot sr^{-1}\ \mu m^{-2}}$. It follows from the brightness theorem (stemming from the second law thermodynamics) that these values set upper limits on the pump modal power and brightness launched into the Raman gain fibre (RGF), which cannot be increased by passive elements such as lenses and apertures. For the GRIN fibre, $V = \pi \times 62.5\ \mu\mathrm{m} \times 0.275 / 0.95\ \mu\mathrm{m} = 56.8$ at 950 nm. Given a parabolic refractive-index profile, this supports 404 "scalar modes" (i.e., not counting polarization multiplicity). Since this is fewer than the number of modes exiting the diode-laser pigtail, it is in principle possible to maintain the power per mode in the GRIN fibre. However, its V-value is (slightly) higher than $V_{eff} = 52.8$. It is therefore not possible to simultaneously fill the GRIN fibre's numerical and physical aperture, in case of an imaging optical coupling system with lenses. This does mean that the launched power into each of the GRIN fibre's modes will be reduced from the ideal 0.181 W per mode in the incident beam (this reduction can be avoided with non-imaging optics). The actual launched power will also be degraded by Fresnel losses and other imperfections in the optical system. Thus, I conclude that the assumption of all modes being equally excited in the GRIN fibre, for a brightness of 0.14 $\mathrm{W \cdot sr^{-1}\ \mu m^{-2}}$ at 950 nm, is fully consistent with the calculated ideal limit of 0.20 $\mathrm{W \cdot sr^{-1}\ \mu m^{-2}}$.

Figure 3.12 shows a typical 2D power distribution, at maximum pump as reconstructed by a beam profiler (Thorlabs BP104-IR) from the 1D distributions it measured in orthogonal transverse directions.

3.3.3 Simulation

In our previous work [2] with spectrally narrow pumping of a longer piece (1.5 km) of the same fibre, the author reached a significantly higher slope efficiency (80%) than now (51%). Although the difference in fibre length and propagation loss may explain some of this, the much wider pump spectrum I have now also reduces the efficiency in the experiments. I investigated this further with simulations. I considered a simplified system with three bi-directional waves at 950 nm, 976 nm, and 1020 nm (i.e., the two pumps and the primary Stokes wavelength), according to the following coupled differential equations:

$$\pm\frac{1}{P_i^{\pm}}\frac{dP_i^{\pm}}{dz} = -\alpha_i + \left(\sum_{i>j}\frac{g_{R_{ij}}}{A_{i,j}}\left(P_j^{+} + P_j^{-}\right) - \sum_{i<j}\frac{g_{R_{ij}}}{A_{i,j}}\left(\frac{\lambda_j}{\lambda_i}\right)\left(P_j^{+} + P_j^{-}\right)\right) \ with\ i,j = 1,2,3 \quad (3.1)$$

These equations are a straightforward extension of common Raman equations [3] to multi-wavelength bi-directional propagation (**Sect. 2.1.3**). The wavelengths λ_1, λ_2, and λ_3 correspond to 950 nm, 976 nm, and 1020 nm, respectively, and α_i is the background loss and $P_i^{\pm}$ is the power in channel (wave) i. The superscript +/– indicates the direction of propagation. Furthermore, $g_{R_{ij}}$ is the Raman gain coefficient between λ_i and λ_j, and $A_{i,j}$ is the effective area for the interaction, which is inversely proportional to the intensity overlap between wave i and j. Note that this model implies that the excited modes in one wave are coupled so that all light propagating in one direction at one wavelength can be treated as a single entity. Otherwise, A_{ij} would change along the fibre. This was a restriction of the simulation software. The near- and far-end cavity reflectances were set to 0.04 and 0.8, respectively, for all waves.

Figure 3.13 shows the results of our simulations, together with experimental data. Here, I assumed that the pump intensity distribution everywhere along the fibre was given by the sum of the intensity distribution of the lowest 109 modes with equal power, out of a total of 351 modes. (The number of modes here is obtained by a mode solver in "RP fiber power" at 976 nm. That is why the value is somewhat different from the previous calculation (404) in **Sect.3.3.2.2**) Although I believe more modes than that are actually excited at the launch, this gave good agreement with the experimentally determined threshold. A tentative explanation is that even though the 109 modes are a small subset of the actually excited modes, they still result in an effective area close to that in the experiments, as a power-weighted average along the fibre. For the signal distribution, I assumed that only the 13 lowest modes were excited, with equal power. This is motivated by the measured signal beam quality, which is significantly better than the value (M^2 = 18) if all signal modes are equally excited. Based on these distributions, I then calculated effective Raman gain coefficients as the local Raman gain coefficient for the wavelengths in question weighted by the intensity distributions of the interacting waves. In turn, the local Raman gain coefficient was determined from the local Ge-concentration, which is proportional to the local increase in the refractive index [4], [5]. The gain coefficients

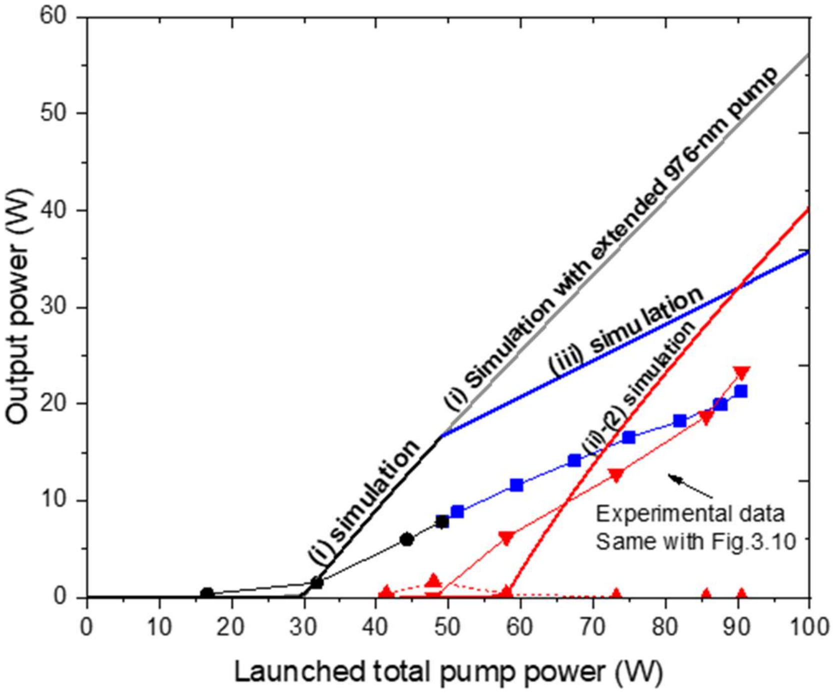

Figure 3.13. Simulations, together with experimental data of FRL pumped simultaneously at 950 nm and 976 nm. Simulations of single wavelength 976-nm pumping (grey line) are also shown. Labelling as in **Figure 3.10**.

become 6.40 × 10^{-14}, 9.17 × 10^{-15}, and 1.19 × 10^{-13} m/W for $g_{R_{12}}, g_{R_{13}}$, and $g_{R_{23}}$, respectively. The effective areas were calculated by estimating the overlap between waves in the same manner as in ref. [2]. They become $A_{1,2}$ = 1559 μm^2 and $A_{1,3} = A_{2,3}$ = 985 μm^2. Likewise, the loss coefficients were determined from the intensity distributions and the dependence of the loss on the wavelength and the (local) Ge-concentration [5], [6]. They become 5.7, 4.8, and 5.2 dB/km for α_1, α_2, and α_3, respectively. These are higher than the experimental values for the 500-m long fibre. Given that the local loss varies between ~ 1 dB/km and 6.5 dB/km depending on the local Ge-concentration, this can perhaps be explained by intensity-distribution differences and changes as the waves propagate through the fibre.

The agreement with experiments is still relatively poor, and we found it difficult to improve it within our simple model. The reason for this may be that the modes cannot be treated as a single entity and therefore propagate with different loss and Raman gain. It was still possible to achieve good agreement with experiments, if we assume that an increasing number of modes are excited at higher power levels. This has some support from the beam quality values in **Table 3.1**, although the quantitative agreement was modest. A model which better describes the spectral evolution and the mode-coupling may be needed to improve the agreement with experiments.

I can still use our simplified model to estimate the penalty of dual-wavelength vs. single-wavelength pumping at 976 nm (also shown in Fig. 4). When the 976-nm pump is at full power (49 W), an increase in the 950-nm pump yields a slope efficiency of 37%. The output power reaches 32 W when the 950-nm pump reaches its full 41 W of power. If instead the 976-nm pump is increased beyond 49 W, the slope efficiency becomes 78%. This difference is significant, but I note that the experimental difference in slope is smaller. Furthermore, the brightness of available diode lasers is limited, and launching more power at a single wavelength may not be possible.

3.4 Summary

A FRA with two different lengths (1.5 km and 0.5 km) of a GRIN gain fibre seeded and pumped directly by diode lasers was demonstrated. The 0.5-km long fibre was better than the 1.5-km one. Aided by QCW operation, it finally ended up with a positive gain (+0.82 dB) with a high seed power of 36.9 W. Higher gain and output power are expected with more pump power as the slope did not show any sign of saturation.

A FRL that emits in a single Stokes order at ~1020 nm when pumped simultaneously at 950 nm and 976 nm by diode lasers is demonstrated for the first time. The output reached 23 W with a slope of 50 % when the 976-nm power is varied while the 950-nm pump is at full power. Although the spectral separation of 270 cm^{-1} is both substantially larger than the Raman linewidth of ~ 100 cm^{-1} and substantially smaller than the Raman peak shift of 440 cm^{-1}, the addition of the 950-nm diode almost triples the output power over that achieved with only the 976-nm diode.

In both experiments, the higher conversion efficiency and output power would have been possible with more launched pump power. In regard to that, **Sect.4.4** presents GRIN FRA and FRL experiments with more pump power added at additional wavelengths.

3.5 References

[1] S. Hong, Y. Feng, and J. Nilsson, “Off-Peak Dual-Wavelength Multimode Diode-Laser- Pumped Fiber Raman Laser,” *IEEE Photonics Technol. Lett.*, vol. 30, no. 18, pp. 1625–1628, 2018, doi: 10.1109/LPT.2018.2863559.

[2] T. Yao, A. Harish, J. Sahu, and J. Nilsson, “High-Power Continuous-Wave Directly-Diode-Pumped Fiber Raman Lasers,” *Appl. Sci.*, vol. 5, no. 4, pp. 1323–1336, 2015, doi: 10.3390/app5041323.

[3] G. P. Agrawal, *Nonlinear Fiber Optics*, 4th ed. London: Elsevier, 2006.

[4] S. T. Davey, D. L. Williams, B. J. Ainslie, W. J. M. Rothwell, and B. Wakefield, “Optical gain spectrum of GeO_2-SiO_2 Raman fibre amplifiers,” *IEE Proc. J - Optoelectron.*, vol. 136, no. 6, pp. 301–306, 1989, doi: 10.1049/ip-j.1989.0047.

[5] J. W. Fleming, “Dispersion in GeO_2–SiO_2 glasses,” *Appl. Opt.*, vol. 23, no. 24, pp. 4486–4493, 1984, doi: 10.1364/AO.23.004486.

[6] M. N. Zervas and R. I. Laming, “Rayleigh Scattering Effect on the Gain Efficiency and Noise of Erbium-Doped Fiber Amplifiers,” *IEEE J. Quantum Electron.*, vol. 31, no. 3, pp. 468–471, 1995, doi: 10.1109/3.364401.

Chapter 4: Wide-Span Multi-wavelength high power diode laser pumped fibre Raman laser

4.1 Introduction

This chapter describes three FRL experiments with different Raman gain fibres (RGFs) that were pumped by five high power diodes lasers at 976, 969, 950, 940, and 915 nm, which were spectrally combined before launched into the fibre. The first RGF in this chapter is custom-made with a pure-silica step-index core. The second RGF is the same standard telecom GRIN fibre with a high Ge-concentration as used in chapter 3. The third RGF is custom-made with a Ge-concentration that is even higher in a quasi-step-index core. More details of the fibres are specified in **Appendix A**.

The total span of the five pump wavelengths is 683 cm^{-1} which is two and a half times wider than the separation of the two pump wavelengths in **Chapter 3**. The total span exceeds the maximum Raman shift in silica of 1100 cm^{-1} when I include the signal wavelength as well. Furthermore, it is more than double the shift to the Raman gain peak (e.g., 440 cm^{-1}). This means that the short-wavelength pumps will go through multiple Raman scattering process to be converted into the signal wavelength. Therefore, the questions I am trying to answer in this chapter are if it is even possible to make the laser emission at single wavelength using such a spectrally broad pump source and if it is, how efficient it is.

Section 4.2 demonstrates a spectrally combined pump beam which was used for pumping various laser setups in following sections.

In **section 4.3**, I used a multimode silica-core step-index fibre for the RGF. A pure-silica core increases the Raman linewidth, which may be beneficial for multi-wavelength pumping, but the absence of Ge reduces the Raman gain compared to telecom GRIN fibres. I did not reach threshold with single wavelength pumping, but with multi-wavelength pumping, with all diode lasers at full power, I reached 31.5 W of output power at 1018 nm with overall slope efficiency of 0.42. This result was published in ref. [1].

In **section 4.4**, I revisit the 1.5-km GRIN fibre in chapter 3 to see how it performs with increased pump power and pump bandwidth, in laser and amplifier configurations. The laser output power reached 67 W with a slope of 0.35 and the amplifier had a positive gain of 2.3 dB at the maximum seed power (33 W), thus reaching 56.5 W.

In **section 4.5**, I use the spectrally combined diode-laser source to demonstrate the first 100-W multi-wavelength pumped FRL. The RGF had a high germanium-concentration, and was designed to achieve higher Raman gain as well as a high NA whilst keeping the increase of the background loss over that of a silica-core fibre acceptable. This fibre was fabricated by Jaesun Kim at Taihan Fiber Optics. I reached 101 W with an overall slope efficiency of 65% (50% of optical-to-optical efficiency).

4.2 The spectral combination of diode-laser pump source

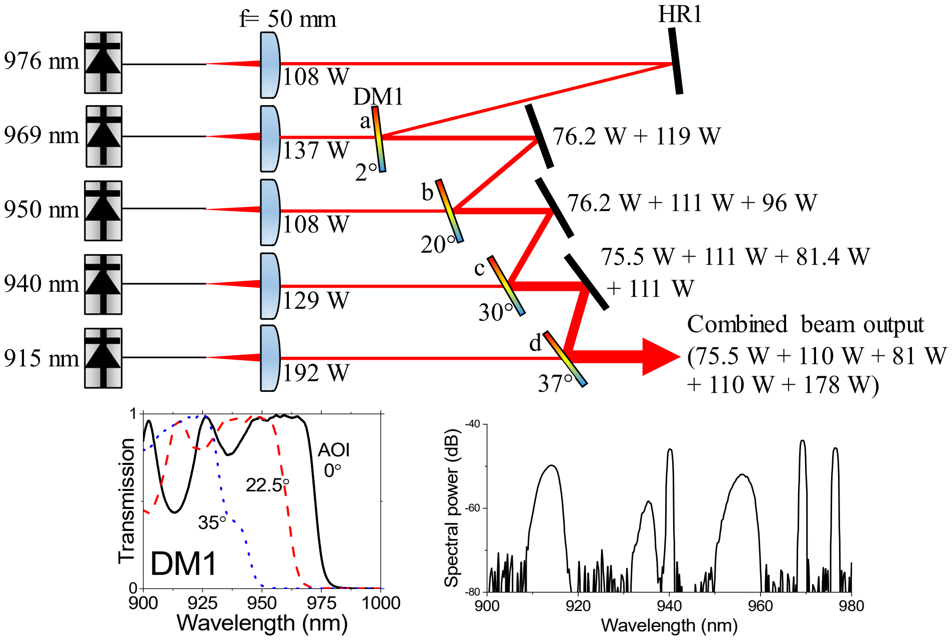

Figure 4.1 Layout of spectral combining of pump diode lasers, the transmission of DM1 at different angles-of-incidence, and the spectrum of the combined beam.

The spectrally combined pump source comprised five diode lasers with emission wavelength of 976, 969, 950, 940 and 915 nm. See **Figure 4.1**. The lasers at 976, 969, and 940 nm were wavelength-locked and their emission spectra were therefore more stable and narrow, although the 940-nm laser had significant unlocked emission at shorter wavelengths. All five diodes have 105/125 µm, 0.22 NA pigtails and are specified to have over 95% of the power within an NA of 0.15.

The beams were collimated individually with f = 50 mm aspheric lenses. This relatively long focal length allowed the pump beams to expand sufficiently to ensure that they remained well collimated over the relatively long free-space beam paths (3 m - 5 m for the different wavelengths). The collimated beams were spectrally combined, one after another from long to short wavelengths, in dichroic mirrors (DM 1). Each mirror transmits the wavelength that is added, and reflects the other wavelengths. The mirrors had the same custom coating but were tuned to different angles-of-incidence (AOIs) from 2° to 37° (specified in **Figure 4.1**) in order to shift the transmission edge. The AOI of each mirror was adjusted in succession to maximise the combined power after the adjusted mirror, with the diode lasers at full power, starting from the longest wavelength. The power reached 555 W (combined), and 76, 110, 81, 110, and 178 W at each wavelength in descending order. This corresponds to an overall combination efficiency of 83%, whereas the combination efficiency of individual diode lasers becomes 70%, 80%, 75%, 85%, and 93%, respectively.

The loss of an added wavelength is significant, upon transmission through the DM. The loss of the reflected wavelength closest to the transmission edge is significant, too. The loss of other reflected wavelengths is negligible. It follows that although our angle adjustment approach leads to nearly the maximum combined power, a slightly higher power can be achieved if the transmission edge is shifted towards the shorter, added, wavelength. Since reflected wavelengths suffer negligible loss in subsequent mirrors, and since longer-wavelength pump power can be expected to be converted more efficiently to the FRL output, the reflected light is more valuable than that transmitted by a mirror. Thus, the mirror angles should be biased towards low reflection loss. Consequently, there is some limited room for improving the beam combination with the same equipment. In addition, the mirrors can be improved, e.g., with different coatings for different mirrors.

4.3 Pure-silica-core fibre Raman laser

4.3.1 Cavity and pump launching

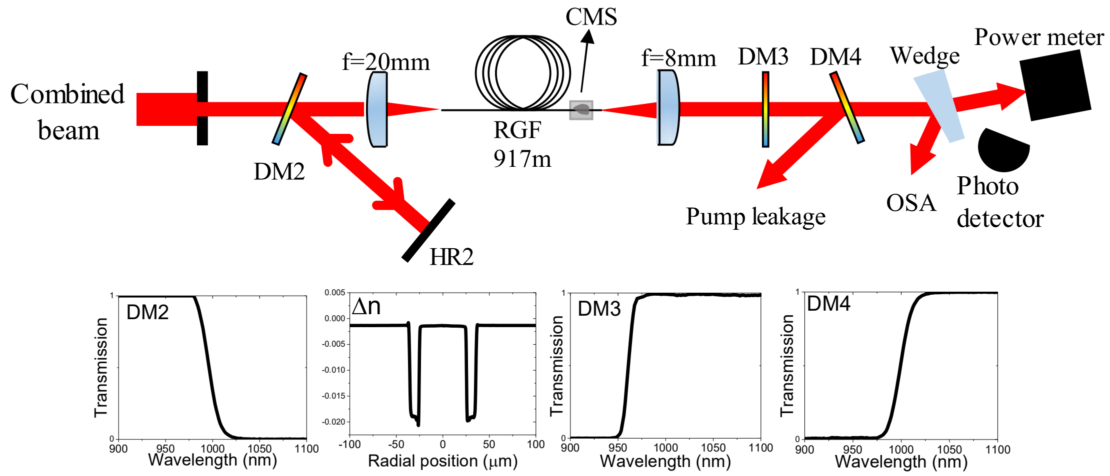

Figure 4.2 FRL cavity and measuring positions. Inset graphs depict the transmission of DM2, DM3, and DM4 as well as the index profile of RGF

TABLE 4.1
POWER AT DIFFERENT STAGES

	976	969	950	940	915	Total power
Model	nLight e18	nLight e18	JDSU Stingray	nLight e18	nLight e18	
Wavelength locked?	Yes	Yes	No	Yes	No	
Power from pigtail	108	137	108	129	192	674
Power after DM 1a	76.2	119				195.2
Power after DM 1b	76.2	111	96			283.2
Power after DM 1c	75.5	111	81.4	111		378.9
Power after DM 1d (power in combined beam)	75.5	110	81	110	178	554.5
Power after aperture	58	86.3	54	67.4	97	362.7
Power after DM 2	56.8	85.4	53.3	66.7	96	358.2
Launched power (To the Silica-core fibre)	24.5	47.5	21.5	33.2	58.5	185.1
Launch efficiency relative to incident power	43%	56%	40%	50%	61%	52%
Launched power relative to diode-laser power	23%	35%	20%	26%	30%	27%
Transmitted power with single diode laser on	18.8	36.3	15	22.2	42.6	134.9
Fibre loss (dB/km)	1.25	1.28	1.7	1.9	1.5	
Power at threshold*	24.5	38.2	20	17.9	0	100.6

Unit: W (if not specified.)

Before the combined pump beam is launched into the RGF, it passes through a 10-mm aperture. This clips pump light with poor launch efficiency, which otherwise adds to the thermal load at the launch point. Then, the beam passes through another dichroic mirror (DM2) with 98% transmission for the combined pump beam and > 97% reflection for the Stokes beam at 1018 nm and is launched into the RGF through an f = 20 mm aspheric lens. The incident pump power was measured before the focusing lens to 57, 85, 54, 67, and 96 W in descending wavelength order.

The RGF is 917 m long and is designed for core-pumping. Its 50-µm diameter, 0.227-NA, step-index silica core is surrounded by 10-µm-thick fluorine doped layer and a 345-µm diameter silica cladding. The refractive index profile is shown in **Figure 4.2**. The fibre was pulled in-house from a preform fabricated by Heraeus (Fluosil Q SWS6.95/SWU1.4). The fibre is coated with low-index polymer to reduce the absorption of any light that escapes from the core. Although cladding-guided pump light penetrates into the core and contributes to SRS in the core, the large cladding area makes this effect negligible, because of the low intensity of cladding-guided pump light. Thus, despite the double-clad fibre structure, the pump needs to be launched into the core. The loss of the core was measured to 1.25, 1.28, 1.70, 1.90, 1.50, and 1.07 dB/km at wavelengths of 976, 969, 950, 940, 915, and 1020 nm, by white-light transmission measurements with a cut-back of (nearly) the full length of the fibre. In contrast to GRIN fibres, I do not expect any significant loss difference between core-guided modes. The fibre was perpendicularly cleaved in both ends and a cladding-mode stripper at the far end facilitated core launch alignment and characterisation. The pump powers launched into the core were 24.5, 47.5, 21.5, 33.2, and 58.5 W at the different wavelengths in descending order, as calculated from the transmitted power and the fibre background loss. Thus, the launch efficiencies for each wavelength are 43%, 56%, 40%, 50%, and 61%. **Table 4.1** summarises the power of respective diodes at different stages.

However, there was some crosstalk among the diode lasers, presumably caused by the wavelength drift due to the thermal load so that the total launched power when all the diodes were at their maximum (175 W) was lower than the sum of the powers from each diodes when individually turned on to the maximum (185 W). I compensate for this effect in the data I present. For example, although the launched powers from the two longest-wavelength diode lasers in isolation are 24.5 and 47.5 W, with a sum of 72.0 W, the power actually launched became 62.7 W. Thus, the power increment of the second diode laser was not 47.5 W but 38.2 W. This is the power used in presented data, and it is to be understood that the actual launched power at a single wavelength depends on which other wavelengths are present. The adjusted (incremental) launched pump powers were 24.5, 38.2, 20, 37.3, and 54.9 W in descending order of pump wavelengths.

In the far end of the fibre, a collimating lens and a third dichroic mirror (DM3) serves to double-pass the shorter-wavelength pumps at 950, 940, and 915 nm. The reason why I double-pass only the shorter pump wavelengths is that these amplify the longer wavelengths, which can lead to high-power backward-propagating light at long wavelengths, if those are seeded by light reflected in DM3. Although it may be possible to avoid this when the laser is operating with substantial amounts of 1st-Stokes power at ~1020 nm, this is challenging to ensure. Thus, initial experiments in which all pump wavelengths were double-passed led to strong backward-propagating 976-nm radiation which damaged the 976-nm diode laser and degraded its power from ~140 W to 108 W. Note also that if higher powers are available, then the benefits of double-passing the pump become smaller. This may then become the preferred configuration, and may also help to suppress temporal instabilities, which appeared in some configurations.

To form a cavity for the FRL, a mirror (HR2) back-reflects the beam reflected from DM2 in the pump launch end of the RGF. In this arrangement, the alignment of the launching stage needs to not only optimise the pump launch but also the collimation of the signal beam for efficient feedback of the Raman signal. Therefore, I first maximised the launched pump power, and then realigned the position of the fibre's launch end to maximise the 1st-Stokes SRS, induced by the 976-nm pump and as monitored at the far end output. Then lastly, I optimised the position of each pump pigtail. This does not guarantee that optimum alignment is reached, but it should come close.

In the other end of the cavity, the fibre is perpendicularly cleaved to form a 4%-reflecting output coupler. In addition, residual signal reflection from DM3 adds to the feedback, but this was not quantified. A fourth dichroic mirror (DM4) separates leaked pump (976 and 969 nm) from the out-coupled signal. A 4%-reflecting glass wedge samples the out-coupled beam for spectral measurements. The output power was measured with a thermal power meter. A 350-MHz biased silicon photodetector (DET10A, Thorlabs) connected to a 200-MHz oscilloscope (DSO X2022A, Agilent) captured scattered light from the power meter's surface in order to measure temporal traces. I estimate the temporal resolution to 2 ns.

4.3.2 Results

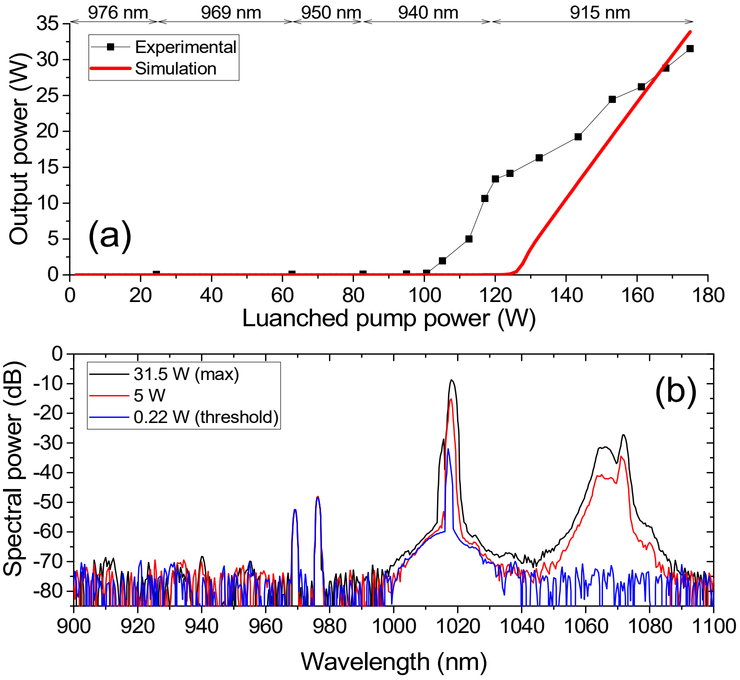

Figure 4.3 (a) Output power *vs*. total launched pump power with simulation **(b)** optical spectra of the output signal measured with 1 nm resolution after DM4, which suppresses the pump waves.

For investigation of the laser characteristics, I increased the pump power by turning on diode lasers one by one in descending order of wavelength. I reached the FRL threshold when the 4th diode laser at 940 nm was turned on to 48% of its maximum power for 101 W of total pump power (24.5, 38.2, 20.0, and 17.9 W at 976, 969, 950, and 940 nm, respectively. The threshold in simulations is 126 W. See **Sect. 4.3.3** for simulation details.) Then, the signal output power increased with average slope of 0.42 and reached 31.5 W when the 940-nm and 915-nm pumps reached their maximum values. This is shown in **Figure 4.3(a)**, together with the result of simulations. In detail, the slope when the 940-nm pump power increases is 0.68. The slope for subsequently adding 915-nm pump power is 0.33. The slope efficiency in the range of 113 – 120 W of launched pump reaches 1.12. I note that the nonlinear pump depletion in a FRL means that the slope efficiency can exceed unity over a limited range of powers. Another possible explanation for slope efficiency > 1, as measured, is drifts in wavelength or alignment, which may have affected the launch into the core at high power. The nonlinear character of a FRL makes this difficult to monitor. The residual pump power in the range 960 – 980 nm was measured to 61 - 64 W for all powers above the laser threshold, in fair agreement with simulations (69 – 80 W).

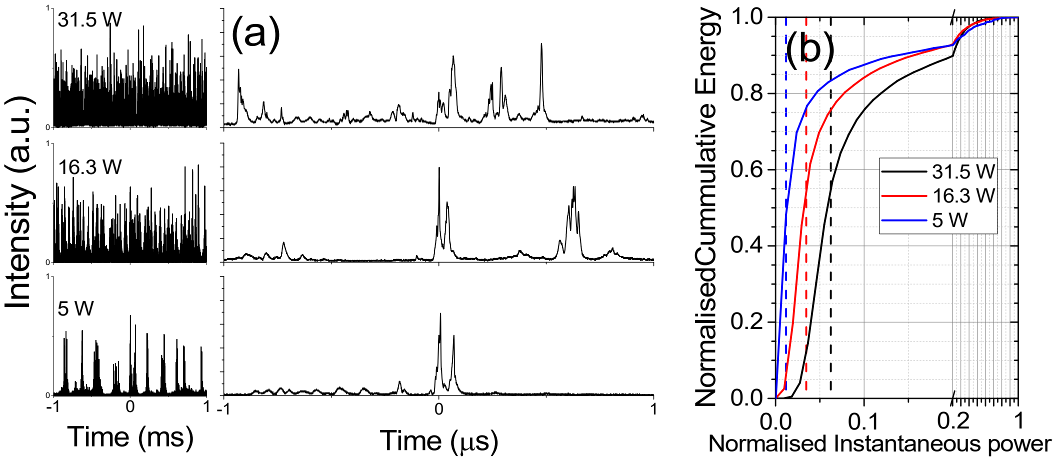

Figure 4.4 **(a)** Temporal traces and **(b)** normalized cumulative energy *vs.* normalized instantaneous power. Dotted lines depict the average power of each curve.

The signal wavelength was 1018 nm, which lies in the wavelength range of the 1st-Stokes of a pure-silica core, both for pumping at 969 and 976 nm. The linewidth was < 2 nm (**Figure 4.3(b)**). Second-order Stokes emission emerged too, in the 1060 - 1075 nm region in the shape of the typical Raman gain curve of silica fibre. The 2nd-Stokes power was no more than ~3% of the 1st-Stokes power even at maximum pump power. The 2nd-Stokes power is included in the reported laser output powers. If necessary, higher Stokes orders can be reduced or even effectively eliminated by improved wavelength selection, e.g., in DM 2. Elimination of broadband feedback from perpendicularly cleaved fibre ends can also improve wavelength selection.

Figure 4.4(a) shows temporal traces in 2-ms and 2-μs spans. The output signal was pulsing, seemingly randomly without a clear trend. The pulse duration ranged from ~6 ns to ~50 ns (full-width at half-maximum) as observed in the 2-μs spans. The maximum instantaneous power within the 2-ms spans was ~424 ~470, and ~505 W at ~5, 16.3, and 31.5 W of average output power, respectively. In addition, there is a continuous wave (CW) component in the output power of at least 31.5 W. To assess the power fluctuations, I calculated the cumulative energy against the instantaneous power (**Figure 4.4(b)**) for those three power levels. The distributions are normalised to their maximum instantaneous powers. Some power may be in higher Stokes-orders, which would reduce

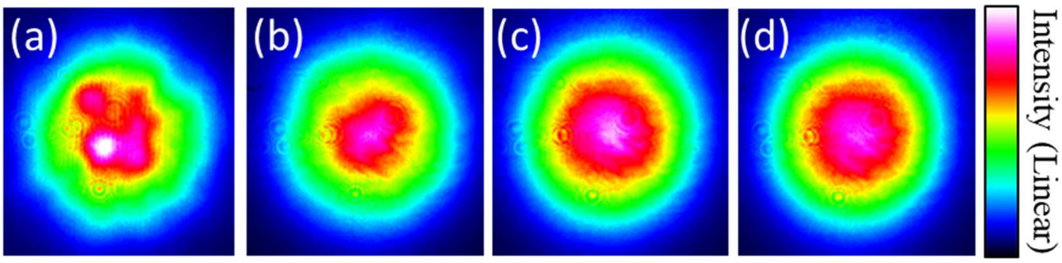

Figure 4.5 Beam images of relative intensity at signal output power of **(a)** 0.3 W, **(b)** 3.5 W, **(c)** 16.3 W, and **(d)** 31.5 W. The intensity is scaled differently in different images.

the power transfer from the pump and effectively clamp the peak power. The fraction of the energy with instantaneous power below half the average power was 15%, 10%, and 4%, and the fraction with instantaneous power below twice the average was 56%, 73%, and 78%. Thus, the power stability increases at higher output power. The random pulsation may be occurring in only some spatial modes. Unfortunately, I cannot check it as the data of temporal traces had no spatial differentiation.

Beam images at four different output powers captured by a silicon CCD camera (Thorlabs BC106N-VIS) with 2 ms exposure time are shown in **Figure 4.5**. Near threshold (**Figure 4.5(a)**), the beam profile is non-circular with significant structure. It was also temporally unstable. This may be because near threshold, only a small subset of the fibre modes is excited through the SRS. At higher pump power, more modes are expected to be excited, and furthermore, the images are averaged over a large number of pulses that are generated in 2 ms, according to **Figure 4.4**. Thus, the beam images became closer to circular, smoother, and temporally stable. The beam quality (M^2) was 6.8 at full power (31.5 W) and 6.1 at 16.3 W (equal in orthogonal directions within ~3%). It could not be measured at lower powers. The beam diameter was measured at the 13.5% intensity-level by a scanning-slit beam analyser on a motorised stage (Thorlabs M2SET-IR). This was controlled by a computer, which also calculated M^2 (Thorlabs Beam Analyzing Software v. 2.3). The M^2-value is markedly lower than the expected ~V/2 = 17.5, if all modes are equally excited.

4.3.3 Simulations

I used simulations to better understand our system. The model is the same as in ref. [2] (**Sect. 2.1.3** and **3.3.3**), except that the effective area was taken to be the same for all wavelengths and the feedback reflectances at both ends were set differently for each wavelength in accordance with the experimental setup.

$$\pm\frac{1}{P_i^{\pm}}\frac{dP_i^{\pm}}{dz} = -\alpha_i + \frac{1}{A_{eff}}\left(\sum_{i>j} g_{R_{ij}}\left(P_j^{+} + P_j^{-}\right) - \sum_{i<j} g_{R_{ij}}\left(\frac{\lambda_j}{\lambda_i}\right)\left(P_j^{+} + P_j^{-}\right)\right), \qquad (4.1)$$

$$with\ i,j = 1,2,3,4,5,6,7$$

The values of parameters used for the simulation are given in **Table 4.2**. The parameter r_{fi} and r_{bi} are the launching end and far end reflectances at λ_i. These values were used also for the simulation curve in **Figure 4.3(a)**. The simulated output power *vs*. fibre length is shown in **Figure 4.6**. The optimum fibre length is 1510 m, where the 2nd Stokes appears. I view this as undesired, but the appearance of the 2nd-Stokes is irrelevant if the total laser output power is the primary objective, or even desired if emission around 1066 nm is the objective. (Although higher-order conversion step does increase the losses, this is captured by the simulations.) The output power at the optimised length is calculated to 68 W and the pump leakage to 8.8 and 10.1 W for 976 and 969 nm, respectively. All other powers were negligible. This suggests that a longer fibre than I had available, or alternatively a higher pump power, can increase the efficiency.

All simulations are CW and I have not tried to analyse the temporal fluctuations and stability of the system. I note that a coupled nonlinear system may lack stable solutions.

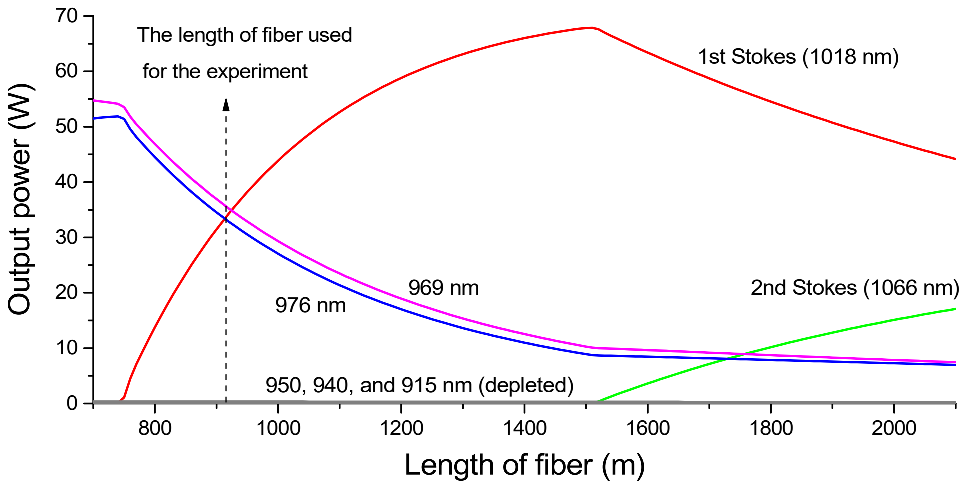

Figure 4.6 Simulated output powers in the far end of the fibre (after DM3) *vs*. fibre length. The power at 915, 940, and 950 nm is negligible.

TABLE 4.2

PARAMETERS FOR SIMULATION

Parameter	Value	Unit	Parameter	Value	Unit
L_f	917	M	A_{eff}	1964	µm^2
λ_1	1066	nm	r_{f1}	0.9	-
λ_2	1018		r_{f2}	0.9	
λ_3	976		r_{f3}	0.04	
λ_4	969		r_{f4}	0.04	
λ_5	950		r_{f5}	0.04	
λ_6	940		r_{f6}	0.04	
λ_7	915		r_{f7}	0.04	
α_1	0.89	dB/km	r_{b1}	0.04	
α_2	1.06		r_{b2}	0.04	
α_3	1.21		r_{b3}	0.04	
α_4	1.27		r_{b4}	0.04	
α_5	1.72		r_{b5}	0.99	
α_6	1.91		r_{b6}	0.99	
α_7	1.43		r_{b7}	0.99	

Raman gain coefficient ($g_{R_{ij}}$) [fm/W]

	$j = 2$	3	4	5	6	7
$i = 1$	$g_{R_{ij}} = 49.0$	4.52	1.99	1.74	1.63	0.74
2		50.2	45.0	3.91	9.13	2.95
3			9.41	28.7	48.5	4.41
4	($g_{R_{ji}} = g_{R_{ij}}$)			18.8	36.4	17.6
5					12.8	51.2
6						32.3

4.4 1.5-km GRIN fibre revisited

The performance with the pure-silica core in **Sect 4.3** reaches a respectable slope efficiency, but it still falls short of the 60% achieved with the telecom GRIN fibre in **Sect. 3.2.2.1** with dual-wavelength pumping. The simulations suggest that a longer silica-core fibre would perform better, but this was not available. Therefore, I decided to test the telecom GRIN fibre also with multi-wavelength pumping. I demonstrate both laser and amplifier made with 1.5-km of the telecom GRIN fibre in this section.

4.4.1 Laser

4.4.1.1 Setup

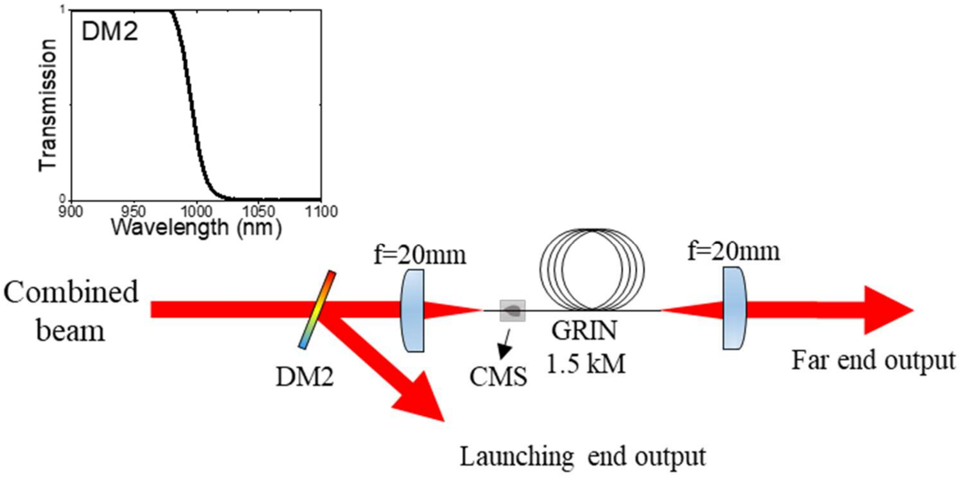

Figure 4.7 Experimental setup of 1.5-km long GRIN fibre laser pumped by five spectrally combined diode lasers.

Figure 4.7 shows the experimental setup of the fibre Raman laser. The Raman gain fibre is a 1.5 km long GRIN fibre, which was introduced in **Sect. 3.2.1.3**. The fibre has a high-index coating which absorbs any power in the cladding. Therefore, a cladding-mode stripper (CMS) at the launch end was used to protect the fibre from being damaged by pump power not coupled into the core. The launched pump powers were 41.3, 61.9, 41.0, 52.1, and 70.9 W for the different wavelengths in descending order. This adds to 267 W of total launched pump power.

The cavity setup is similar to that in **Sect. 4.3.1** except there is no mirror at the far end that adds feedback to both signal and pump. The fibre was normally cleaved on both sides to form a cavity with 4% reflectors at both ends. The output of the laser is double-ended and expected to be symmetric, because of the symmetric feedback in the two ends.

The laser output was characterised by power meters, an optical spectrum analyser, and photo detectors, which are the same equipment as in **Sect. 4.3.1**. The spectra and output power were measured at each power level at both ends. The measured spectra were integrated over different ranges in order to separate the output power into three bands, namely pump, signal (the 1st Stokes), and the 2nd Stokes (i.e., as before). The 3rd and 4th Stokes order were measured and considered in calculations only for the maximum output at the launch end as it is insignificant in other cases. The 3rd and 4th Stokes order were not considered on the far end because the spectra measured on the far end contains the leaked pump which is certainly much bigger than the 3rd and 4th Stokes order. This makes the total integral bigger, therefore, the difference in calculating the power of signal that the 3rd and 4th Stokes order brings becomes negligible even if they are similar size to that of the launching end. Temporal traces are only measured for the launch-end output beam.

4.4.1.2 Results

Figure 4.8(a) shows the leaked pump power, laser output power in the 1st Stokes (i.e., “signal”) in both ends, and the 2nd and higher order Stokes against total launched pump power. **Figure 4.8(b)** shows the optical spectra at three different total laser output powers (16.6, 38.5, and 66.9 W), measured at both ends.

The threshold of the laser was around 75 W (41 W of 976 nm plus 34 W of 969 nm). The signal output power on both sides showed similar output power throughout the different pump levels. The total output power from both ends reached 66.9 W (far end: 34.9 W, launching end: 32.0 W) with an overall slope efficiency of 35%. The initial slope, from the threshold to 100 W of the pump power, records 0.59 which agrees with the result of **Sect. 3.2.2.1**. The 2nd order Stokes appears when the total pump power reaches around 140 W. The total power of the 2nd and higher Stokes orders from both ends was 23.8 W at maximum pump power. This means 90.7 W was converted from 267 W of total launched pump power.

Including the leaked pump, the total output power from both ends is 142 W. This is only 53% of the total launched pump power. Most of the other 47% represents the fibre loss

(**Sect. 3.2.1.3**), whereas the quantum defect in the Raman conversion is only estimated to be around 5%. At the same time, a big fraction of the pump power stays unconverted despite the long fibre. This is because of the early build-up of the higher order Stokes already at relatively low power. Once the power reaches the 2nd Stokes order (or higher), its contribution to the depletion of the pump is weak. (This is discussed more in chapter 5.) These two indications, namely the high background loss and the early build-up of the higher order Stokes, suggest that the fibre was too long.

Figure 4.9(a) shows temporal traces of the signal at different power levels taken at the far end output. It shows a periodic behaviour, which becomes more pronounced as the output power grows. A close-up at maximum output power over two cycles is shown in **Figure 4.9(b)**. The detector is Si-based. The measured trace is dominated by the signal i.e., the 1st Stokes) rather than higher Stokes orders although the sampled beam a mixture of all the wavelengths reflected from DM2 because the responsivity of the detector for the signal is about four times higher than that for the 2nd order Stokes, and the average power of the signal is about three times as large as that of the higher-order Stokes waves.

The output voltage from the detector was recalculated to optical power using the average voltage (1.24 mV) over a long span (2 ms) and the "dark" voltage (-0.3 mV). These were measured to correspond to average optical power of 32 W and 0 W of the launching end output. This is shown as the y-axis on the right side of the plot in **Figure 4.9(b)**. The trace is smoothed by the Savitzky-Golay method with a 300-points (150 ns) of window for better visibility.

The period of a cycle is 18.5 μs. This is comparable to the round trip time of the cavity (14.5 μs) although the difference is not negligible. This may mean that the modulation is not directly related to the round trip except the similarity in the order of magnitude.

The instantaneous peak power reaches 90 W, which was ramped up from the zero in ~ 3.1 μs. Then it drops down to zero over around 10.5 μs of time. During the descent, the trace exhibits sub-peaks, and there is also one sub-peak in the zero-power region 1.6 μs before the trace starts to ramp up to the 90-W main peak again. Unfortunately, the temporal trace from the other end was not taken. However, it is expected that the trace at the other end also has a repetitive cycle with

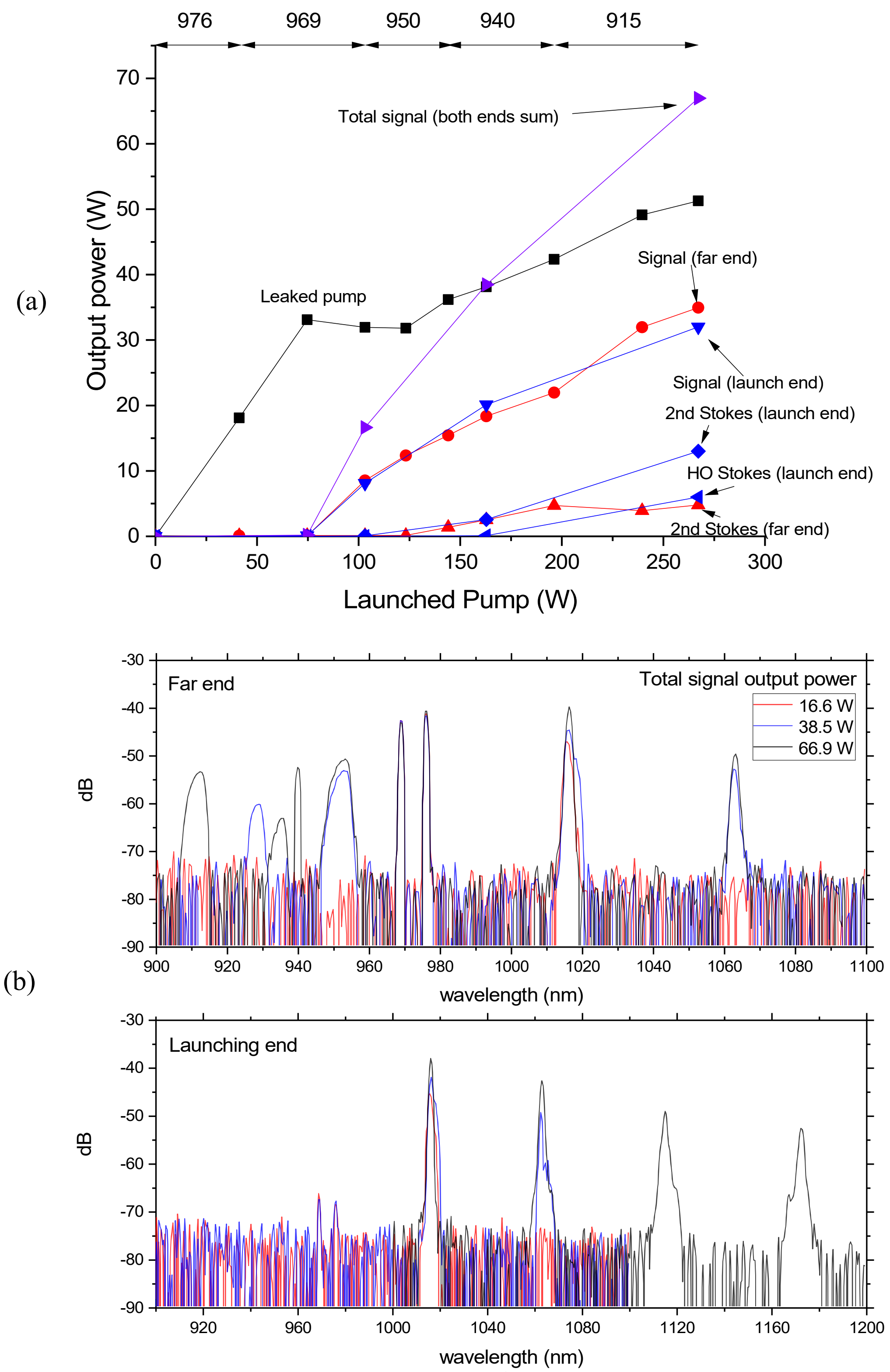

Figure 4.8 (a) Output power of the signal, the 2nd Stokes at the far and launching ends, and the higher order Stokes at the launching end together with the summed signal output from both end and the leaked pump *vs*. total launched pump power with the indication of pump wavelength. **(b)** The optical spectra taken from **(top)** the far end and **(bottom)** the launching end side at the total signal output power of 16.6, 38.5, and 66.9 W.

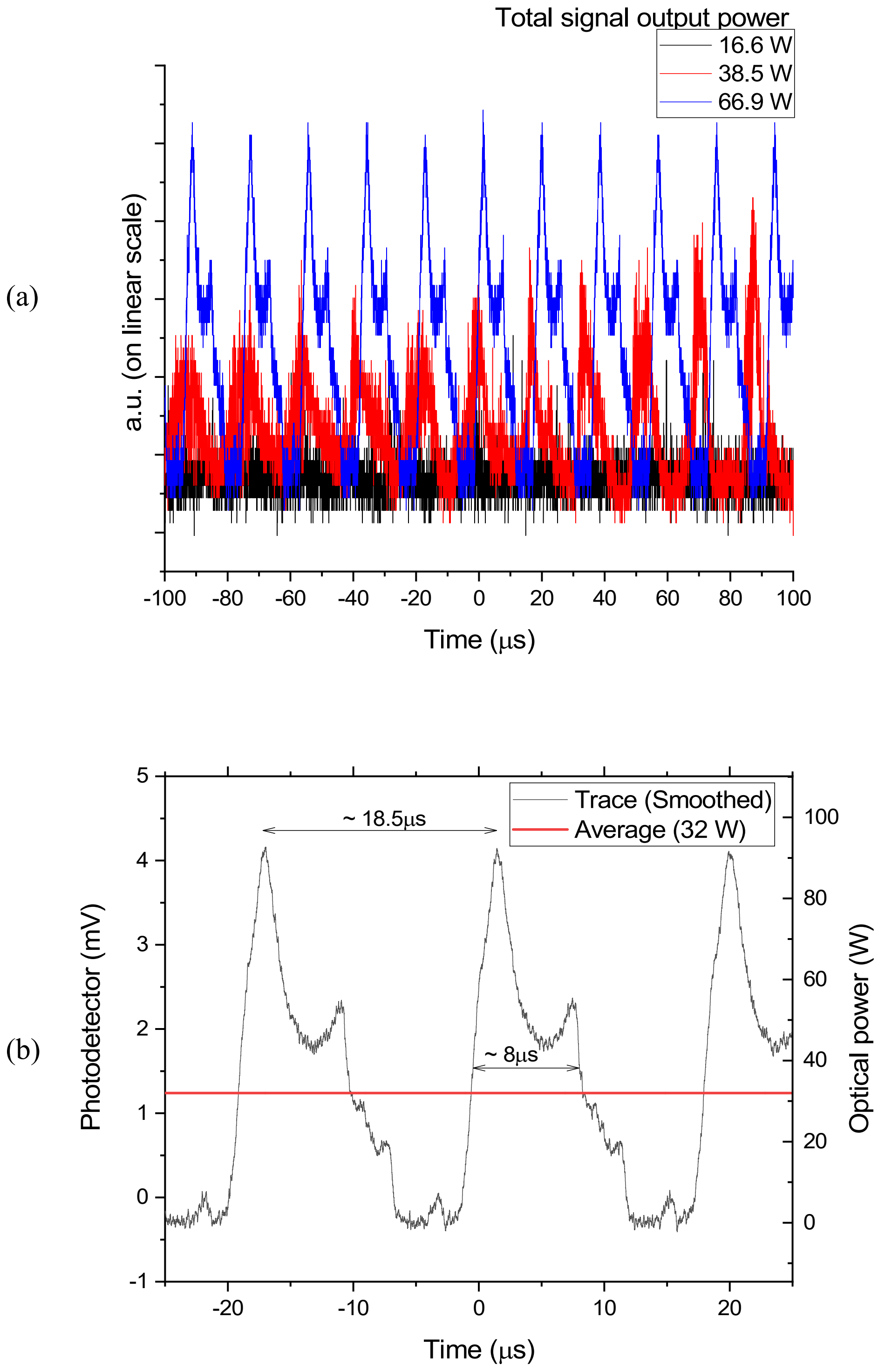

Figure 4.9 (a) Temporal traces over 200-μs spans taken at the launching end output at the total signal power of 16.6, 38.5, and 66.9 W. **(b)** Enlarged temporal trace of the maximum signal output at the launching end that contains two cycles. The instantaneous optical power is indicated by the axis on the right side.

same period, and may have a main peak, as well. The time difference between the main peaks from each end can be an interesting measurement.

The pulsing of the FRL output has been already presented in **Sect. 4.3**. In the present case, however, the CW component does not increase for the higher output power. Instead, the repetition of a certain shape of cycle becomes more regular. While the cause of the pulsing is not clear, one thing that is commonly observed so far is that the pulsing and the higher Stokes orders always emerge together. This is not surprising, as the pulsing leads to higher instantaneous powers, which then drives nonlinearities such as SRS.

Though it is from two ends rather than in a single beam, almost 70 W is reached in total. This is more than twice as much as in the silica-core experiment in **Sect. 4.3** even though the GRIN fibre was longer and lossier. One of the reason for this is the higher launched pump power. In total, 267 W was launched which is an 82-W increase from **Sect. 4.3**. This is made possible by the larger size and NA of the core, which allows more pump power to be launched. Another reason is the higher Raman gain coefficient that promotes the SRS. The germanium content in GRIN fibre increases both the NA and the Raman gain coefficient. On the other hand, the high germanium doping also increases the background loss of the fibre which might outweigh the benefit of a higher Raman gain.

4.4.2 Amplifier

High-power, high-brightness radiation at 0.98 μm is attractive for pumping of erbium and ytterbium. My experience with laser configurations suggested that the shorter-wavelength diode lasers could pump fibre Raman amplification of the 976-nm diode laser. I demonstrated this with single-wavelength pumping at 950 nm in **Sect.3.2**, but the achieved output power was limited. To investigate this with the multi-wavelength pump source, the far end of the 1.5-km telecom GRIN fibre (see **Figure 4.7**) is angle-cleaved to raise the laser threshold and thus prevent lasing. This transformed the laser into an amplifier. The 976-nm diode laser provided the signal seed while the diode lasers at 950, 940, and 915 nm pumped the amplifiers. The 969-nm diode was not used as it would deplete the pumps rather than amplify the signal at 976 nm. The launched power for each wavelength was now 33.9, 41.0, 55.5, and 86.3 W for 976, 950, 940, and 915 nm respectively. The 976-nm power is reduced by 18% whereas those at 940 and 915 nm are 6.5% and 22% higher than before. Output power, spectra, and temporal traces were measured at the far-end output. The relative output power for each band (pump, signal, and the higher order Stokes) were determined by integrating output spectra. The temporal trace (**Figure 4.10(c)**) is a mixture of all the output waves as there was no spectral filtration for the temporal trace measurement.

The pump diodes were turned up in the order of longer to shorter wavelengths. **Figure 4.10(a)** shows the output power vs total launched pump power. The launched 33.9 W of signal power is affected by fibre loss, so in the absence of pumping, the signal output power becomes 18.0 W. From there the signal grows up to 56.5 W and then it reduced down 56.0 W at the maximum pump with the emergence of the 2nd Stokes. Overall, the conversion efficiency was 26% (at the maximum signal output, 56.5 W). The conversion from 940 nm was higher (41%) than from other wavelengths.

Temporal traces in **Figure 4.10(c)** show a random modulation starting at the maximum signal output (ii) and growing stronger for increased pump power (iii). The modulation does not drop below the level (i) where the pump power is ~100 W.

A positive net gain of 2.20 dB was achieved by increasing the number of wavelengths, and thus the pump power, compared to the single-wavelength pumping in **Sect.3.2.2** (but note that the pump was at 950 nm, which is not ideal). If I take away the loss of fibre for the seed (-2.75 dB), the Raman gain is calculated to be 5.95 dB.

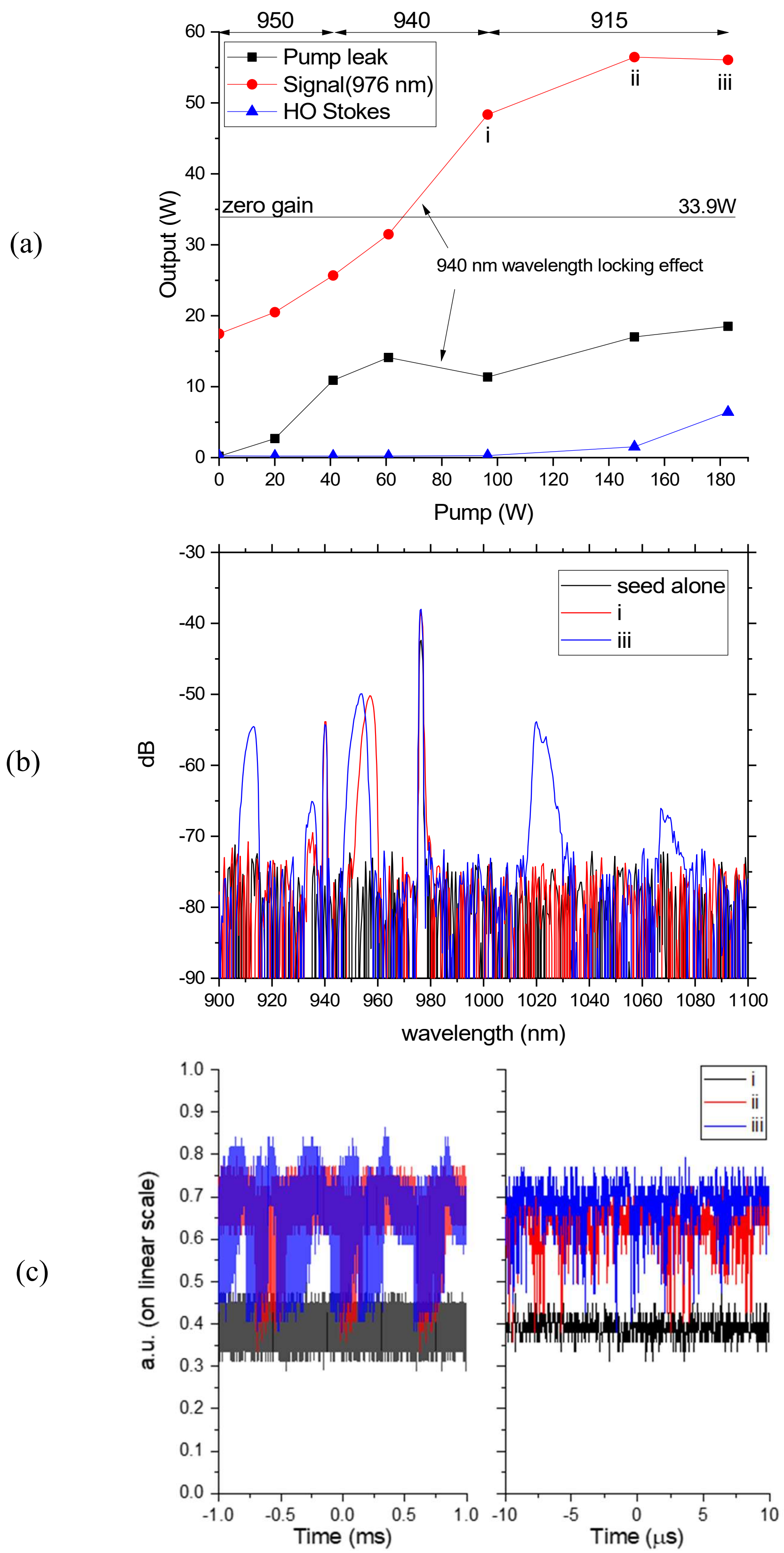

Figure 4.10 (a) Output power of the signal (976 nm), the higher order Stokes (the sum of the 2nd and 3rd Stokes), and the leaked pump *vs.* launched total pump power (power of the individual pump wavelength indicated on the top of the graph). **(b)** Output spectra. **(c)** Temporal trace of span 2 ms and 20 μs. The indicators **(i, ii,** and **iii)** mark the points in **(a)** corresponding to the spectra and temporal traces in **(b)** and **(c)** .

4.5 High germanium fibre Raman laser

As discussed briefly at the end of the **Sect. 4.4.1**, the experiment benefits from the GRIN fibre's higher germanium concentration. This gives a higher Raman gain coefficient as well as a higher refractive index that increases the NA, which in turn makes it possible to launch more pump power into the fibre for the same core area. This increases the pump intensity and thus the Raman gain. Therefore, it is desirable to try an even higher germanium concentration and NA, as long as the background loss remains sufficiently low.

Luckily, I had a chance to collaborate with a fibre fabricator, Jaesun Kim at Taihan Fiber Optics, and ask for a custom-made high-germanium fibre. This section presents results obtained with the resulting fibre.

4.5.1 Setup

4.5.1.1 QCW operation

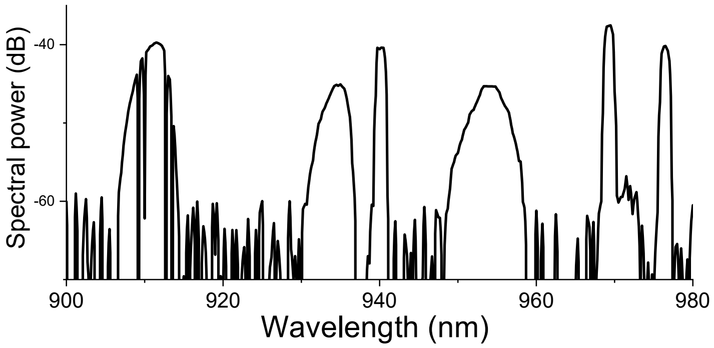

Figure 4.11 Spectrum of spectrally combined pump beam at maximum pump power.

The same wavelength-combined pump beam introduced in **Sect. 4.2**. was used for this experiment. Thus, the pump consists of five wavelength-combined diode lasers at 976, 969, 950, 940, and 915 nm. However, in this experiment, the drive currents of the pump diode lasers are modulated in a quasi-continuous wave (QCW) form. This decreased the average power due to the low duty cycle and reduced not only the thermal stress in optics which degrades the optical alignments and pump launching efficiency but also the heating of the diodes, which leads to wavelength drifts in the diode lasers. The change to QCW operation induced a minor shift of peak wavelengths of non-wavelength-locked diodes and thus their respective powers within the combined beam also changed from the set up in **Sect. 4.2** (the subset of **Figure 4.1**). The new spectrum of the combined pump when driven QCW at maximum power is shown in **Figure 4.11**.

The repetition rate and the duty cycle of the current modulation of diodes were set to 1 kHz and 10%. The average 20%-80% rise and fall time of the output power from the five diodes at their maximum power is measured to 11 and 7.9 µs, respectively. The synchronisation among the generated pulses from the different diode lasers was kept within ~10 µs.

The maximum average powers at the different wavelengths of the diode lasers measured in the combined beam were 5.94, 11.4, 7.50, 10.0, and 14.3 W in the descending order of wavelength. This combined beam was, then, steered to the FRL cavity. Before being launched into the Raman gain fibre (RGF), the pump beam passed through a dichroic mirror (DM2) which transmits 98% of the power of the combined pump beam and reflects > 97% of the signal. Then, the beam was focused into the core of RGF by an aspheric lens with 20-mm focal length.

4.5.1.2 Cavity

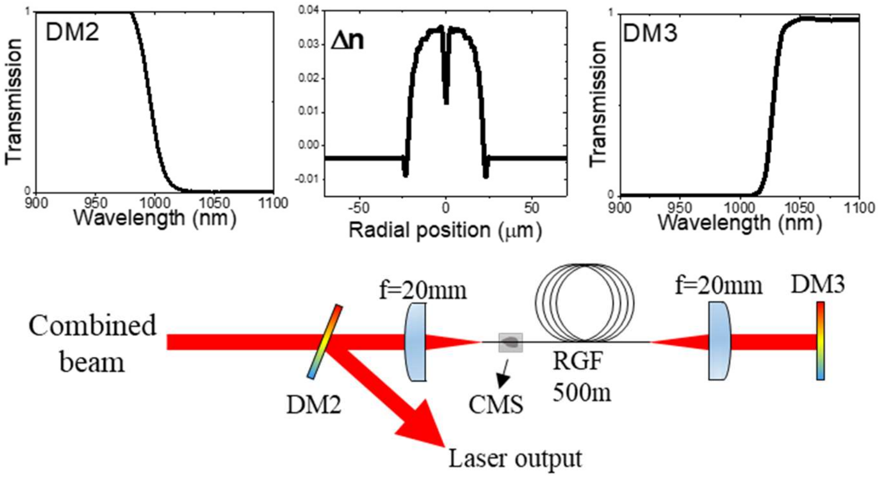

Figure 4.12 Setup of the FRL cavity. The insets show the transmittance of DM2 and DM3 as well as the refractive index profile of the RGF.

The RGF was designed for core pumping. It was fabricated by Taihan Fiber Optics co., Ltd. It has a germanium-doped core that is surrounded by a silica cladding. The diameters of the core and the cladding varies from 39.4 / 141.4 μm (core /cladding, at the top of the bobbin) to 44.1 / 145.0 μm (bottom of bobbin). The length is 500 m and the numerical aperture of the core is 0.34. The refractive index profile is shown in **Figure 4.12**. The fibre has a polymer coating with refractive index lower than that of the cladding. Thus, the cladding guides light, which helps to avoid coating-damage caused by light escaping from the core. However, although some pump light is likely to propagate in the cladding, its intensity is too low to lead to any significant Raman gain.

Since the Ge-concentration is higher than in the telecom GRIN fibre, the Raman gain coefficient and the background loss are expected to be higher, too. The background loss of the core at the wavelengths of our interest (1063, 1016, 976, 969, 950, 940, and 915 nm) are measured to 2.19, 2.98, 3.76, 4.55, 4.91, 5.14, and 4.71 dB/km, respectively. This was done by white-light transmission measurements with a cut-back of (nearly) the full length of the fibre. This is close to the lowest loss level that can be found in the world, for fibres with a germanium concentration of 30% (mol) [3].

For laser experiments, both ends of the fibre were normally cleaved and a clad-mode stripper (CMS) was applied 1 m from the launching end of the RGF to make the core launch alignment easier.

The average pump powers launched into the core were estimated to 2.99, 5.71, 3.43, 5.02, and 5.78 W, based on the transmitted power and the background loss. The launching efficiencies were 50%, 50%, 46%, 50%, and 40% for the individual pumps in descending wavelength order.

At the far end of the fibre, there is another lens which collimates the output light. This is followed by a dichroic mirror (DM3) at normal angle of incidence in order to reflect the signal and the pumps back into the RGF, after they are refocused in the lens. The transmittance of DM3 is 2.5% and 97% at 1016 and 1063 nm, respectively. These are the wavelengths of the 1st Stokes (i.e., the signal) and the 2nd Stokes, therefore DM3 serves as a high reflector at the far end of the cavity for the signal but not for the higher-order Stokes. This suppresses the higher-order Stokes. The reflectance of DM3 at the pump wavelengths is higher than 99.9%. Although the direct measurement could not be made, I estimate the overall feedback efficiency at the far end to be near unity, seeing that lasing threshold increases by 28.8 W when the pump was prevented from being double-passed by an extra dichroic mirror placed at a certain angle, while the leaked pump power was 30 W. At the launching end of the cavity, the normally cleaved facet served as a 4%-reflecting output coupler. Thus, the generated signal is out-coupled at the launch end and reflected out from the pump beam path by DM2.

The output beam was then sampled by a wedged window. This leads to two reflected beams, each carrying ~4% of the out-coupled power. These were used for measuring spectra and temporal traces, while the transmitted beam (~92%) was used for measuring the optical power. The optical spectrum analyser (ANDO AQ-6315) was triggered to capture the output beam 30 μs before the trailing edge of the pump pulses. Temporal traces were measured by a 350-MHz biased silicon photodetector (Thorlabs, DET10A) which was connected to a 200-MHz oscilloscope (DSO X2022A, Agilent). The temporal traces of the incident pump were measured in the beam reflected in DM2 with the same photodetector.

4.5.2 Calibration of instantaneous power

Calibration of the peak power of both pump and signal was needed due to the pulse shape with QCW modulation. The optical pulses were not perfectly “square” and the rise and fall time were relatively long. For example, the peak power, which is expected to be ten times of the average power at 10% of duty cycle, differed by between -5.6% and +16.2% from the expected value at different pump wavelengths. Furthermore, the signal pulses were shorter than the pump pulses because of temporal offsets between pump pulses at different wavelengths.

The calibration was done by comparing the measured optical average power to the temporal trace which was measured by a photo detector. The voltage levels of all data points in the temporal trace of one period were averaged at the different power levels. Then, a graph of the average (optical) power *vs*. the average voltage level was plotted and linearly fitted to find calibration coefficients for converting voltage to optical power. The power levels were then read out from the individual temporal traces where the curve stabilises after the initial spike. See **Figure 4.14(a)**. The validity of this calibration depends on the assumption that the linearity of the photo detector is adequate and that the fraction of the power that reaches the detector stays the same during a cycle.

The time interval when there is no optical power in the cavity is not of interest. Thus, hereafter, the powers presented in this section (**Sect. 4.5**) means the average power in the duration that the pulse is effectively on unless noted otherwise.

The pulse-on powers of the launched pumps were determined to 28.2, 52.9, 35.0, 58.4, and 59.8 W, in descending wavelength order, for a total of 234 W.

4.5.3 Results

For pumping, I turned up the diode lasers in the order of 976, 969, 950, 940, and 915 nm. **Figure 4.13(a)** shows the signal output power and the corresponding simulations *vs.* the total launched pump power. The same model as in **Sect. 4.3.3** was used for the simulations in **Figure 4.13(a)**, with fibre parameters corresponding to the new fibre.

The laser threshold was reached with full power at 976 nm and a third of the full power at 969 nm, for a total of 43.7 W. The output power grew up to 101 W as the pump power was increased with the overall slope efficiency of 65%. The conversion efficiency at this point is 50%. The slopes for individual pump wavelengths were 93%, 57%, and 60% for 969, 950, and 940 nm pump respectively. The slope for the 915-nm pump was unclear because the signal started to oscillate rapidly. This made it difficult to determine the peak power. Also, cascaded SRS beyond the first Stokes was observed when oscillations appeared.

To investigate what causes the oscillation as well as to verify that the 915 nm pump can be converted into signal, I reduced the pump powers of the other four wavelengths to approximately 80% of their maximum. This is also plotted in **Figure 4.13 (a)** (curve with pink square dots). The slope efficiency for the 915-nm pump was 36%, while the oscillation was suppressed. This suggests that the oscillation is related to high signal power, *e.g.*, as a result of pump depletion or higher-order Stokes generation.

The signal traces in **Figure 4.14(a)** show delayed responses relative to the pump traces in **Figure 4.14 (b)**. Although I have not verified it, I tentatively conclude that the cavity build-up and the time for all diodes to turn up delays it. That can explain why the delay is bigger at low power. When the pumping is just above threshold, all diodes need to reach their set output power (*e.g.*, the black curves in **Figure 4.14**) for lasing to commence.

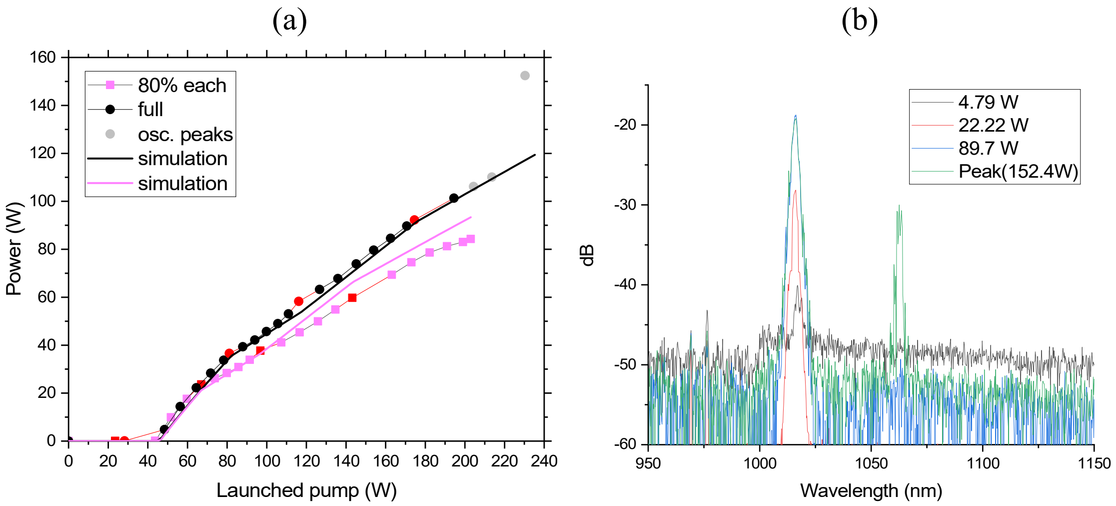

Figure 4.13 (a) Experimental signal output power and that of corresponding simulations vs. total launched pump power for case 1: the power of each pump diode turned fully up in succession, and case 2: the power of the first four pumps turned up to 80% of their maximum power in succession, after which the 915-nm pump is turned up fully, to allow the 915-nm pump to contribute to the conversion before oscillations appear. Red data points are where the pump wavelength changes. **(b)** signal output spectra at the signal power of 4.79, 22.2, 89.7, and 152.4 W (the last one is the oscillation peak).

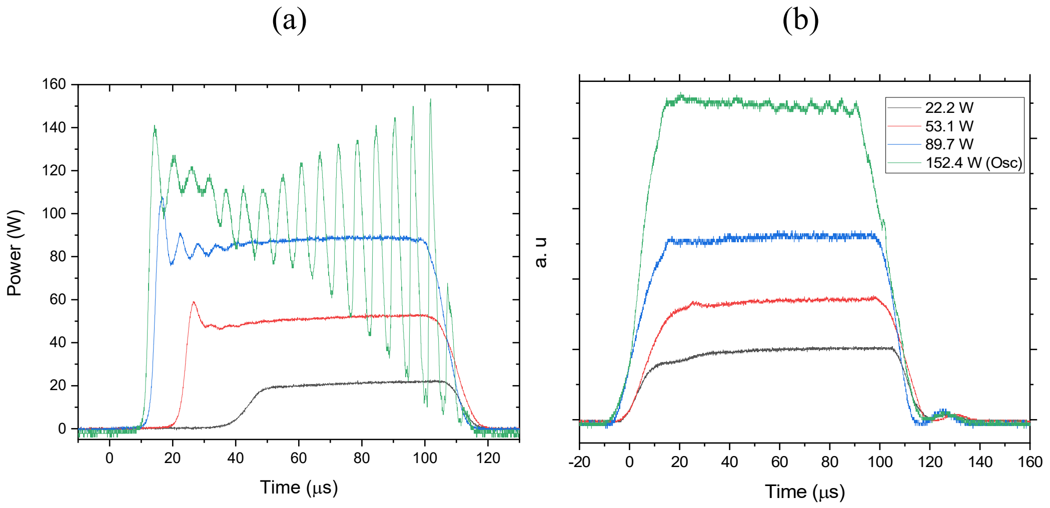

Figure 4.14 (a) Temporal traces of the signal and **(b)** temporal traces of the pump at the signal power of 4.79, 22.2, 89.7, and 152.4 W (the last one is the oscillation peak). For the pump traces, the incident pump beam as reflected by DM2 was measured. Since the launching efficiency is different for different wavelengths, the absolute size of the pump trace is not proportional to the launched pump power.

Also, the green curve of **Figure 4.14(b)** suggests that the strong oscillation of the signal feeds back to the pump diode.

The pattern of the temporal signal traces evolved through several stages as the pump power increased. First, the signal trace takes after the pump trace when the power of the signal is small compared to the total pump power. Secondly, when the signal power reaches 40 W (about half the total pump power), the trace exhibits an initial spike that will deplete the pump for a short time. It then relaxes to a stable state. At still-higher power, the relaxation time becomes longer and starts to show an oscillation that decays within 30 μs. Lastly, the oscillation grows instead of decaying when the signal power exceeds 100 W. The period of oscillation was ~5.8 μs, which is similar to the cavity roundtrip time.

The spectra in **Figure 4.13 (b)** show that 1st-order (signal) and 2nd-order Stokes were at 1016 and 1063 nm. The spectrum of the 2nd Stokes looks jagged because it was oscillating more strongly than the signal. Notwithstanding the oscillation, the average power of the 2nd order Stokes remains insignificant but is about to grow. (~10 dB lower than the signal in terms of the spectral power at the maximum pump power) This indicates that the length of fibre is near the optimum.

Since the higher order Stokes wave was not spectrally filtered out from the output beam, the temporal traces shown in **Figure 4.14** include not only signal but also any higher order Stokes. Moreover, their summed optical power does not correspond directly to the voltage trace because the responsivities of the silicon detector at the signal and higher order Stokes wavelengths are different. The responsivity of the photodetector is around four times larger at the 1st-Stokes signal wavelength (1016 nm) than at the 2nd-Stokes wavelength (1063 nm). Thus, the actual optical power (summed) is bigger than the power determined by a calibration at 1016 nm because the optical power at 1063 nm will be represented by a voltage corresponding to one fourth of its actual power. In addition, the power in higher order Stokes is estimated to be less than 5% of the signal power from the spectrum shown in **Figure 4.13(b)** even at maximum pumping. Therefore, it is safe to say that the traces in **Figure 4.14** are mostly of signal.

The beam quality (M^2) was measured to 7.5, 10.9, and 11.6 at the output powers of 14, 58, and 92 W, respectively. **Table 4.3** summarises the brightness of the signal and pump and the brightness enhancement factor at three output powers. The beam quality factor (M^2) of the launched pump is 22 under the assumption that all the modes in the fibre are equally excited. The brightness enhancement factor decrease from 1.92 to 1.70 near the maximum output power as the beam quality degrades.

TABLE 4.3

BRIGHTNESS ENHANCEMENT

Launched pump power [W]	Signal output power [W]	Conversion efficiency	Measured signal beam quality (M^2)	Brightness of signal (B_s)$^{(1)}$ [$W \cdot sr^{-1} \cdot \mu m^{-2}$]	Brightness of pump (B_P)$^{(2)}$ [$W \cdot sr^{-1} \cdot \mu m^{-2}$]	Brightness enhancement (B_s / B_P)
58	14	24%	7.5	0.24	0.13	1.92
120	58	48%	10.9	0.47	0.26	1.82
180	92	51%	11.6	0.66	0.39	1.70

(1) Calculated with the measured beam quality.

(2) Calculated under the assumption that all the modes in the fibre are equally excited.

4.6 Comparison of three fibres as Raman gain fibre

TABLE 4.4
THREE FRLS SUMMARY

	unit	Pure-silica core fibre	GRIN fibre	High-germanium fibre
Germanium concentration(1)	mol%	0	18.5	30
Length (L)	m	917	1500	500
Loss at 976 nm (α_{976})	dB/km	1.25	1.7	3.76
L × α_{976}	dB	1.15	2.55	1.88
Core diameter	µm	50	62.5	40
NA		0.227	0.275	0.34
BPP	mm×mrad	5.7	8.6	6.8
Peak g_R @ 1um	$\times 10^{-13}$ m/W	0.5	1.19	1.7
FoM(2)	$\times 10^{-12}$ $m^2/(W \bullet dB)$	2.06	5.29	5.23
Launched pump power (P_L)	W	185	269	234
P_L/BPP^2	W/(mm×mrad)	5.74	3.64	5.06
Pump intensity(3)	W/µm^2	0.094	0.088	0.186
Max signal output power	W	31.5	66.9	101
Conversion eff.		17%	25%	50%
BE factor(4)		1.20	-	1.70

(1) Estimated from NA
(2) Figure of merit (FoM) is calculated by $NA^2 \times g_R/\alpha_{976}$
(3) Assuming the intensity profile is flat in the core. (or, averaged intensity)
(4) At maximum signal output power. Assuming the launched pump equally excited all supported modes in the RGF. Unfortunately, brightness enhancement (BE) factor for the GRIN fibre experiment is missing as the beam quality data of signal is missing.

Table 4.4 summarises the results of three FRLs and the key specifications of each Raman gain fibre. Although the experiments (e.g., the fibre length) should be optimised to allow for accurate comparisons, **Table 4.4** still gives good insight.

What stands out for the high-germanium fibre is the pump intensity, which is almost double that of the other two fibres. Its high NA made it possible to launch power similar to, or more than, that of the other fibres, while the smaller core area enhances the pump intensity which directly boosts the SRS (**Eq. (2.1)**). In addition, the higher concentration of germanium increases the Raman gain. Therefore, it showed the best efficiency with the shortest length.

In addition to the fibre, the attained performance depends also on the details of the optical setup and the alignment. Here, the launched pump power (P_L) divided by the square of beam product parameter (BPP^2) can indicate how successful the pump-launching is, given the BPP of the different fibres, because the square of the BPP of the fibre is proportional to the maximum pump power that can be launched into the fibre when the fibre is overfilled. (*i.e.*, when the BPP of the beam is bigger than that of the fibre.) According to this launching factor (P_L/BPP^2), the launching into the GRIN fibre may seem the poorest. However, it is not so obvious because its refractive index is graded, which brings down the effective NA for all the area within the core. (*e.g.*, in a geometric ray-like picture, the edge of the core would not be able to capture light incident at an angle corresponding to an NA 0.275) Furthermore, a GRIN fibre's parabolic refractive-index profile leads to higher intensity at the centre, which can promote SRS into the lower signal modes and thus improve the beam quality as discussed and assumed for the simulation in **Sect. 3.3.3**.

On the other hand, the pure-silica core FRL, which has a similar pump intensity, has no effects brought about by germanium. Thus, it needs larger length to reach the optimum. This induces more loss. Therefore, even at the optimised length, the output power suffers, and the simulation showed only 68 W in **Sect. 4.3.3**. On the other hand, multiwavelength-pumping should benefit from the SRS linewidth of pure silica, which is larger than that with Ge-doping.

The brightness enhancement (BE) factor is also found to be higher in high-germanium fibre than in pure-silica core fibre. However, the high-germanium fibre appears to be closer to the optimised length than the pure-silica fibre. If the output power of the pure-silica fibre can double as the simulation predicted, it will also double the BE factor making it higher than that of the high-germanium fibre. Meanwhile, the BE factor of the GRIN fibre could have been the best out of three because GRIN fibre is known for its beam clean-up effect [4]. Also, the BE factor of GRIN in **Sect.3.3**, which was ~3, is higher than both pure-silica and high-germanium fibres.

Currently, the record value of BE factor among diode-laser-pumped fibre Raman lasers is 73. This is thanks to the mode-selective feedback that was achieved by special fibre Bragg gratings (FBGs) that were directly inscribed in a GRIN fibre near the fibre axis by a femtosecond laser [5].

Brightness enhancement should involve some kind of intermodal interaction. Thus, a BE factor larger than one is only possible in either multimode fibre (for core pumping) or clad-pumping. (A core-pumped single mode fibre does not allow for a BE factor larger than one even if the conversion efficiency is 100%.) A BE factor of around 2000 was suggested to the maximum value in a cladding-pumped fibre Raman amplifier [6] This was determined from the limit set by higher-order Stokes generation under the assumption that this cannot be (or is not) suppressed by distributed filtering along the length of the fibre. Therefore, the BE factor of 1.2 - 3 in my experiments are a rather unexpected positive result for the cases of core-pumping without any pre-consideration for BE.

4.7 Temporal modulation and 2nd order Stokes

Unintended temporal modulation ("self-modulation") of the signal, either periodic or (seemingly) random, was repeatedly observed in the lasers which exhibited 2nd-order Stokes generation. Studies of the dynamics of fibre Raman lasers with multiple Stokes orders can be found also in ref. [7], [8].

When the conversion self-modulates, higher Stokes orders are more likely to be generated as the instantaneous peak power is much higher than the average power. (For example, in **Figure 4.4**, the peak power is hundreds of times higher than the average power.) A possible mechanism is that the 2nd Stokes depletes the signal. This reduces the pump depletion so that more energy remains in the pump, which then increases the signal gain so that a 1st-Stokes signal pulse can build up. In turn, the high signal peak power leads to 2nd-order SRS, whereby the cycle repeats. Such oscillations are more likely to occur when there are counter-propagating waves so that the time-of-flight introduces a delay in the conversion process.

It is unclear which of temporal modulation and 2nd Stokes starts first. It could be the pump power that is accumulated lengthwise within the cavity that produces an initial spike of the signal that initiates the process. This initial spike is shown in numerical simulations [7]. However, the initial spike is expected to be smaller in experiments because of the slow switching-on of the pump. It took tens of microseconds (several round-trip times) even with the relatively fast driver I have used for the high-power diodes. Hence, the gain for the initial signal is always same as the laser threshold regardless of the targeted pump power.

The modulation may relax in short time (a few tens of cavity round trip time) converging to a stable solution as in ref. [8] in numerical simulation but in most of the real experiments presented in this thesis (except for the signal output up to 100 W in **Sect.4.5**) and in ref. [8], it was chaotic or periodic. On a side note, the oscillation of signals in ref. [8] shows some similarity to that in **Sect.4.4.1** (**Figure 4.9(b)**), including the discrepancy between the cavity round trip time and the oscillation period.

Separately monitoring the temporal traces of the different Stokes orders (pump, signal, and the 2nd order) as in ref. [8] will give a better picture and understanding of the dynamics in these configurations, including in the initial period of time when the pump is switched on.

Seeing from the fact that even the numerical model, which excludes any unknown parameters that can be added in real experiments, can simulate self-oscillation, I tentatively conclude that they are inevitably caused by an intrinsic instability in the basic equations describing the interactions among the different wavelengths and modes.

4.8 Summary

FRLs with three different fibres were built and tested – namely with fibres with pure-silica step-index core, high-germanium GRIN core, and high-germanium quasi-step-index core. These reached 31.5, 66.9, and 101 W of output power, respectively. From this, I conclude that the effects of higher germanium concentration, such as higher NA and higher Raman gain, facilitate higher output power as long as the background loss is sufficiently low. The results were also discussed in terms of brightness enhancement (BE). The BE factor higher than unity for core-pumping without any pre-consideration of BE is an unexpected positive result. Here it should be noted that the theoretically suggested maximum BE-value of 2000 and the experimental record value of 73 are achieved with a modal restriction such as cladding-pumping or mode-selective feedback.

A FRA with a 1.5-km-long GRIN was revisited and a higher gain (+2.20dB) than in **Sect.3.2.3.2** is achieved, thanks to the higher pump power made possible through multi-wavelength pumping.

The temporal behaviour was also discussed. Although there is not enough data for a robust analysis of the causes of the instabilities observed in experiments and simulations, or how it persists in time, I tentatively conclude that they are inevitably caused by an intrinsic instability in the basic equations describing the interactions among the different wavelengths and modes, rather than by, e.g., unstable pumping. Separately monitoring temporal traces from different spatial modes and different Stokes orders will help with the analysis and identification of the cause of the temporal modulation.

4.9 References

[1] S. Hong, Y. Feng, and J. Nilsson, “Wide-Span Multi-Wavelength High-Power Diode-Laser Pumping of Fiber Raman Laser,” *IEEE Photonics Technol. Lett.*, vol. 31, no. 24, pp. 1995–1998, 2019, doi: 10.1109/LPT.2019.2953195.

[2] S. Hong, Y. Feng, and J. Nilsson, “Off-Peak Dual-Wavelength Multimode Diode-Laser- Pumped Fiber Raman Laser,” *IEEE Photonics Technol. Lett.*, vol. 30, no. 18, pp. 1625–1628, 2018, doi: 10.1109/LPT.2018.2863559.

[3] E. M. Dianov, “Advances in Raman fibers,” *J. Light. Technol.*, vol. 20, no. 8, pp. 1457–1462, Aug. 2002, doi: 10.1109/JLT.2002.800263.

[4] K. Krupa *et al.*, “Spatial beam self-cleaning in multimode fiber,” *Nat. Photonics*, vol. 11, no. 4, pp. 3–8, 2016, doi: 10.1038/nphoton.2017.32.

[5] A. G. Kuznetsov, S. I. Kablukov, E. V. Podivilov, and S. A. Babin, “Brightness enhancement and beam profiles in an LD-pumped graded-index fiber Raman laser,” OSA Contin., vol. 4, no. 3, p. 1034, 2021, doi: 10.1364/osac.421985.

[6] J. Ji, C. A. Codemard, J. K. Sahu, and J. Nilsson, “Design, performance, and limitations of fibers for cladding-pumped Raman lasers,” Opt. Fiber Technol., vol. 16, no. 6, pp. 428–441, Dec. 2010, doi: 10.1016/j.yofte.2010.09.011.

[7] B. Burgoyne, N. Godbout, and S. Lacroix, “Transient regime in a nth-order cascaded CW Raman fiber laser,” Opt. Express, vol. 12, no. 6, p. 1019, 2004, doi: 10.1364/opex.12.001019.

[8] P. Suret, N. Y. Joly, G. Mélin, and S. Randoux, “Self-oscillations in a cascaded Raman laser made with a highly nonlinear photonic crystal fiber,” Opt. Express, vol. 16, no. 15, p. 11237, 2008, doi: 10.1364/oe.16.011237.

Chapter 5: Numerical Simulation on Multi-Wavelength Pumping of Double Clad Fibre Raman Amplifiers

5.1 Introduction

For power-scaling of fibre Raman sources, pumping with multimode laser diodes has recently been demonstrated, of multimode as well as double-clad fibres [1],[2]. This approach combines the well-established and well-controlled fabrication, the potentially high resilience to photodarkening, and the high damage threshold, of "passive" high-silica fibres (e.g., germanosilicate fibres) with the simplicity of high-power direct-diode-laser pumping, the brightness enhancement enabled by double-clad fibres, and the advantages of SRS such as wavelength-agility, immunity to high-energy self-Q-switching, and non-local gain saturation [3]. However, SRS is a relatively weak process so high diode brightness and pump intensity is required to reach sufficient Raman gain. This can be analysed in terms of a figure of merit (FoM), given by the induced peak Raman gain relative to the background loss, i.e., $I_P\, g_R\, (\nu_{peak}) / \alpha$, where I_P is the pump intensity, $g_R\, (\nu)$ is the Raman gain coefficient, ν_{peak} is the frequency shift to the Raman gain peak, and α is the fibre background loss, which for simplicity is sometimes assumed to be the same for pump and signal. It was found that a value of the FoM of at least five [1] was needed for efficient conversion in an ideal cavity, whereas a higher value would be required in laser cavities and amplifiers with high gain or excess loss beyond the propagation loss. Today's continuous-wave (CW) diode lasers can provide 140 – 200 W of output power at 0.9 – 1 µm from a 105-µm core pigtail at an NA of 0.15. In combination with a low-loss fibre with a low-Ge-concentration core (e.g., NA < 0.1) and a pure-silica inner-cladding with NA of 0.3 and thus inner-cladding diameter of 52.5 µm to accommodate the pump, this allows for a figure-of-merit of around 10, which is adequate for efficient conversion. There is however an additional requirement for efficient conversion in cladding-pumped fibre Raman sources (including amplifiers). The inner-cladding / core area ratio must not exceed approximately eight, insofar as cascaded SRS to higher Raman orders is to be avoided [4]. An inner-cladding diameter of 52.5 µm thus requires a core diameter of at least 18.6 μm. Larger cores and thus inner claddings are possible, but make it increasingly difficult to maintain single-mode operation. Thus, the standard power-scaling approach of an increasing number of pump ports on a pump combiner with an increasingly large common port to reach targeted power is limited by the limited brightness of diode-laser pump sources and the limited core size for single-mode operation. I note also that a pump combiner degrades the pump brightness [5]. This may render the brightness inadequate even with state-of-the-art multimode diode lasers. An alternative route to further power-scaling is then to use a brighter pump source, e.g., a Yb-doped fibre laser, which excels in this regard [6]. Another potential route to high-brightness pumping is to spectrally combine diode lasers at different wavelengths. Such diode laser sources are pursued vigorously for direct-diode materials processing [7]–[9]. This makes spectrally combined diode lasers attractive candidates for cladding-pumping of fibre Raman sources, which retains the attractions of pumping directly with diode lasers.

However, the pump acceptance bandwidth of SRS in high-silica fibres is limited to the Raman linewidth of ~5 THz (~15 nm at 1 μm) in the conventional case of first-order Raman conversion with high Raman gain coefficient g_R, i.e., when the pump wavelength is separated from the Stokes wavelength by approximately the peak Raman shift ν_{peak}. This is around 12 – 15 THz in silica, corresponding to 400 – 500 cm^{-1} or ~ 40 – 50 nm at 1 μm. Pumping with any single wavelength within the pump acceptance bandwidth is expected to allow for efficient operation of a high-silica fibre Raman device. Likewise, pumping with spectrally combined pump lasers with a wavelength span below 15 nm is expected to behave similarly as single-wavelength pumping, with similar efficiency. However, the 15-nm pump acceptance bandwidth for (effectively) single-wavelength pumping is much smaller than the wavelength-range of spectrally combined diode laser sources for materials processing. This is largely determined by the wavelength range over which diode lasers perform best, and may be 50 - 100 nm. Interestingly, however, high-efficiency pumping over a wavelength range exceeding the 15-nm Raman linewidth has been demonstrated recently, through pumping on several Raman orders [10] (i.e., with 400 – 500 cm^{-1} pump separation) as well as through dual-wavelength pumping with 26-nm wavelength separation. Interestingly, the 26-nm separation is significantly larger than the Raman linewidth but still different from the peak Raman shift [11] (**Sect. 3.3**). Though the 26-nm span is still smaller than that of many spectrally combined diode lasers, these results still suggest there may be considerable potential for pumping at multiple wavelengths over spans exceeding the Raman peak shift, even at off-resonance wavelengths which are not necessarily carefully selected and do not correspond to the Raman peak shift, or multiples thereof.

Section 5.2 presents a numerical simulation of a FRA with an area ratio of eight pumped by discrete multiple wavelengths of fixed and optimised spacings for realistic fibre parameters (e.g., diameter of core and clad and background loss). A FoM at each individual pump wavelength of up to 80 is considered although FoM exceeding 10 may be unrealistic with contemporary state-of-art diode lasers. It is also possible to evaluate the FoM of the wavelength-combined pump as the sum of the FoMs at the individual wavelengths, but, I always mean that of a single wavelength. The conversion efficiency and acceptable pump bandwidth are extensively examined for up to 10 discrete pump wavelengths of the same power, for fixed as well as optimised wavelength spacings. This work was published in ref. [12]. Although this work was started by the first author, Zhao, the major contributions I made to this work justifies its inclusion in my thesis.

In **section 5.3**, a theoretical lossless fibre (thus, with infinite FoM) is considered, to investigate limits of this approach in terms of total pump wavelength span, wavelength spacing, and area ratio. With infinite FoM, the absolute power and fibre length are irrelevant, so the results only depend on initial power distribution of the pump wavelengths. Then lastly, I estimate the loss in conversion efficiency at optimised fibre lengths for some selected realistic conditions.

5.2 Raman fibre amplifier pumped by discrete multiple wavelengths with fixed and optimised spacings

In this section, I present simulation results of multi-wavelength cladding-pumping in the 0.9 – 1 μm wavelength range of a high-power fibre Raman amplifier (FRA) in the continuous-wave regime, with fixed and optimised pump wavelength spacings of 5 – 30 nm. I use a signal in the 1st Stokes order of the longest-wavelength pump and reach up to 71% power conversion efficiency (PCE) with narrow optimised pump wavelength spacing at a FoM of 10 at each pump wavelength (200 W per pump wavelength). The

PCE remains above 68% for up to ten pump wavelengths. Furthermore, for all considered FoMs (between 10 and 80), the PCE can be higher with two pump wavelengths, and often with more than two, than with only one pump wavelength. Depending on the value of the FoM, the PCE can remain higher than with a single pump laser up to a span of 100 nm. These simulations confirm the potential for multi-wavelength diode-laser off-resonance pumping with total pump bandwidth significantly larger than the Raman linewidth for further power scaling and improved efficiency of diode-laser-pumped fibre Raman sources. Notably, this applies to important multi-kW spectrally combined diode-laser sources in rapid development for direct-diode materials processing.

5.2.1 Theory and simulation model

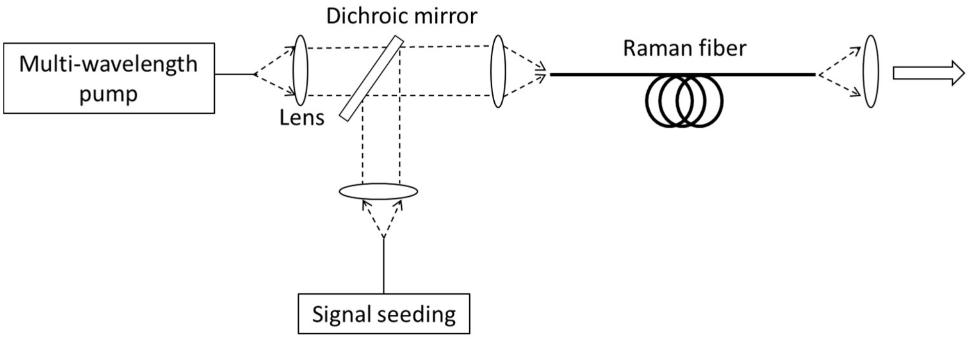

Figure 5.1 Layout of simulated multi-wavelength-pumped fibre Raman amplifier.

Figure 5.1 shows the layout of the multi-wavelength-pumped FRA I simulate. A signal seed and a multi-wavelength pump are combined and launched, respectively, into the core and inner cladding of a double-clad FRA in the same (forward) direction. All pump and Stokes waves are unpolarised. The first, longest-wavelength, pump is always at 980 nm, with additional pumps added at predetermined or optimised wavelengths on the short side of 980 nm. The signal is seeded by 10 W at around 1024 nm, which corresponds to the Raman gain peak (i.e., 1st Stokes order) with 980-nm pumping (separation ~440 cm^{-1}). The double-clad Raman gain fibre considered for these simulations has a 19.1-µm-diameter core with low Ge-doping in a 54-µm-diameter pure-silica inner-cladding, for an area ratio of eight. A larger area ratio allows for higher-power pumping, but in the absence of spectral filtering, this leads to cascaded Raman conversion into higher Stokes orders, which in the case of single-wavelength pumping significantly reduces the conversion efficiency into the 1st Stokes for area ratios larger than eight [4]. (This becomes somewhat worse for multi-wavelength pumping, for which area ratios of up to ~7 appear better. This is further discussed in **Sect. 5.3**.) Thus, although I include such cascaded conversion to the 2nd and 3rd Stokes orders in my simulations, it is a parasitic process relative to amplification of a signal in the 1st Stokes order. All reported efficiencies relate to the 1st-Stokes signal power. The Raman gain spectrum and fibre loss spectrum I used are adopted from Ref. [13], [14] and are shown in **Figure 5.2**, for silica fibre with low Ge-content. Obviously the Raman gain depends strongly on the separation between pump and Stokes, but even for a fixed Raman frequency shift, the Raman gain coefficient is approximately inversely proportional to the pump wavelength [13]. To account for this, as well as for the polarisation, I scaled g_R (v) with the inverse of the wavelength of each pump [13], and reduced it by half for unpolarised pumping. The pump power is the same for each wavelength, and can be 200 W, 400 W, 800 W, and 1600 W per wavelength, corresponding to FoM of 10, 20 40, and 80. Here, and throughout this section, I calculate the FoM based on the power of a single pump wavelength, 980 nm, where the propagation loss becomes 1.92 dB/km and the Raman gain coefficient 51 fm/W. The diode lasers at other wavelengths are assumed to have the same power but different loss according to **Figure 5.2**, as well as peak Raman gain in inverse proportion to the wavelength. Therefore, the FoMs at other pump wavelengths differ somewhat from that at 980 nm. Whereas current state-of-the-art diode lasers are bright enough for 200 W single-wavelength pump power and FoM = 10, higher power may be difficult to achieve at present. However, Yb-doped fibre lasers would be able to reach a FoM of 80, and can then be used for spectrally combined pumping in the 1 – 1.1 μm wavelength range with very high FoM.

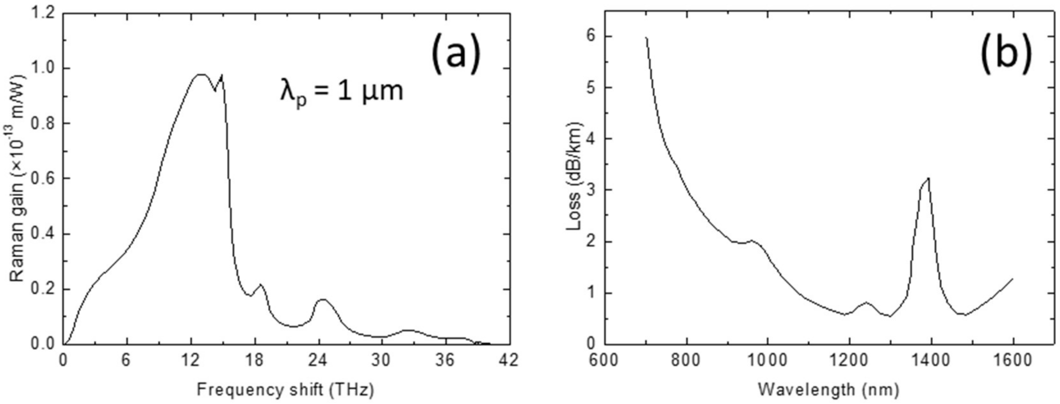

Figure 5.2 (a) Spectral dependence of Raman gain coefficient g_R (v) vs. Raman frequency shift v for silica fibre with polarised pumping at wavelength λ_p = 1 μm [13]. **(b)** Silica fibre loss spectrum [14].

With multi-wavelength pumping, SRS between pumps, between pumps and Stokes, and between different Stokes orders need to be taken into consideration. **Eq. (5.1)** is a rewritten form of **Eq. (2.7)** and **(2.8)**. It describes the evolution of the pump and Stokes powers for a discrete number n of interacting waves in the continuous-wave (time-independent) regime:

$$\frac{dP_i}{dz} = -\alpha_i P_i + \sum_j G_{ij} P_i P_j \tag{5.1}$$

Here, i and j vary from 1 to n, P_1 to P_{n-3} are pump powers, P_{n-2} to P_n are Stokes powers in the 1st, 2nd, and 3rd Stokes order (relative to the longest-wavelength pump at 980 nm), and α_i represents the fibre loss. Furthermore, if ν_k is the optical frequency of wave k and $g_{ij} = g_R\,(|\nu_i - \nu_j|)$,

$$\begin{cases} G_{ij} = +g_{ij}/A_{eff} & if\ \nu_i < \nu_j\ (gain\ for\ signal\ i) \\ G_{ij} = 0 & if\ \nu_i = \nu_j \\ G_{ij} = -(g_{ij}/A_{eff})(\nu_i/\nu_j) & if\ \nu_i > \nu_j\ (depletion\ of\ pump\ i) \end{cases} \tag{5.2}$$

$$\begin{cases} A_{eff} = A_{core} & if\ i\ and\ j\ are\ both\ in\ core \\ A_{eff} = A_{clad} & if\ i\ or\ j\ is\ in\ cladding \end{cases} \tag{5.3}$$

I implemented **Eq. (5.1) – (5.3)** in Matlab using a Runge-Kutta solver (Matlab ODE45) for numerical integration. The Matlab code is short and straightforward to write. I then used it to evaluate multi-wavelength-pumped FRAs with different parameters. In all cases, I chose the fibre length to yield the highest conversion into the 1st Stokes. Note that there is no backward-propagating light due to unseeded SRS or Rayleigh scattering in the model, and therefore no coupling with counter-propagating waves. Therefore, the solution of **Eq. (5.1)** as integrated in the forward direction, is at every position equal to the output power distribution of a fibre of the corresponding length. The computer run-times for determining the optimum length and the corresponding output power for a given set of input wavelengths and powers are therefore small, typically less than 1 s on a standard personal computer.

The simulations do not treat individual spatial modes, but rather assume that the pump powers are distributed uniformly over the whole core and cladding area. Although each pump mode has a different overlap with the core, a practical, well-designed cladding-pumped fibre should counteract mode-selective pump depletion through mode-coupling and / or non-circular cladding geometries. Although the relatively small inner cladding leads to large mode spacings that hamper mode-coupling, mode-coupling may still be significant, given the fibre lengths needed for SRS. An interesting question is what effect cascaded Raman conversion of the pump has on the spatial pump homogeneity, but this is beyond the scope of this thesis.

As it comes to the core, this could in principle be strictly single-mode, for strictly single-mode signal propagation. However, this requires a core-NA of 0.041 or less, for which the waveguiding may be too weak. Therefore, I assume an NA of 0.1. The core then supports around eight spatial modes, but it may still allow for fundamental-mode operation, if higher-order signal modes are not excited at the launch and mode-coupling is small (thanks to the relatively large mode-spacing in a 19.1-μm core). Although the effective area of the signal depends somewhat on the partition of power between modes, I neglect this and use the core area as the effective area for cascaded SRS from the 1st Stokes order to higher orders. These are seeded by vacuum fluctuations of power 14.8 μW for the 2nd Stokes wave at 1073 nm and 14.1 μW for the 3rd Stokes wave at 1126 nm. These levels correspond to the power in eight modes in two polarisations within a gain bandwidth of 5 THz. Bendloss-filtering [15] could perhaps suppress higher-order spatial modes in the Stokes orders, but this has not been considered.

5.2.2 Results

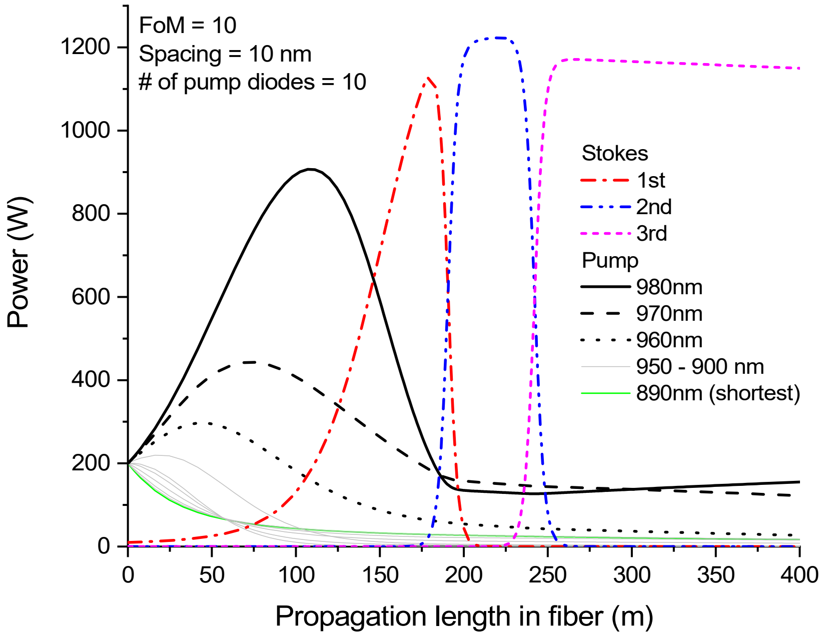

Figure 5.3 Power evolution of waves vs. propagation length in fibre for the case of FoM = 10 with ten diodes with 10-nm spacing. Because all waves propagate in one direction, the powers for a given propagation length are equal to the output powers for a fibre of that length.

Figure 5.3 shows the power evolution of the waves along a fibre simulated with our model for a FoM of 10 with 10 pumps separated by 10 nm. The evolution as well as the conversion efficiency depends on the parameters, but this is a representative example. In the beginning of the fibre, SRS transfers power from the pumps at shorter wavelengths to those at longer wavelengths, and most of all to the longest-wavelength pump at 980 nm. The 1^{st}-Stokes signal grows from the start, and at some point, reaches a power where it depletes the 980-nm pump so fast that also the 980-nm pump power decreases. The 1^{st} Stokes also amplifies the 2^{nd} Stokes (seeded by vacuum fluctuations). Once the 1^{st}-Stokes wave has reached sufficient power, the 2^{nd}-Stokes wave grows rapidly, and rapidly depletes the 1^{st} Stokes. Then the SRS cascades to the 3^{rd} Stokes, and would continue to higher orders, but those are not included in the simulations. The power and the length at the position of the 1^{st}-Stokes peak were taken as the signal output power and optimised length throughout this section. Note that the maximum power of 2^{nd} Stokes is 5 - 10% higher than that of 1^{st} Stokes due to a considerable amount of residual pump. During the depletion of the 1^{st}-Stokes power, SRS continues to transfer power from the pumps to the 1^{st}-order Stokes, and this power will add to the 2^{nd}-Stokes power which thus can reach a higher level than that of the 1^{st} Stokes.

Incomplete pump depletion occurs also for single-wavelength cladding-pumping, when the area ratio exceeds around eight, because of the smaller effective area and thus higher rate of SRS from the 1st to 2nd Stokes than from the pump to the 1st Stokes. Multi-wavelength pumping reduces the overall rate of SRS from the pumps to the 1st Stokes and thus exacerbates this problem. For the area ratio of eight used here, the residual pump power when the 1st-order Stokes power reaches its maximum varies from 17% to 66% of the total power, depending mainly on the wavelength spacing but also on the FoM. If I only consider cases with conversion efficiency above 60%, then the leakage varies in the range 17% - 30%. It is possible to counteract this with a smaller area ratio. For an area ratio of four, the residual pump power range reduces to 6% - 55% (6% - 18% for cases that reach over 60% conversion efficiency), and the maximum powers of the 1st and 2nd Stokes become almost the same. The effect the of area ratio is discussed further in **Sect. 5.3**.

Figure 5.4 shows the 1st-Stokes conversion efficiency obtained with 5, 10, 15, 20, and 30 nm pump wavelength spacing, for different FoMs and number of pumps. The 1st-Stokes signal was seeded at a fixed wavelength of 1024 nm, i.e., 438 cm^{-1} or 13.1 THz from the longest pump-wavelength. Throughout this section, each pump laser is either on or off. Thus, the pump power increases in discrete steps, and the lines between data points only serve to guide the eye. As expected, a narrower spacing generally allows for higher conversion efficiency. Furthermore, in many cases, multi-wavelength-pumping allows for higher conversion efficiency than single-wavelength pumping does, especially for small FoMs and narrow wavelength-spacing. The efficiency remains high with 5 and 10 nm spacings even with 10 pump sources, which is the highest number I considered. The total pump bandwidth of up to 90 nm (31 THz) is then considerably larger than the conventional pump acceptance bandwidth of ~ 5 THz, and even exceeds twice the shift to the Raman gain peak. The 31-THz bandwidth is approximately equal to the maximum Raman frequency shift in **Figure 5.2(a)**, but I believe this is a coincidence. The power conversion efficiency stays largely above 55%, 65%, 70%, and 72% for FoM of 10, 20, 40, and 80, respectively. For 5 nm spacing, for those FoMs, the PCE stays above 65%, 70%, 73%, and 75%, respectively, for 2 – 10 pumps. By contrast, for 20 – 30 nm spacings, the efficiency deteriorates rapidly as the number of pumps increases. Note also that whereas InGaAs diode lasers are available with largely constant specifications from ~0.9

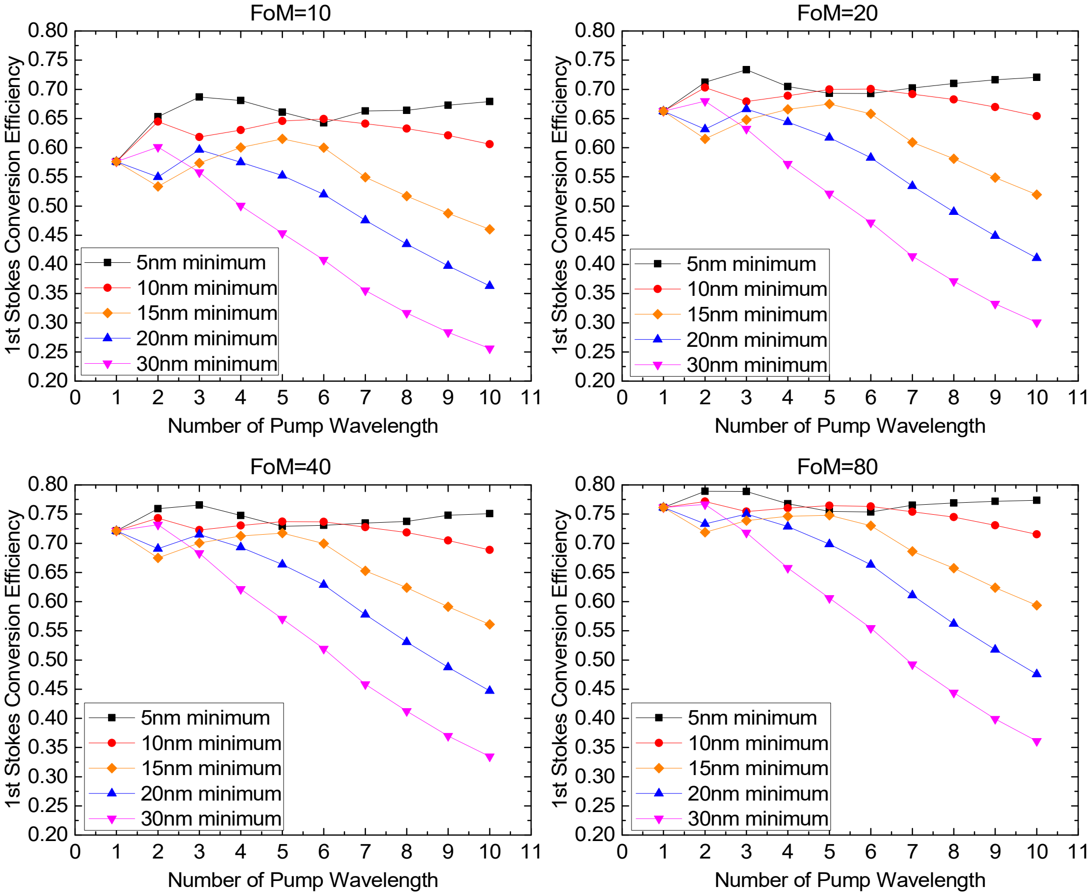

Figure 5.4 Power conversion efficiency to 1st Stokes with 5, 10, 15, 20, and 30 nm pump wavelength spacing at different pump powers as represented by different FoM.

to ~1 µm, the largest total wavelength range in **Figure 5.4** is 270 nm. This range is difficult or impossible to cover with diode lasers of adequate performance.

Whereas the trends in **Figure 5.4** for the dependence on the number of pump wavelengths, wavelength spacing, and FoM are expected, some details are less clear and suggest that further improvements are possible. For 15 nm and 20 nm spacings, two wavelengths are worse than one and three. Furthermore, 30 nm is significantly better than 20 nm spacing for two pumps, and there are also other examples where a larger wavelength spacing is comparable to, or better than, a smaller spacing. A smaller spacing is more difficult to achieve, so a larger spacing is more attractive in those cases (subject to diode laser availability).

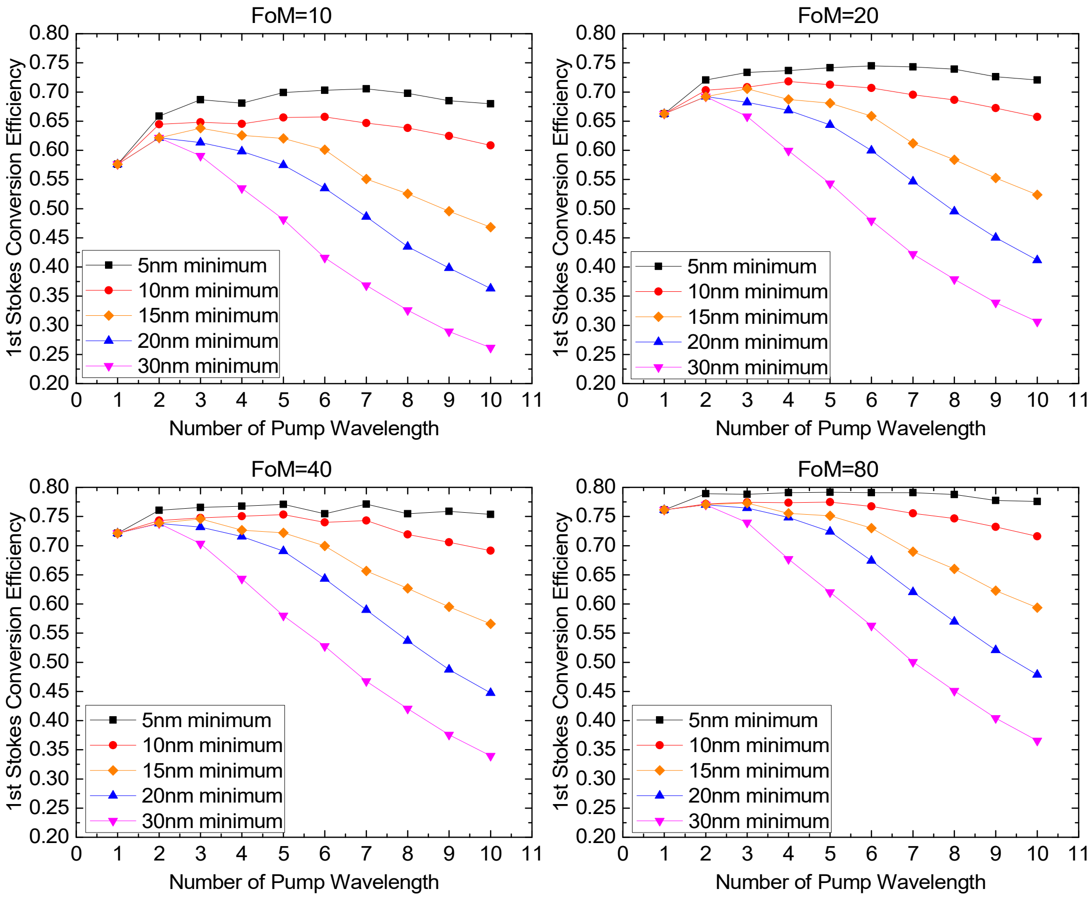

Figure 5.5 1^{st} Stokes power conversion efficiency with optimised pump wavelength spacings with 5, 10, 15, 20, 30 nm minimum spacings at different pump powers as represented by the FoM.

To investigate if such anomalies can be avoided, and if further improvements are possible, I next consider the case of optimised pump wavelengths. This is shown in **Figure 5.5**, for different numbers of pump diodes, and with different minimum wavelength-spacings of 5, 10, 15, 20, and 30 nm. This requires nonlinear optimisation. I used the Matlab routine FMINCON to optimise the wavelength spacings under the constraint of a minimum spacing and with the longest pump wavelength fixed at 980 nm. Also the signal wavelength was optimised over a wavelength span corresponding to the width of the 1^{st}-Stokes peak. Thus, the number of optimisation variables is equal to the number of pump wavelengths. In the optimisation procedure, for a given set of wavelength spacings and signal wavelength, the signal output power in the 1^{st} Stokes is calculated as in the fixed-wavelength case, and the maximum signal power, at the optimum length for this set of spacings and signal wavelength, is returned to the optimisation procedure. This is repeated until the optimisation procedure has found a set of wavelength-spacings and signal wavelength that maximises the signal power. This will be a local maximum, since nonlinear optimisation is not guaranteed to find the global maximum, but the results can be sanity-checked through the character of plotted curves. Furthermore, FMINCON was run several times with different starting spacings and signal wavelengths. In all cases, the minimum spacing was included as one starting set, so this set will always be included in the optimisation procedure. **Figure 5.5** shows that a smaller minimum spacing is better, but the minimum value would be dictated by the capabilities of the spectral combination technology. Furthermore, the anomalies are gone, except perhaps for some minor dips in efficiency in some cases. These and other minor anomalies in the results may be caused by imperfect optimisation.

In all cases, two pump wavelengths are better than a single pump wavelength. Furthermore, with 5 nm minimum spacing, multi-wavelength pumping is for all considered FoMs and number of diodes (i.e., up to ten) more efficient than single-wavelength pumping. Up to 68% power conversion efficiency is maintained with FoM = 10 even with the number of pumps extending to 10. The PCE is impacted by the energy difference between photons. The quantum conversion efficiency becomes 73%.

The 1st-Stokes output power dependence on the total pump power is plotted in **Figure 5.6**, as I increase the number of pumps, both for non-optimised fixed and optimised minimum pump wavelength spacings. This is based on the same data as used for **Figure 5.4** and **5.5**, with equal pump power at each wavelength, but re-calculated in terms of total pump power and 1st-Stokes output power. Since the different FoMs correspond to different amounts of pump power in each wavelength, the increment between data points is different for the different FoMs. The general conclusion is that there is little difference between fixed and optimised wavelength spacings, although there are a few cases in which the difference is non-negligible. For the 5 – 10 nm cases, optimised as well as fixed, the output power increases almost linearly when adding more pump power by adding more wavelengths. No roll-off is observed even for ten pumps. The slope efficiency is approximately 70%, 73%, 76% and 78% for FoM = 10, 20, 40 and 80 with 5 nm minimum spacing. For 10 nm, it is approximately 62%, 66%, 69% and 71%. Note that for example, a FoM of 10 with 5-nm spacing is more efficient than a FoM of 20 with 10-nm spacing. This is further studied in **Sect. 5.3**. A possible explanation is that a smaller wavelength spacing with the same spectral power density allows for more routes for cascaded SRS, of which the most efficient ones are favoured. For spacings of 15 – 30 nm, the output power rolls over to the point where there is no further increase for additional

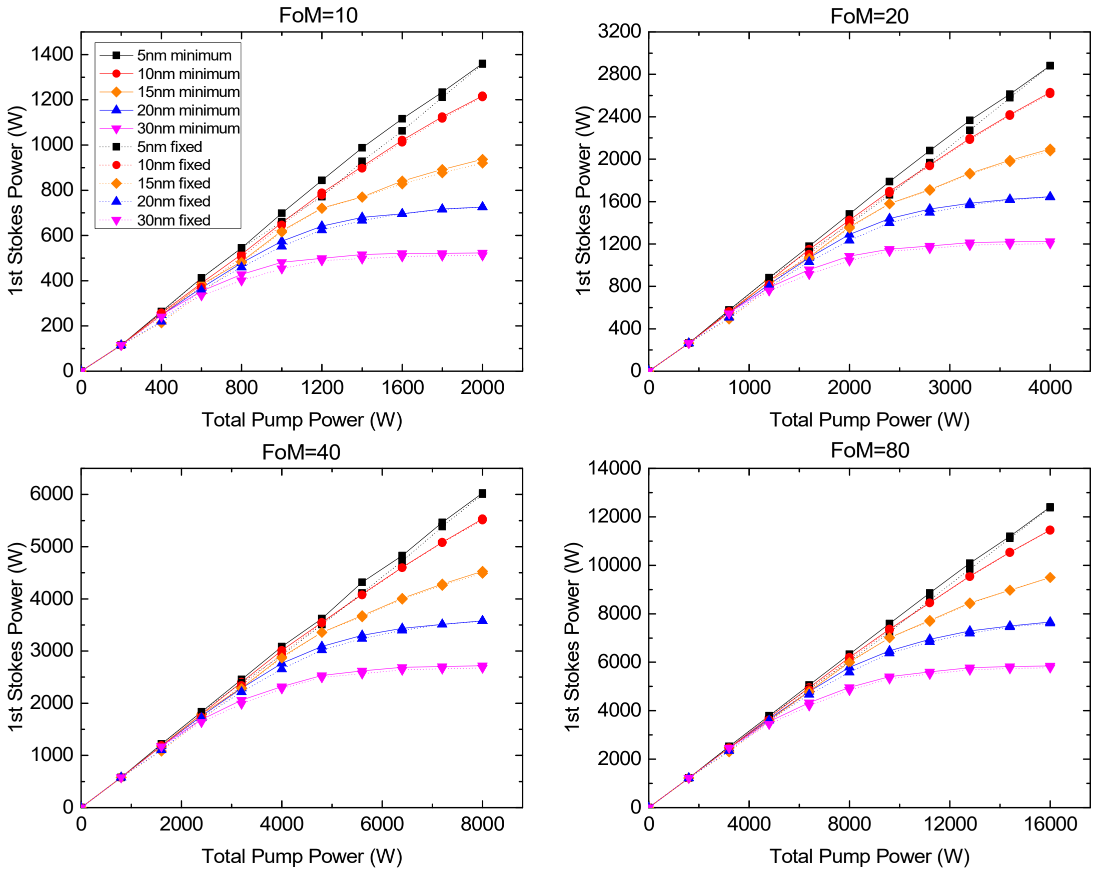

Figure 5.6 1st-Stokes output power vs. total pump power with non-optimised and optimised pump wavelength spacings with fixed or minimum spacings of 5, 10, 15, 20, and 30 nm at different FoMs (corresponding to different power per pump wavelength). The curves for fixed wavelengths are largely indistinguishable from those with optimised wavelengths.

pump wavelengths. The higher loss at the shorter wavelengths used with large numbers of pumps contributes to this roll-over, and I note that the higher FoMs, which are less affected by loss, show slightly weaker roll-off. Note also that the highest signal power density in **Figure 5.6** exceeds 40 W/μm^2, and may well lead to optical damage. A larger signal core would reduce the signal power density. (By contrast, the efficiency and optimum length are expected to depend more on the pump intensity than the signal intensity).

The optimised fibre lengths corresponding to **Figure 5.5** are plotted in **Figure 5.7**, for the case of optimised wavelength spacings. This confirms that the fibres are significantly shorter with higher FoM, as well as with increasing number of pumps. This is particularly beneficial for small FoM when the total background loss is large, and explains at least in

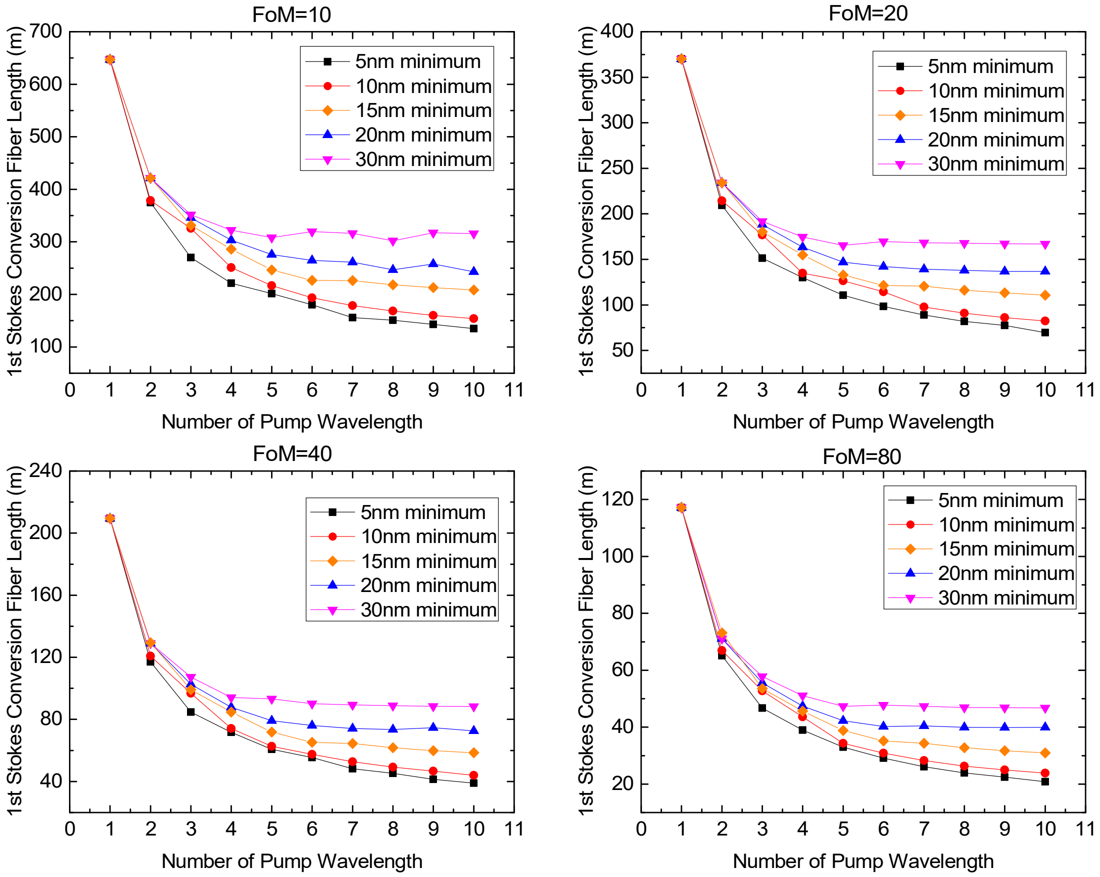

Figure 5.7 Optimised 1st Stokes conversion fibre length with 5, 10, 15, 20, and 30 nm minimum pump wavelength spacings at different pump powers

part why the case of FoM = 10 shows the biggest efficiency-improvement with dual-wavelength pumping in **Figure 5.5**.

Compared to the 5-nm results without optimisation in **Figure 5.4**, the efficiency with optimisation in **Figure 5.5** is increased by nearly 5%, for five and six pump wavelengths. By contrast, the improvement is less significant or even negligible for smaller as well as larger numbers of pump wavelengths, as well as for 15 – 30 nm spacing. This is also shown in **Figure 5.6**. This is primarily a result of low efficiency in the case of five and six fixed wavelengths, so cannot be attributed to imperfect optimisation. To help us understand why the optimisation leads to bigger improvements for some combinations than for others, **Figure 5.8** plots the optimised wavelengths used in **Figure 5.5** for FoM = 10. For small pump numbers, the optimised wavelengths vary and, in some cases, lead to spacings approximately equal to the Raman peak shift, even when the minimum (i.e., smallest allows) spacing is much smaller. When adding more pumps, the wavelength spacings are optimised to the minimum value, or close thereto, and thus close to the fixed spacing used in **Figure 5.4**. For example, the pump wavelengths are optimised to 980 nm, 954 nm and 934 nm for three pump sources with 20 nm minimum spacing. When pumped with 10 wavelengths, the spacings are at or close to the 20-nm minimum spacing. Other FoMs showed this pattern, too.

I conclude from **Figure 5.8** that for large numbers of pump wavelengths, the spacing should be as small as possible. Still, even with optimised spacings, **Figure 5.6** shows that the number of pumps that can contribute effectively is limited, at least in the case of large minimum spacings. This is also shown in **Figure 5.9**, which plots the incremental conversion efficiency, defined as the increase in laser output power as a pump laser is added, relative to the power of that pump laser, for optimised spacings (fixed spacings gave similar results). In this case, the abscissa is the total wavelength span rather than the number of diodes. I note that in some cases in **Figure 5.8**, the total pump wavelength range is smaller for a larger number of pumps. This affects the behaviour of the curves in **Figure 5.9**. Furthermore, the differentiation used for **Figure 5.9** can exacerbate any unusual behaviour in the optimisation, or indeed in the physics of cascaded SRS. Nevertheless, overall, the decrease in incremental conversion efficiency for larger wavelength spans is similar for the different FoMs and different minimum wavelength spacings. If I define the endpoint of the maximum usable wavelength span for pumping as the wavelength for which the output power increases by 60% of the power added by one diode then this becomes approximately 55 nm, 76 nm, 85 nm, and 91 nm for FoM of 10, 20, 40, and 80, respectively. The span, $\Delta\lambda_{60}$, is plotted in **Figure 5.10** for 10, 20, and 30 nm minimum wavelength spacings. Surprisingly, the largest span is in most cases obtained for a 20-nm minimum spacing. Anomalous optimisation is one of many effects that may explain this. One can also speculate that in some cases, the optimisation or the nature of cascaded SRS means that the efficiency of the last diode within the bandwidth $\Delta\lambda_{60}$ may have a relatively weak dependence on the wavelength, and may therefore shift significantly due to irregularities in the SRS cascade or the optimisation. The incremental efficiency of an added diode laser also depends on the efficiency of the previous diode lasers. If this is below par then one can expect that the incremental efficiency an additional diode laser is higher than it would otherwise be, and possibly above rather than below the threshold of 60% used in **Figure 5.10**. Thus, I believe the details of the curves are less significant than the bigger trends.

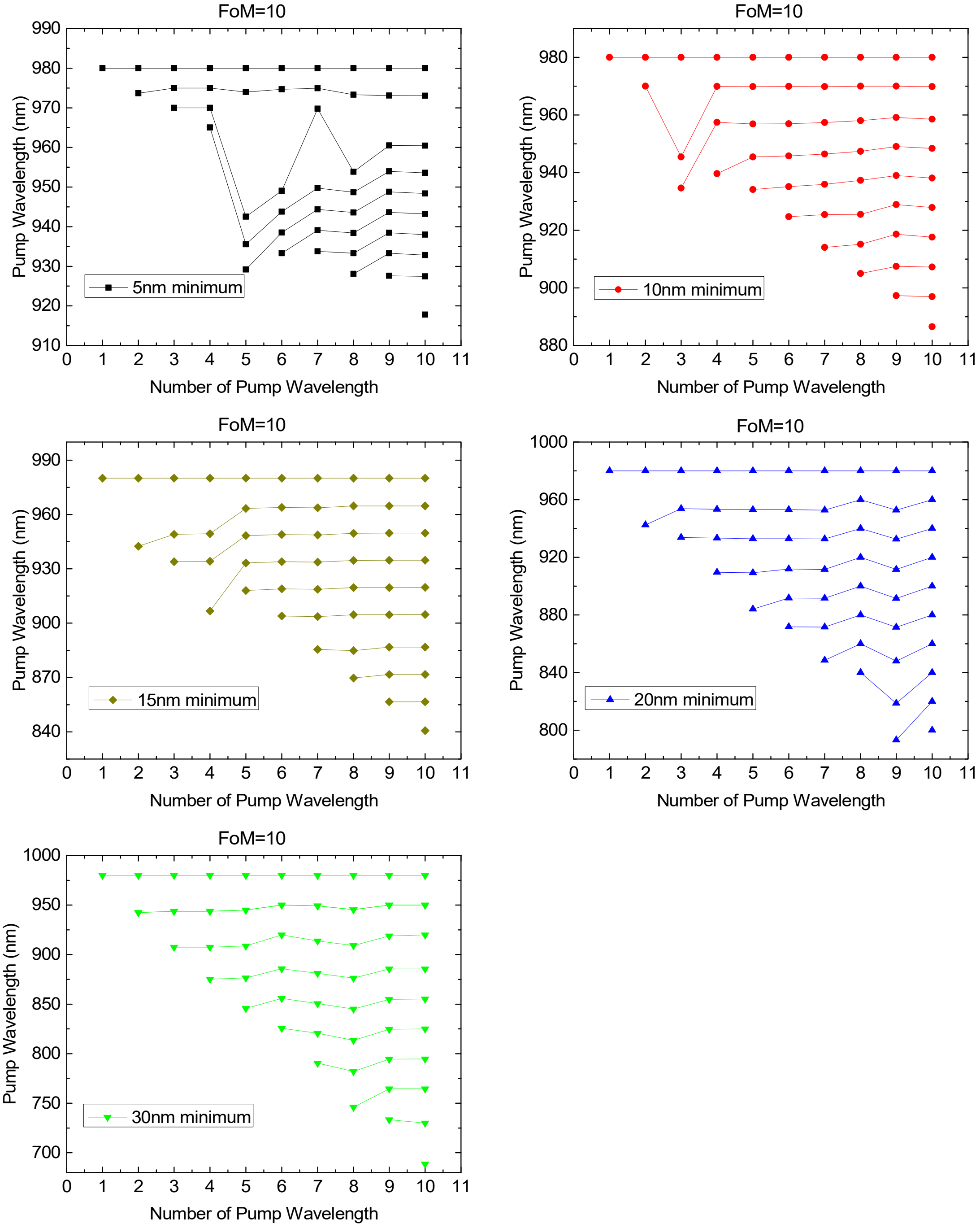

Figure 5.8 Optimised pump wavelengths with 5, 10, 15, 20, and 30 nm minimum spacings at FoM = 10.

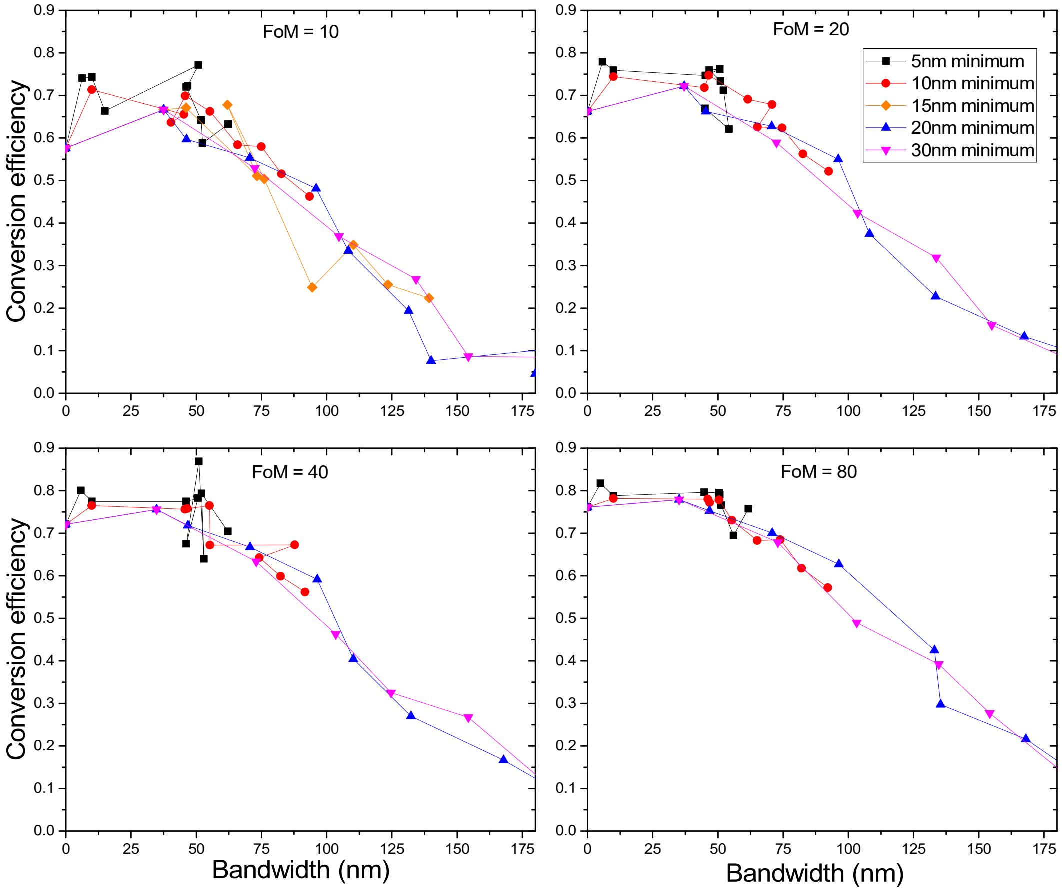

Figure 5.9 Incremental conversion efficiency as pump lasers are added *vs*. total pump bandwidth for FoM = 10, 20, 40 and 80.

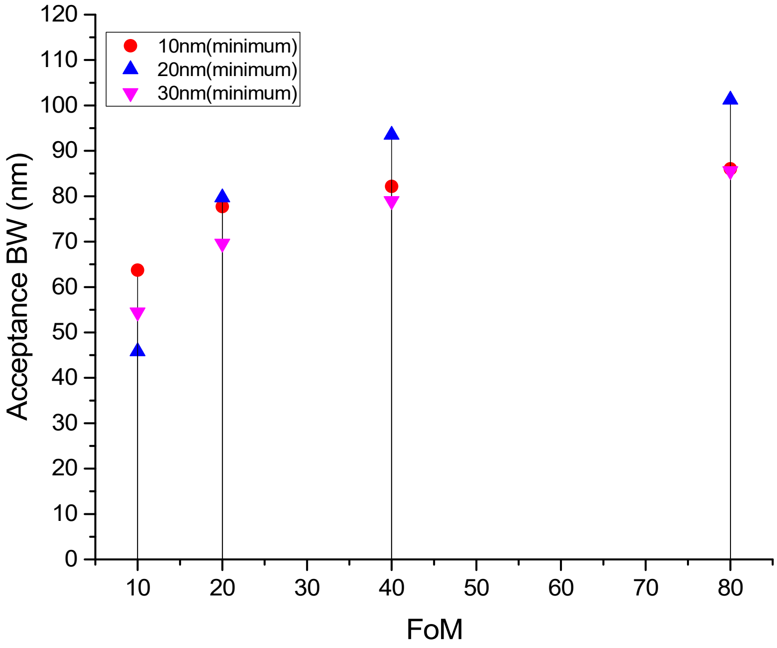

Figure 5.10 Pump acceptance bandwidth $\Delta\lambda_{60}$ defined as the bandwidth for which the incremental conversion efficiency exceeds 60% *vs*. FoM for optimised pump wavelengths with different minimum spacings.

Figure 5.11 summarises the results in terms of the relation between spectral power density, actual used bandwidth, and efficiency, for the case of optimised wavelength spacings. Points connected by lines correspond to similarly connected data points in **Figure 5.5**. Only data points with bandwidths smaller than $\Delta\lambda_{60}$ are included. The spectral power density in **Figure 5.11** was calculated as $P_{tot}/(\Delta\lambda_R^2 + (\lambda_{max} - \lambda_{min})^2)^{1/2}$ where P_{tot} is the total pump power and λ_{max} (= 980 nm) and λ_{min} are the wavelengths of longest and shortest pump wavelength. The expression also includes the intrinsic linewidth of SRS, $\Delta\lambda_R$ = 15 nm. This prevents the spectral power density from diverging, and ensures that it is the same regardless of the minimum pump spacing, in case of a single pump wavelength. The choice of $\Delta\lambda_R$ is motivated by the expected low dependence on the spectral distribution within a span of $\Delta\lambda_R$, as a result of the fundamental properties of SRS. Nevertheless, the bandwidth in **Figure 5.11** is defined as λ_{max} - λ_{min} (as in **Figure 5.9** and **5.10**), i.e., the actual used bandwidth, since this relates to the combination technology rather than to the properties of SRS. For a given bandwidth, a higher spectral power density generally improves the efficiency. A higher spectral power density generally increases the bandwidth that can be used, as well, although in all cases, the efficiency drops at the largest bandwidths for a given FoM.

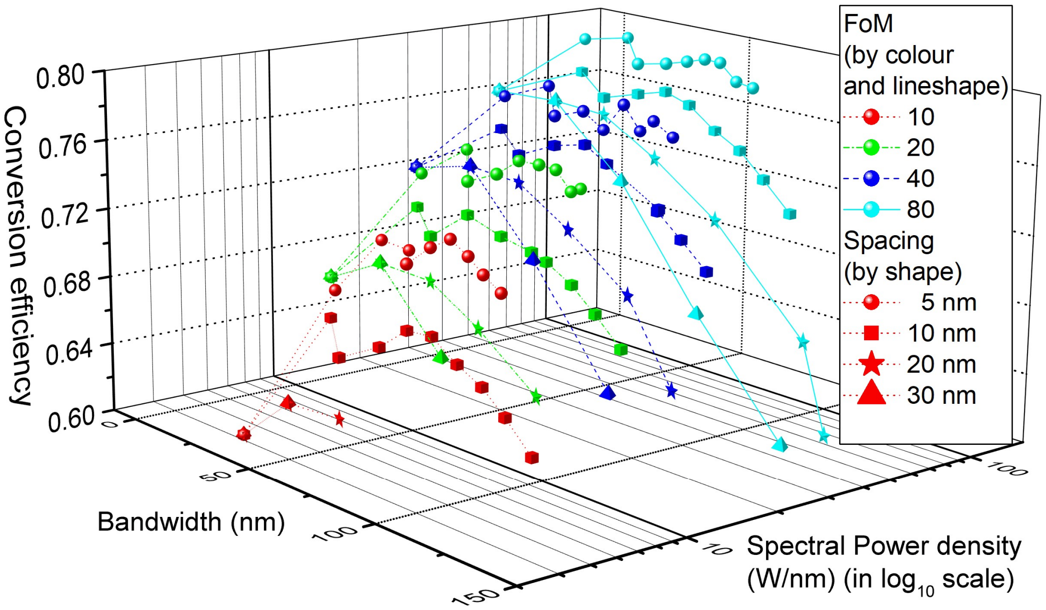

Figure 5.11 Efficiency *vs*. bandwidth and spectral power density for optimised wavelength spacings.

In **Figure 5.11**, two wavelengths (from two diode lasers) are better than one, and the improvement can remain with a larger number of wavelengths, too. However, the improvement becomes smaller for larger FoM. It is easy to realise that for sufficiently high FoM, single-wavelength pumping will be more efficient than multi-wavelength pumping. The Raman conversion losses stem from fibre background loss, quantum defect loss, and pump leakage. For high enough FoM (for high brightness or for low fibre loss), the quantum defect losses and / or the pump leakage will dominate, and in this regime, it is better to use narrow-band pumping close to the signal. Although we fall short of this regime even for a FoM of 80, which is a very optimistic FoM with diode-laser pumping, it may well be possible to reach it through pumping with a fibre laser, thanks to its exceptional brightness. Note however that it is difficult to maintain a high pump brightness through a fused-fibre pump combiner of the type often used for pumping of rare-earth-doped fibres.

It is also interesting to consider the effect of the Ge-concentration. Higher Ge-doping than assumed in this chapter increases the Raman gain coefficient, but also the loss. The increase in the loss depends on wavelength, and I expect that at least for some wavelengths, the FoM can be higher with higher Ge-doping. However, the Raman linewidth and peak shift become smaller, which will also affect the efficiency of multi-wavelength pumping as shown by experiments in **Chapter 4**.

As it comes to the spectral characteristics of the signal, the simulations assume that all power resides at either the pump wavelengths, the signal in the 1st-Stokes wavelength, or at the 2nd or 3rd Stokes orders. The spectrum of an individual wave, including the signal, is therefore not resolved. Spectral distortions of individual waves could occur through SRS as well as other nonlinearities [13] such as four-wave mixing (FWM) and self-phase modulation (SPM) [16], [17]. However, simulations of SRS on a finer grid (not shown here) did not exhibit any SRS-induced line broadening. Although FWM was not included in the simulations, this requires phase-matching and is generally weak for multimode beams (the inner cladding supports approximately 700 modes *LP*-modes, i.e., around 1400 polarised modes. Even if the Stokes power resides in the fundamental mode, this has normal dispersion, which precludes phase-matched FWM between wavelengths in the same spatial mode. FWM to higher-order modes can still be possible, but with reduced strength because of the reduced overlap. SPM can still lead to significant broadening. In **Figure 5.3**, at the output (i.e., where the 1st-Stokes signal peaks), the Raman gain of the

2nd Stokes is ~60 dB. It follows that the nonlinear phase shift of the 1st-Stokes signal becomes $\gamma\, A_{eff} / g_R$ (60/4.343) rad = 35 rad, where γ is the nonlinear parameter that governs SPM. (This assumes all transfer of power to the 2nd Stokes is from the 1st Stokes rather than directly from a pump.) Such large nonlinear phase shift can lead to significant spectral broadening. It is possible to reduce the resulting spectral broadening through improved amplitude stability; however, any multimode interference degrades the stability. Thus, it may be difficult to avoid spectral broadening of the signal in the fibre I consider. Note also that a reduced area ratio reduces the SPM of the 1st Stokes, since this either reduces the signal intensity (in case of a larger core area) or the effective length (in case of a smaller inner-cladding area, which increases the pump depletion rate). Experimentally, in case of a GRIN FRL which was core-pumped at 950 and 974 nm [11] (**Sect. 3.3**), the 1st-Stokes emission linewidth was narrower than the intrinsic Raman linewidth even in the absence of spectral filtering. This suggests that conventional gain-narrowing managed to counteract line-broadening in this case.

I note that in addition to reducing the SPM of the 1st Stokes, a smaller area ratio also reduces the 2nd-Stokes gain. Otherwise, the ~60 dB it reaches in my case may be enough to induce lasing from spurious reflections or possibly even double Rayleigh back-scattering [18]–[20]. I note also that temporal fluctuations of the 1st Stokes can also enhance the rate of conversion to the 2nd Stokes [21]. Any increase in the rate of build-up of the 2nd Stokes reduces the conversion efficiency into the 1st Stokes.

This approach disregards the possibility that power is scattered to a wavelength outside the predefined wavelength set, although I observed this experimentally in ref. [11] **(Sect.3.3)**. However, that was in a laser cavity, in which a relatively low Raman gain can lead to significant SRS. By contrast, insofar as the input power outside the predefined wavelengths is low (if the input spectrum is sufficiently pure), I expect that the Raman gain will be too low to lead to any significant power outside the predefined wavelengths, or in the backward direction.

I have not investigated the details of how a pump photon is converted to the 1st-Stokes signal. **Figure 5.2(a)** shows that direct conversion is possible for frequency differences of up to ~38 THz (from around 910 nm into 1024 nm), but with very low Raman gain coefficient. Therefore, except for the longest pump wavelengths, I expect that cascaded SRS dominates the conversion of pump photons to signal photons. When this happens, it is possible that the effective area of the pump becomes smaller in the cascade through so-called Raman beam cleanup [22]–[26]. My simulations do not include this effect. The details depend on the fibre design, but at least in principle, it opens up for larger area ratios for cascaded pumps.

5.2.3 Conclusion

I have used numerical simulations to investigate multi-wavelength cladding-pumping directly with diode lasers of high-power fibre Raman amplifiers operating on the 1st Stokes wavelength of the longest-wavelength pump. I find that compared to a single pump laser, spectrally combined pump lasers with the same power per wavelength are more efficient. In terms of a figure of merit which depends on the achievable pump intensity and fibre loss, the conversion efficiency reaches 71% for FoM = 10, which is realistic with state-of-the-art pump sources. I considered a cladding / core area ratio of eight, for which the pump leakage is non-negligible. A smaller area ratio as well as core-pumping can reduce the pump leakage and thus improve the efficiency, as discussed in **Sect. 5.3**. The usable pump bandwidth varies between 46 nm and 91 nm with the pump powers and wavelengths spacings considered. I expect that even higher usable pump bandwidths are possible with other parameters. For a given total pump bandwidth, the precise pump wavelengths have a relatively minor effect on the attainable conversion efficiency for the fixed and optimised wavelengths I have studied, but it does depend on the FoM. The general results apply also to single- and multimode core-pumping and to pumping with spectrally combined Yb-doped fibre lasers.

5.3 Lossless fibre Raman amplifier regarding the bandwidth and the spacing of multi-wavelength pump as well as the area ratio

In contrast to the **Sect. 5.2** in which the outcome of multi-wavelength pumping was assessed with respect to the spacings and the number of wavelengths for different FoM, the total pump bandwidth and wavelength spacing are used as the main variables for the assessment in this section. A (theoretical) lossless fibre (thus infinite FoM) is first assumed in order to eliminate the distraction that individual properties of fibre brings to the arguments and focus on the theoretical limits of multi-wavelength pumping at different area ratio (AR). Then, cases with realistic fibre loss are considered. The objective is to fully examine theoretical spectral and spatial boundaries of multi-wavelength pumping for fibre Raman amplifier with single-wavelength signal output.

A modified coupled differential equation to accommodate lossless fibre is introduced in **Sect. 5.3.1** and its result is presented in **Sect. 5.3.2**. In **section 5.3.3**, I estimate loss for lossy fibres for selected conditions.

5.3.1 Simulation model

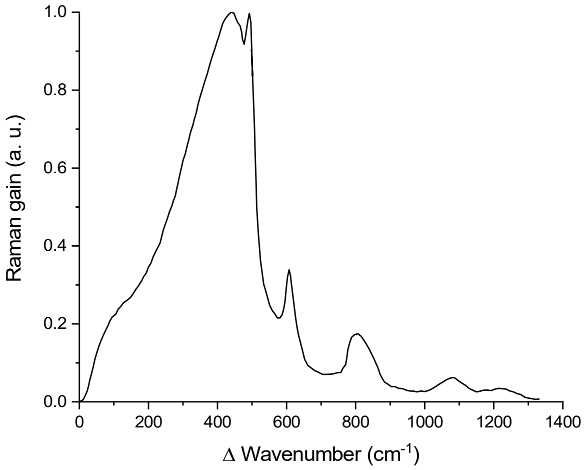

Figure 5.12 Raman gain spectrum of silica fibre. Same as **Figure 5.2(a)** but the unit is changed to cm^{-1}.

The optical apparatus assumed in these simulations of the multi-wavelength-pumped fibre Raman amplifier is identical to those in **Sect. 5.2**, **Figure 5.1** and the material of the Raman gain fibre is pure silica in this section. However, the configuration of the pump wavelengths is changed and the consideration of the AR is added. When considering different ARs, the core size is kept the same as in **Sect. 5.2** while the cladding size is changed.

All pump and Stokes waves are unpolarised. The longest pump wavelength is always set to 976 nm (10250 cm^{-1}) and other pumps are added successively at shorter wavelengths. The wavelength of the signal, the 1st Stokes of the longest pump, was set to 1019 nm (9810 cm^{-1}) where the Raman peak is.

I consider the fibre to be lossless. This makes the results more general, with efficiency independent of the total input power, core diameter (at fixed AR), and following appropriate scaling, the length of the fibre. In realistic terms, this assumption is reasonable when the total loss over the optimum fibre length is small.

The governing equation was modified from **Eq. (5.1)** by inserting $N_i h\nu_i$ into P_i and eliminating the loss term. With additional definitions and reorganisation, the equation writes as below.

$$\frac{1}{n_i}\frac{dn_i}{d\zeta} = \sum_j G_{ij} n_j \,, \qquad with\ i, j = 1, 2, \ldots, l \tag{5.5}$$

$$where\ \zeta = \frac{h\mathbb{N}}{A_{core}} z, \qquad n_i = \frac{N_i}{\mathbb{N}}, \qquad \mathbb{N} = \sum_i N_i \,, \qquad G_{ij} = \frac{\epsilon_{ij} g_{R_{ij}}}{r_{ij}}, \tag{5.6}$$

$$\epsilon_{ij} = \begin{cases} +\nu_j & if\ \nu_i < \nu_j \\ 0 & if\ \nu_i = \nu_j \\ -\nu_i & if\ \nu_i > \nu_j \end{cases} \tag{5.7}$$

and

$$r_{ij} = \begin{cases} 1 & if\ \nu_i, \nu_j \leq 10{,}000\ \text{cm}^{-1} \\ A_{clad} \,/\, A_{core} & else \end{cases} \tag{5.8}$$

N_i is the photon flux (i.e., number of photons per unit time) at the frequency ν_i and $\mathbb{N}$ is the total photon flux summed over all frequencies. Therefore, n_i accounts for the fractional photon flux at the frequency ν_i out of the whole frequency span. The optical power (P_i) at the frequency ν_i calculates to $N_i h\nu_i$, where h is the Planck constant. ζ is a generalised propagation coordinate that is proportional to the total input photon flux density and the actual coordinate, z.

A benefit of changing variables to photon flux from the power (and power density to flux density) is that the total photon flux $\mathbb{N}$ is an invariant in case of a lossless system. On the other hand, the quantum defect is not negligible, especially when the total spectral span of pump is broad. However, this can be roughly estimated by averaging the pump frequency of the used span. Typically, this is close to the middle value. Thus in my case, the factor of 9810 cm^{-1} / (10250 cm^{-1} + total span/2) can be multiplied to the photon conversion efficiency (which is the same as the quantum conversion efficiency, and normally called just the efficiency in this section) to estimate the efficiency in terms of power.

In addition, $g_{R_{ij}}$ is the Raman gain coefficient of silica for the frequency difference $|\nu_i - \nu_j|$. The subscript, i and j, was numbered from low to high frequency. ϵ_{ij} indicates whether n_i is pumping n_j or being pumped by n_j. A_{core} and A_{clad} are the area of core and clad, respectively. The product ($r_{ij} A_{core}$) becomes the effective area for the interaction between i and j, and is equal to either the core or the clad area. When either of ν_i and ν_j is considered as a pump (*i.e.*, either is guided in the cladding), the effective area becomes A_{clad} [21] (and **Eq. (2.7)**). Otherwise, it becomes A_{core}. Light at frequencies smaller than 10,000 cm^{-1} (wavelength longer than 1000 nm) is considered to be guided in the core. Note that the possibility of pump power in skew modes of cladding that does not interact with the core modes is ignored.

475 frequency channels were employed to cover the spectrum from 8510 to 13250 cm^{-1} (755 - 1175 nm in terms of wavelength) with an interval of 10 cm^{-1} (*i.e.*, $l = 475$). The channels that were neither pumped nor seeded were injected by a fictitious photon in order to simulate the triggering of unseeded Stokes waves. This is represented as if a power of $(3.17 \times 10^{-12}) \times \nu_i/c$ [W] is seeded into the ν_i-channel. (*e.g.*, 31.7 μW for the channel at 10,000 cm^{-1}.) This value is calculated according to **Sect. 2.1.4**. Then, this seed power was transformed into the initial value of n_i for the unseeded channel-i in the **Eq.(5.5)** by using the relation $P_i = N_i h\nu_i$ and the **Eq. (5.6)**. By covering broadband with densely positioned channels over this wavelength range, this model cannot only calculate the build-up of Stokes waves up to the 3rd order but also detect the unexpected built-up of the unseeded Stokes waves that can emerge amongst the broadly spaced pumps and

signal. Furthermore, any peaks with a linewidth broader than 10 cm^{-1} can be spectrally resolved. See, e.g., the higher order Stokes waves at 9000 – 9500 cm^{-1} in **Figure 5.13**.

Importantly, **Eq. (5.5)** implies that in lossless fibre, the scaling of the input power by the same factor in each pump and signal channel has no effect other than reducing the length z in inverse proportion to the power. The solution is only affected by the initial distribution of n_i over different frequencies and the G_{ij} matrix. Similarly, the calculations remain the same if core area, cladding area, and length are scaled in proportion.

Meanwhile, the loss term for the ν_i-channel (L_i) which would remain in **Eq. (5.5)** if fibre loss is included (and significant) writes as below.

$$L_i = -\frac{\alpha_i}{h\mathbb{N}/A_{core}} \tag{5.9}$$

The lossless approximation ($L_i \rightarrow 0$) is achieved for very low loss or very high total input intensity ($\alpha_i << h\mathbb{N}/A_{core}$). (Here, the area ratio of cladding to core is fixed. Therefore, A_{core} can be replaced by A_{clad}/the area ratio.) Noticeably, L_i is inversely proportional to the FoM defined in **Sect. 5.1** given that the Raman gain coefficient is the same. It is clear that $L_i = 0$ corresponds to infinite FoM.

For all the cases, one 1200th of the total pump power is injected at 9810 cm^{-1} as a 1st-Stokes signal seed. The 1:1200, the ratio of the seed and the total pump power was selected, to consider the amplifiers in a regime such as 1 W of seed grows to 1 kW with 30-dB gain by being pumped by around six state-of-the-art (~200 W) diode lasers at different wavelengths. Also note that $\mathbb{N}$ is slightly smaller for broader-band pumping for the same total input power because the photons of higher frequency have higher energy.

The simulation is written and executed in Matlab and the internal Matlab function "ode45" was used to solve the differential equation, **Eq. (5.5)**.

5.3.2 Result

As a demonstration, I first present four cases in **Figure 5.13**. The examples show two different total spans (1000 and 3000 cm^{-1}) and spacings (10 and 100 cm^{-1}). For instance, the pump configuration with 3000 cm^{-1} of a total span and 100 cm^{-1} of a spacing means 31 pump wavelengths equally spaced with an interval of 100 cm^{-1} from 10250 to 13250 cm^{-1}. See **Figure 5.13(d)**. The AR is unity in these cases (*i.e.*, the RGF is core-pumped).

The total span and spacing in **Figure 5.13** are (1000 cm^{-1}, 10 cm^{-1}), (1000 cm^{-1}, 100 cm^{-1}), (3000 cm^{-1}, 10 cm^{-1}), and (3000 cm^{-1}, 100 cm^{-1}), respectively, in **(a) – (d)**. For each case, 2D plots that show spectrally integrated power within three groups (pump: 10000 – 13250 cm^{-1}, signal: 9800 – 9820 cm^{-1}, and higher-order Stokes: 8510 – 9500 cm^{-1}) versus ζ are presented alongside the 3D plots, the axes of which are the generalised propagation distance (ζ), the fraction of signal to the total photon flux (n_S), and the wavenumber. The pump with the spacing of 10 cm^{-1} as in **Figure 5.13(a)** and **(c)** can be considered spectrally continuous because the spacing is equal to the spectral resolution of the model and small compared to the Raman linewidth. As soon will be shown in this section, any spacing smaller than the Raman linewidth (~100 cm^{-1}) would be similar to a continuous pump of the same total span, so two such spacings will be nearly equivalent. The 2D plots show that a wider total span reduces the efficiency whereas a larger spacing had almost no impact for the spans and spacings in **Figure 5.13**.

In all four cases, first the signal builds up through SRS from the pump, and soon after, also higher Stokes orders emerge and ultimately cause the signal power to drop. This is similar to single-wavelength-pumped FRAs. A difference is, however, that the increase of signal power can stop or be slowed down even without higher order Stokes. – In case of the single-wavelength pumping, the 1st-Stokes signal continues to build up until the pump depletes unless the build-up of higher-order Stokes take away signal power faster than the pump adds to it. Multi-wavelength pumping introduces an additional effect, which is easiest to observe in wider spans such as in the bottom graphs of **Figure 5.13(c)** and **(d)**. From ζ = 2 to ζ =2.5, the conversion almost stops although no higher-order-Stokes is seen. Strictly speaking, this is also relates to depletion of the pump after all, but the depletion of power in useful pump wavelengths for which the Raman gain for the signal in the 1st Stokes is meaningful. For a too broad total span, the power in the longest pump wavelengths quickly converts into the signal and depletes before the power in shorter pump wavelengths reach the longer wavelengths and thus interact with the signal (note that the rate of conversion from a shorter to a longer pump wavelength, relative to the power in the shorter wavelength, is proportional to the power in the longer wavelength). This thus slows down the cascade from short pump wavelengths to the signal, so that some of the pump power in shorter wavelength is left unconverted. This suggest that the total pump span is another limiting factor for brightness-enhancing in FRL together with the AR shown in ref.[21]. It is interesting to note that one can expect that the efficiency of transfer of power from a given shortest pump wavelength depends on the distriution of pump power at longer wavelengths. Although I have not investgated to what extent such "abandoned" pump power can be avoided, but it may well influence the distribution of optimum pump wavelengths in **Fig. 5.8**.

A set of pump, signal, and higher order Stokes curves (like in the bottom graphs in **Figure 5.13**) can be always determined by the three input variables, namely the total pump span, the pump spacing, and the AR, once I fixed the ratio between seed and the total pump power (in my case, 1:1200. This also assumes a uniform pump spectrum.) In order to find the best efficiency possible for a specific combination of values of those three input variables and the optimised fibre length, the maximum signal power is taken from the signal *vs*. propagation curve such as in **Fig. 5.13** (as in **Sect. 5.2**). The conversion efficiency is plotted against total span and spacing for the AR of one and eight in **Figure 5.14**. The spacing varies from 10 to 570 cm^{-1} and the total span varies from 10 to 3010 cm^{-1}, both with a step size of 10 cm^{-1}. The maximum value of the spacing was selected to exceed the shift to the Raman gain peak. A total span larger than ~3000 cm^{-1} (shortest wavelength: ~750 nm) is uninteresting in practice because the fibre loss increases steeply and the shortest wavelength of suitable commercially available high-power diode lasers now or in the foreseeable future is around 790 nm.

(a)

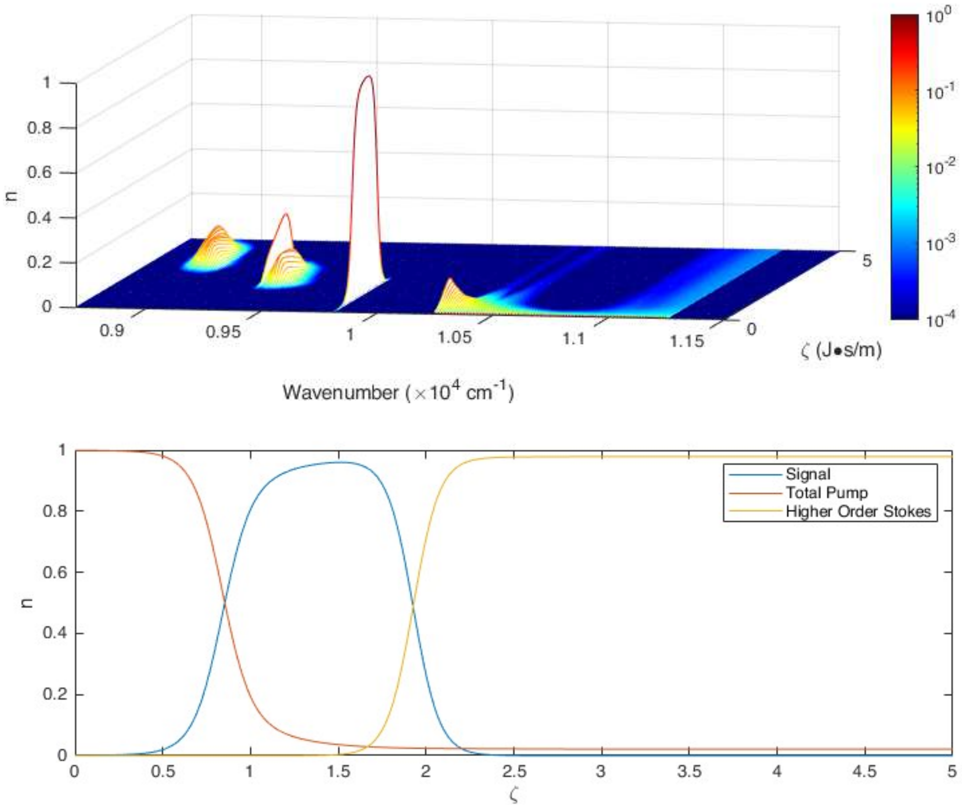
n
0
0.2
0.4
0.6
0.8
1
0.9
0.95
1
1.05
1.1
1.15
Wavenumber ($\times 10^4$ cm^{-1})
0
5
ζ (J•s/m)
10^0
10^{-1}
10^{-2}
10^{-3}
10^{-4}
Signal
Total Pump
Higher Order Stokes
n
0
0.2
0.4
0.6
0.8
1
0
0.5
1
1.5
2
2.5
3
3.5
4
4.5
5
ζ

(b)

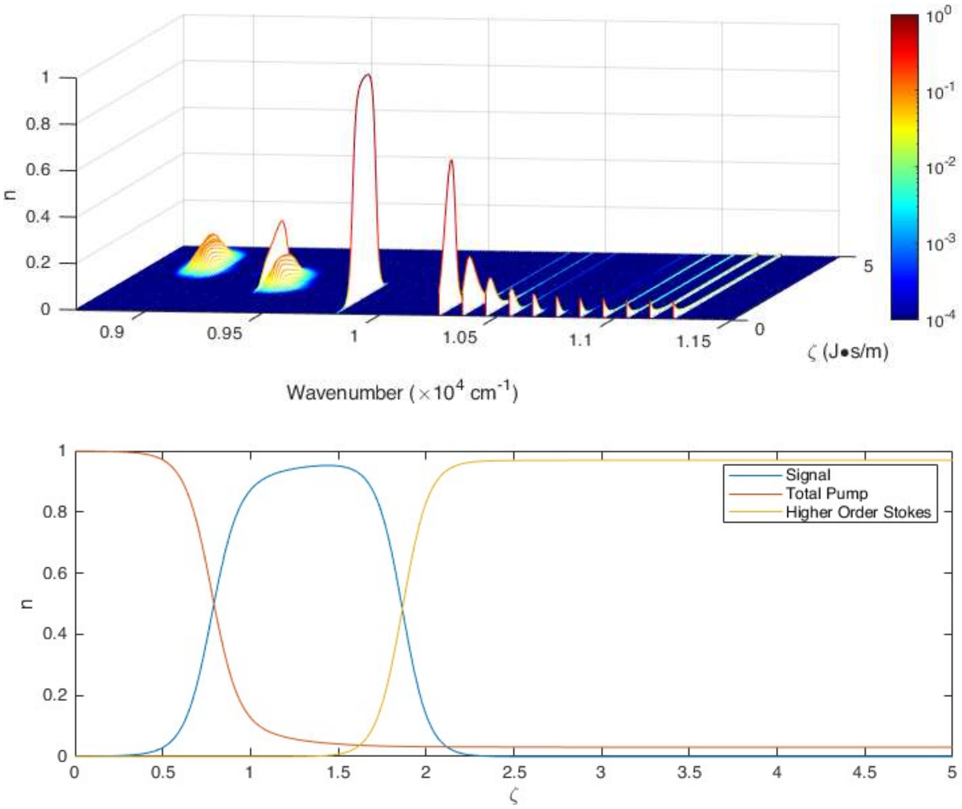
n
0
0.2
0.4
0.6
0.8
1
0.9
0.95
1
1.05
1.1
1.15
Wavenumber ($\times 10^4$ cm^{-1})
0
5
ζ (J•s/m)
10^0
10^{-1}
10^{-2}
10^{-3}
10^{-4}
Signal
Total Pump
Higher Order Stokes
n
0
0.2
0.4
0.6
0.8
1
0
0.5
1
1.5
2
2.5
3
3.5
4
4.5
5
ζ

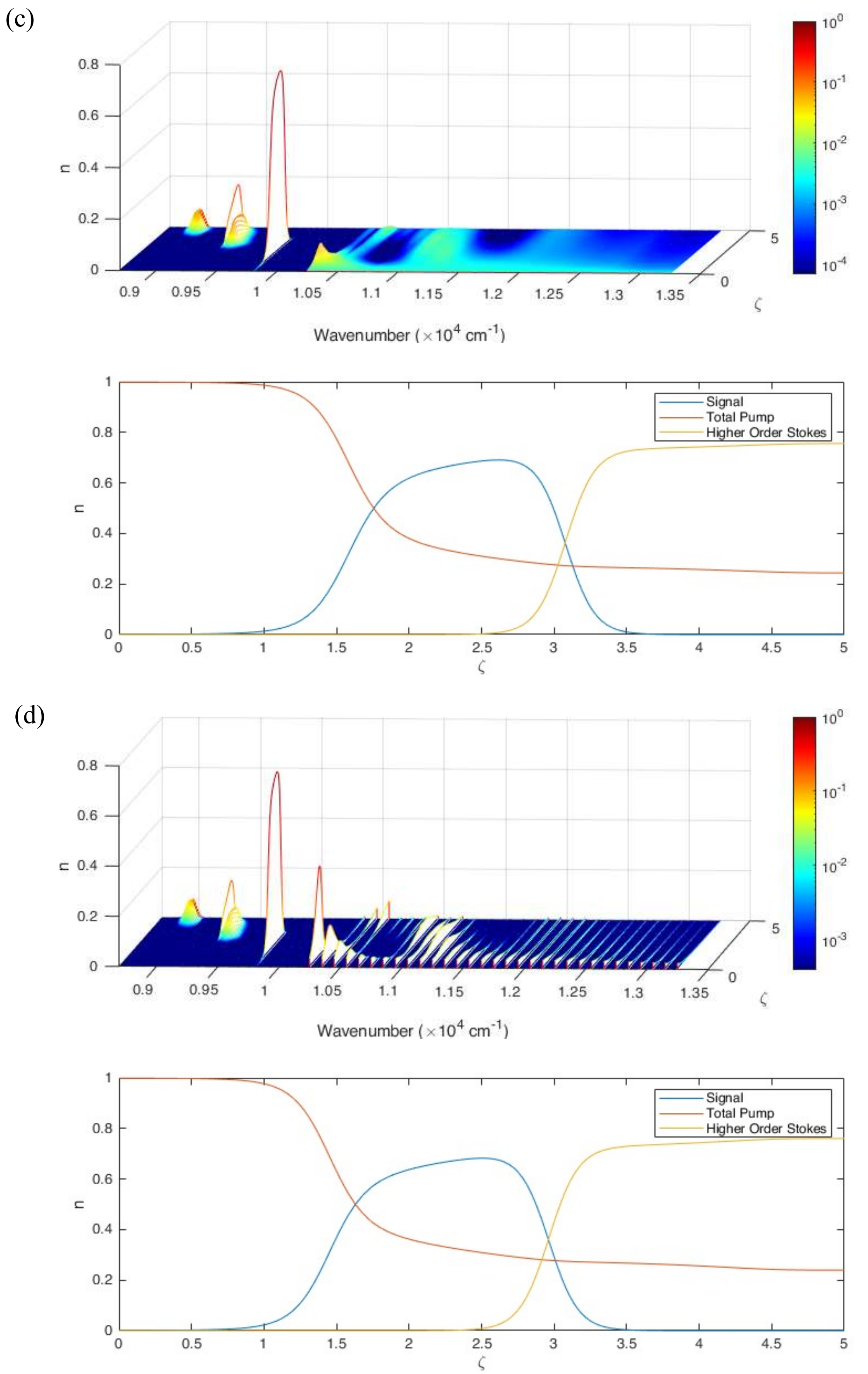

Figure 5.13 (TOP) Spectral evolution of pump and Stokes waves (note that the axis is in wavenumbers rather than wavelength) and **(BOTTOM)** the pump, the signal, and the higher order Stokes power *vs.* ζ for different total spans and spacings of **(a)** 1000 cm^{-1}, 10 cm^{-1} **(b)** 1000 cm^{-1}, 100 cm^{-1} **(c)** 3000 cm^{-1}, 10 cm^{-1} **(d)** 3000 cm^{-1}, 100 cm^{-1}.

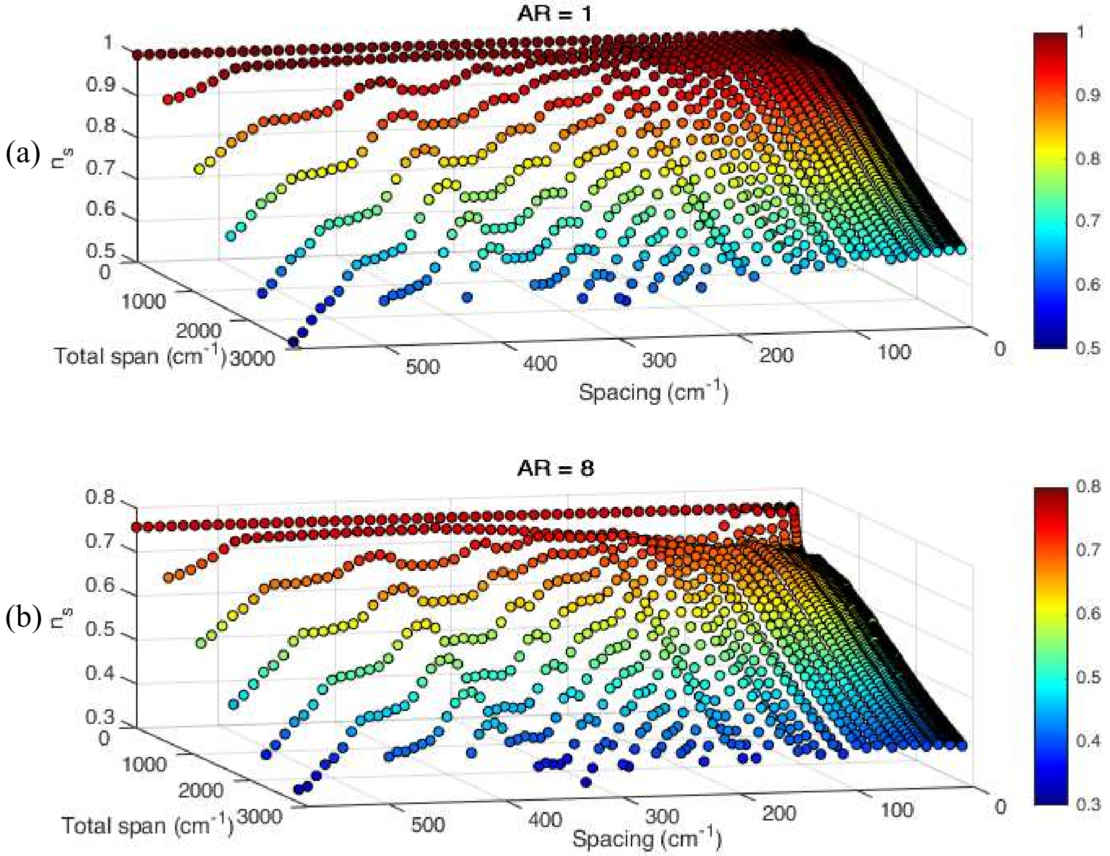

Figure 5.14 Quantum conversion efficiency at optimum fibre length *vs*. span and spacing for AR of **(a)** one and **(b)** eight.

The data points are sparse in some places, because an increase of the total span only increases the number of pump wavelengths once it reaches an integer multiple of a considered spacing. Thus, each of the stripes seen at the wide-spacing end corresponds to a certain, small, number of pump wavelengths.

What stands out at first sight in **Figure 5.14(a)** is that the efficiency stays uniformly high (>95%) over a broad region where the total span and the spacings are smaller than ~1000 and ~200 cm^{-1} as well as the total span less than 800 cm^{-1} for wider spacings. Also remarkably, almost no differences are noticeable for spacings narrower than 100 cm^{-1}. This suggest that a multi-wavelength pump spaced narrower than 100 cm^{-1} and a continuously broad pump are effectively the same, at least, for the AR of 1 in this case of negligible loss.

Consider next the AR of eight (**Figure 5.14(b)**). In this case, the efficiency slightly increases for the wider spacings, especially in the region where the total span is between

120 and 1000 cm^{-1} (e.g., the span-spacing point of 600 and 200 cm^{-1} has 71% of the efficiency which is 5% higher than that of 500 and 10 cm^{-1}). Nevertheless, a good efficiency (65%), which seems not prohibitively smaller than that with single-wavelength pumping (75%), is still achieved for a span of 1000 cm^{-1} even with the AR of eight. Remember also that this is the quantum conversion efficiency, whereas the larger quantum defect at shorter wavelengths makes the power conversion efficiency comparatively lower.

The reason for the increase of the efficiency with the wider spacing at the span of 100-400 cm^{-1} is the smaller number of wavelength. In other words, Narrowly spaced cases (hence, many wavelengths) has significant power at around 60 – 330 cm^{-1} away from the primary pump frequency (10250 cm^{-1} or 976 nm) where SRS interactions with the 976-nm pump as well as with the 1st-Stokes signal is weak [11] (**Sect. 3.3**). It was seen that this region tended to be unpopulated by pumps when the pump wavelengths were optimised and dissimilar spacings were allowed [12] (**Sect. 5.2.2**, **Figure 5.8**). The same happens for unity AR but it is less pronounced than for the bigger ARs

Regardless of the AR, the efficiency reduces as the total span widens except where the span is between 250 and 500 cm^{-1} for narrow spacings. The widening of the spacing also reduces the efficiency when it exceeds the Raman peak separation but, before that, the efficiency can increase for wider spacings, especially in regions near 400 cm^{-1}. The reason is the same as discussed as in the previous paragraph.

I next redraw the data of **Figure 5.14** to more clearly show the effect of the number of pump wavelengths. Thus, **Figure 5.15** depicts the conversion efficiency *vs.* the total pump span for the different number of pump wavelengths when the wavelengths are equally spaced within the given total span. The exact frequencies used in the model are rounded to the nearest 10 cm^{-1} (*e.g.*, for the case of four wavelengths and total span of 1000 cm^{-1}, the frequencies are 10250, 10580, 10920, and 11250 cm^{-1} as the two middle values are rounded from 10583 and 10916 cm^{-1}). As the Raman gain spectrum I used is only 1350 cm^{-1} broad (there is no Raman gain for larger shifts), the cases of two pump wavelengths show no contribution by the added pump wavelength when the span is bigger than 1350 cm^{-1} (and 2700 cm^{-1} for three wavelengths). The slight increase after 1350 cm^{-1} is due to the reduction of the total photon flux ($\mathbb{N}$), which compensates for the shorter wavelength's higher photon energy.

Figure 5.15(b) shows that a lower number of pumps at discrete wavelengths is more efficient than a continuous pump for total spans narrower than 1000 cm^{-1}. This is also observed in **Figure 5.15(a)** although the effect is quite small as the overall efficiency remains high anyway. The reason for this is the same as mentioned before, i.e., that the case of a smaller number of wavelengths happens to have less power in less efficient wavelength regions. As the span widens, a more densely spaced pumps at a larger number of wavelengths and the continuous case (with an infinite number of wavelengths) become more efficient. The cases of the fewer wavelengths are spikier because the peaks in Raman spectrum are more directly projected to them as they have fewer routes to be converted into the signal.

Figure 5.16(a) shows the efficiency *vs.* AR for single-wavelength pumping. This has been shown previously in ref.[21], although it is here plotted in terms of the photon conversion efficiency. As the AR increases from 1 to 12, the efficiency (i.e., the photon conversion efficiency) drops from 100% to ~60%. These values set the upper-limit efficiency for each AR with multi-wavelength pumping as seen in **Figure 5.15(b)**. no line could surpass the dotted line because the efficiency of multi-wavelength pumping cannot exceed that of single-wavelength pumping in the lossless case with infinite FoM.

To visualise the impact of the AR on the conversion efficiency, spans that allow for 70% efficiency for each AR from 1 to 12 are plotted against the spacing in **Figure 5.16(b)**. As the dataset is not complete (*i.e.*, not all the spacing and the total span points are assigned to an efficiency value because there is no new added pump wavelength), the data was

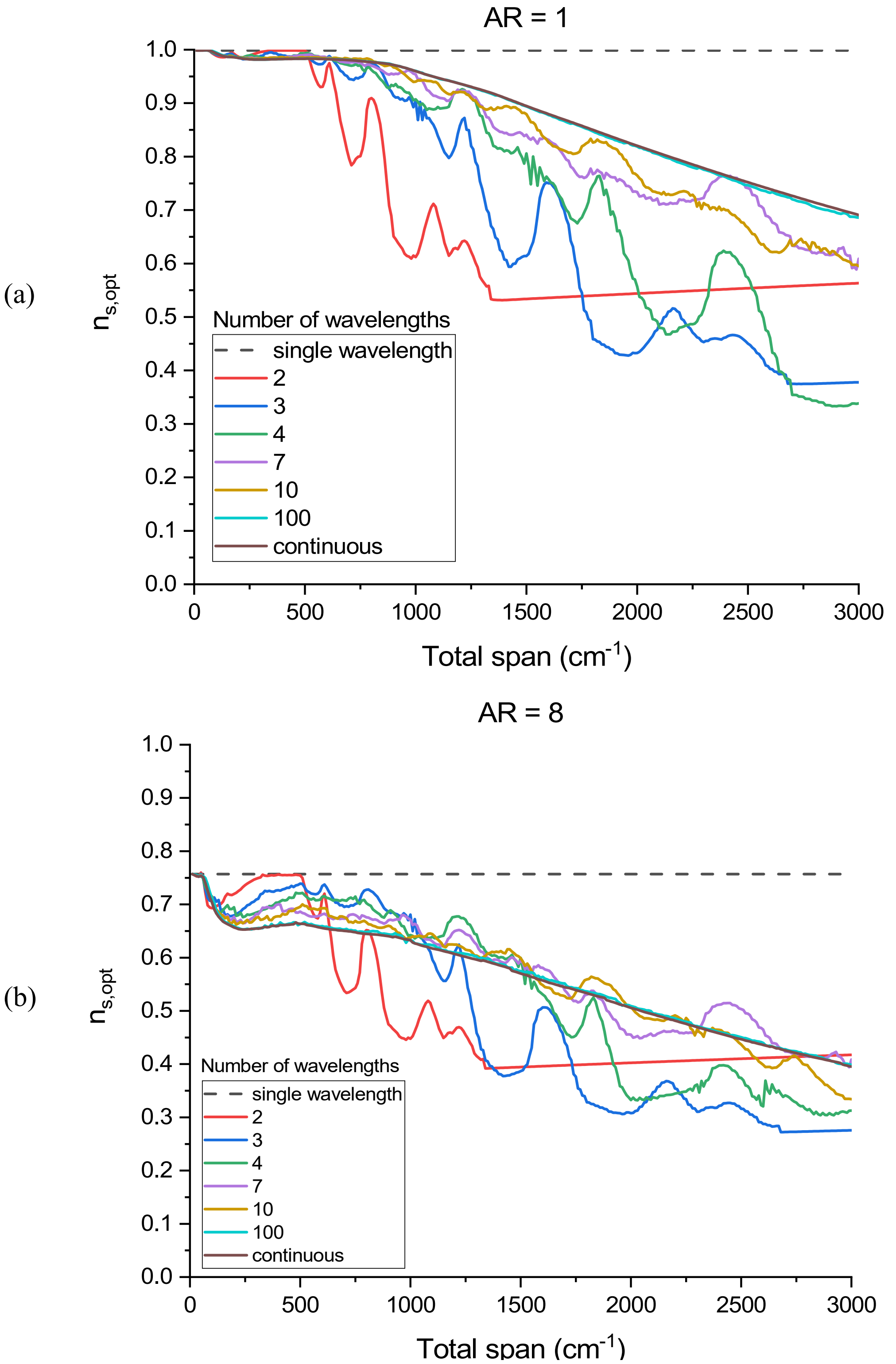

Figure 5.15 Quantum conversion efficiency *vs.* the total pump span of the different number of pump wavelengths for the AR of **(a) 1** and **(b) 8**. Wavelengths are equally spaced within the given total span.

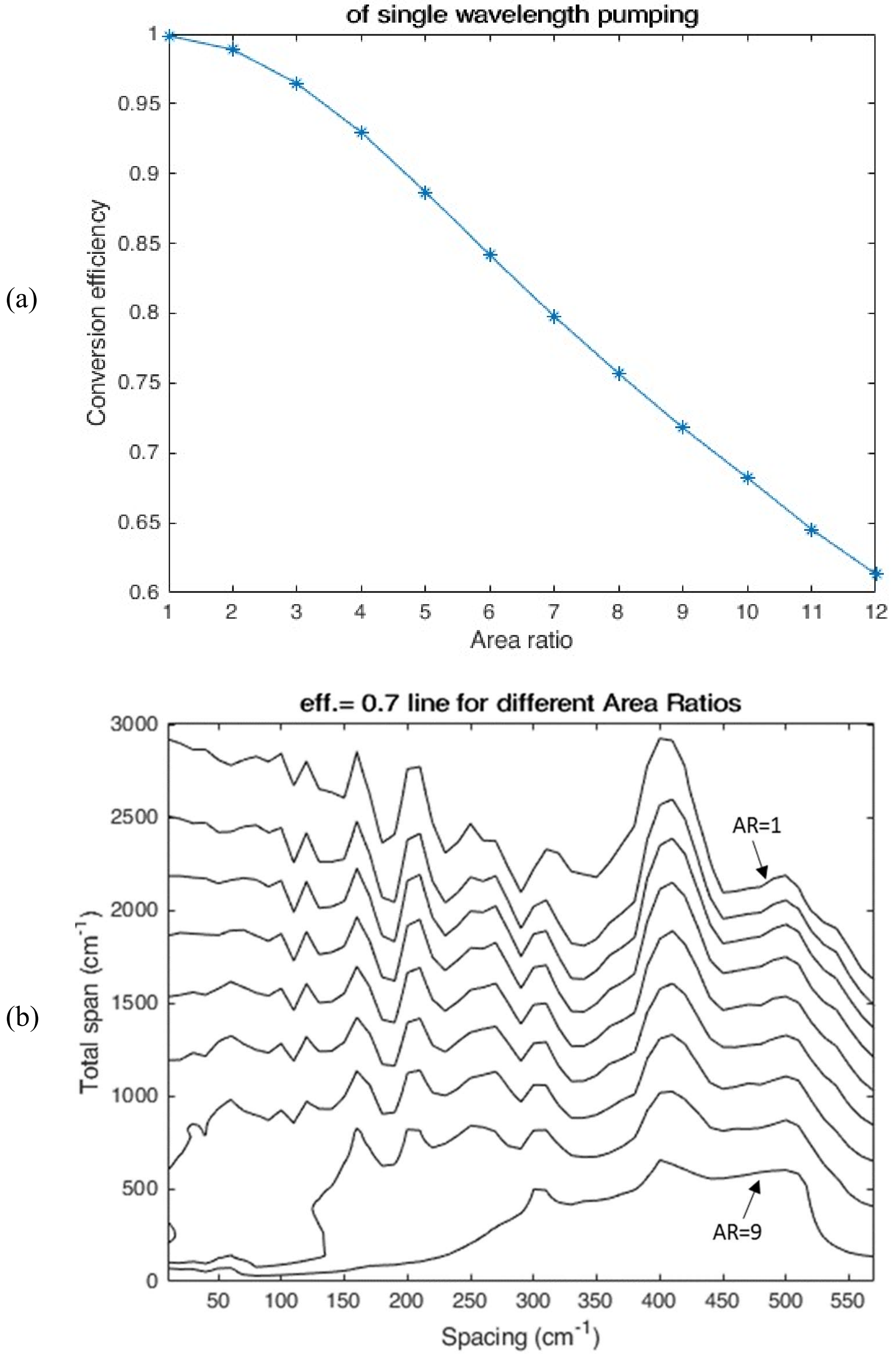

Figure 5.16 (a) Quantum conversion efficiency *vs.* the AR of the single-wavelength pumping. Plotted in terms of the photon conversion efficiency in accordance with the **Eq. (5.5)** **(b)** The contours that marks 70% of the efficiency for each ARs from 1 to 12. Plotted against the total span and the spacing.

linearly interpolated in the direction of the total span. This means that, e.g., at 600 cm^{-1} of total span and 400 cm^{-1} spacing, there is no original data point because no new pump wavelength is being added for a 600 cm^{-1} span. Therefore, it is assigned a conversion efficiency linearly interpolated from the cases of two-wavelength (span = 400 cm^{-1}, spacing = 400 cm^{-1}) and three-wavelength pumping (span = 800 cm^{-1}, spacing = 400 cm^{-1}). The filled data points, although they do not have a direct physical realisation, can be loosely translated into the cases where a fraction of pump power is injected at the wavelength that is to be added next. The efficiency at the (span = 600 cm^{-1}, spacing = 400 cm^{-1}) point would be similar to the efficiency of the case where two full powers are at first and second wavelength and the half of that power is added to the third wavelength.

It is seen in **Figure 5.16(b)** that the region made of the total spans and spacings that result in at least 70% photon conversion efficiency becomes smaller as the AR increases. The AR above 9 is not shown in the plot because it is no longer possible to reach 70% efficiency even with single-wavelength pumping. Note that the AR of 8 and 9 can still reach 70% but only with two wavelengths spaced near the Raman peak separation, as they cannot afford the less efficient wavelength addition near 250 cm^{-1}.

Now, in order to estimate the scalability of the output power regarding both spatial (the AR) and spectral domain (the total span and the spacing) together, I define a parameter, calling it pump-multiplier (PM), that is the product of the AR and the number of pump wavelengths. The amount of (pump) power that can be launched into a fibre from a (pump) laser is limited by the V number of the fibre (i.e., its cladding in case of cladding-pumping) and the brightness of the laser. Assuming the pumps at different wavelengths have the same brightness, the maximum launched total pump power is proportional to the number of wavelegnths and the area of cladding (this is proportional to the AR, since I assume a fixed core size). In other words, the parameter is a multiplier for the unit pump power (the optically allowed power per one wavelength, per core area (when AR=1)) to determine the maximum total pump power that can be lauched. Also, the PM is inversely proportional to the spacing for a given span, so a narrower spacing can expect a higher output power, but not necessarily with a higher conversion efficiency.

Figure 5.17 displays the conversion efficiency and the scalability *vs.* the PM for the AR of 1, 3, 5, … , 11 with the spacing of 50, 100, 200, and 400 cm^{-1}. The black dotted lines indicate 100% conversion efficiency. The scalability is the product of the efficiency and

(a)

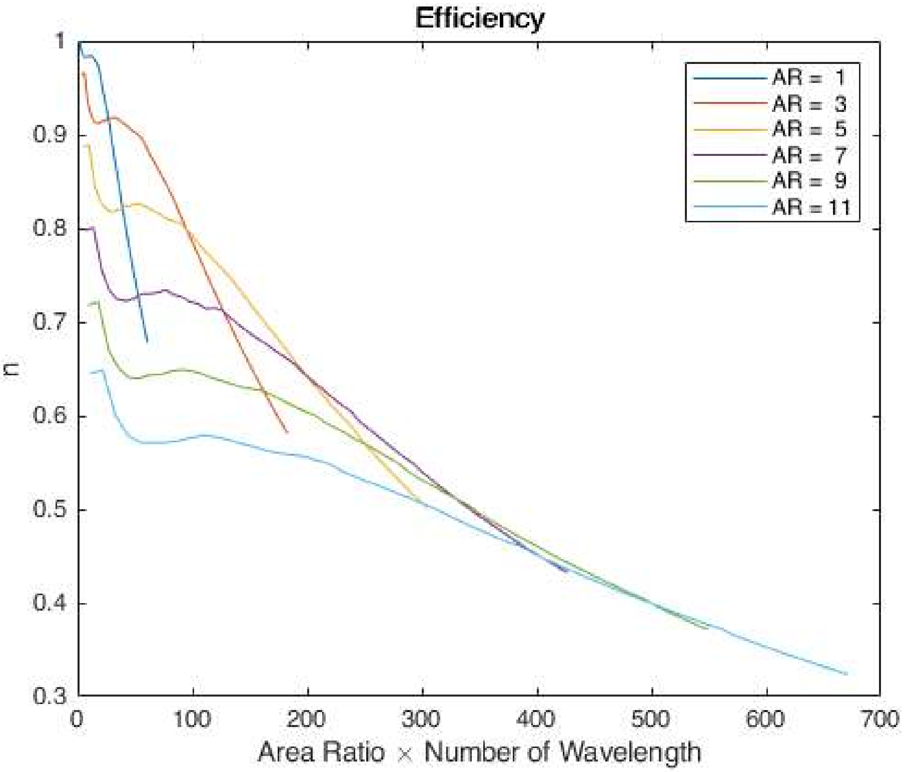
Efficiency
1
0.9
0.8
0.7
0.6
0.5
0.4
0.3
n
0
100
200
300
400
500
600
700
Area Ratio × Number of Wavelength
AR = 1
AR = 3
AR = 5
AR = 7
AR = 9
AR = 11

(b)

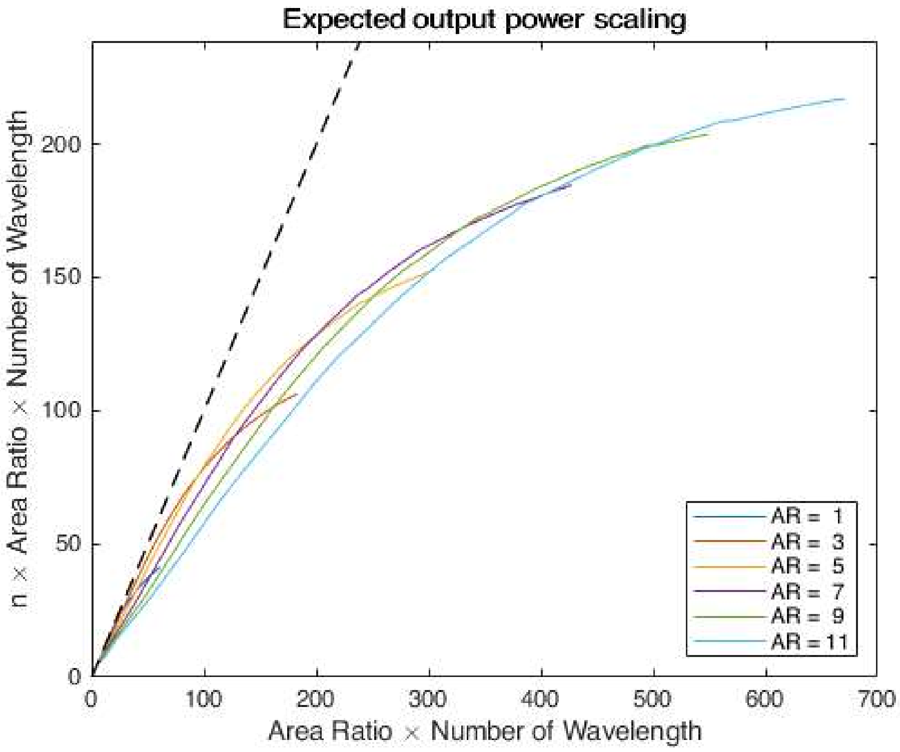
Expected output power scaling
200
150
100
50
0
n × Area Ratio × Number of Wavelength
0
100
200
300
400
500
600
700
Area Ratio × Number of Wavelength
AR = 1
AR = 3
AR = 5
AR = 7
AR = 9
AR = 11

(c)

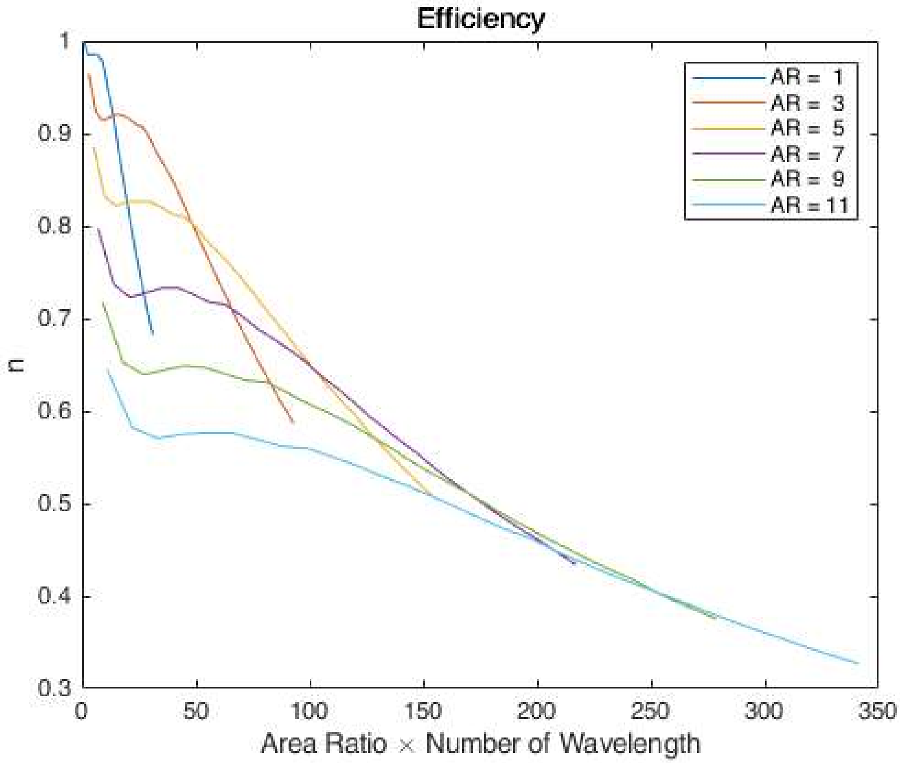
Efficiency
n
Area Ratio × Number of Wavelength
AR = 1
AR = 3
AR = 5
AR = 7
AR = 9
AR = 11
0.3
0.4
0.5
0.6
0.7
0.8
0.9
1
0
50
100
150
200
250
300
350

(d)

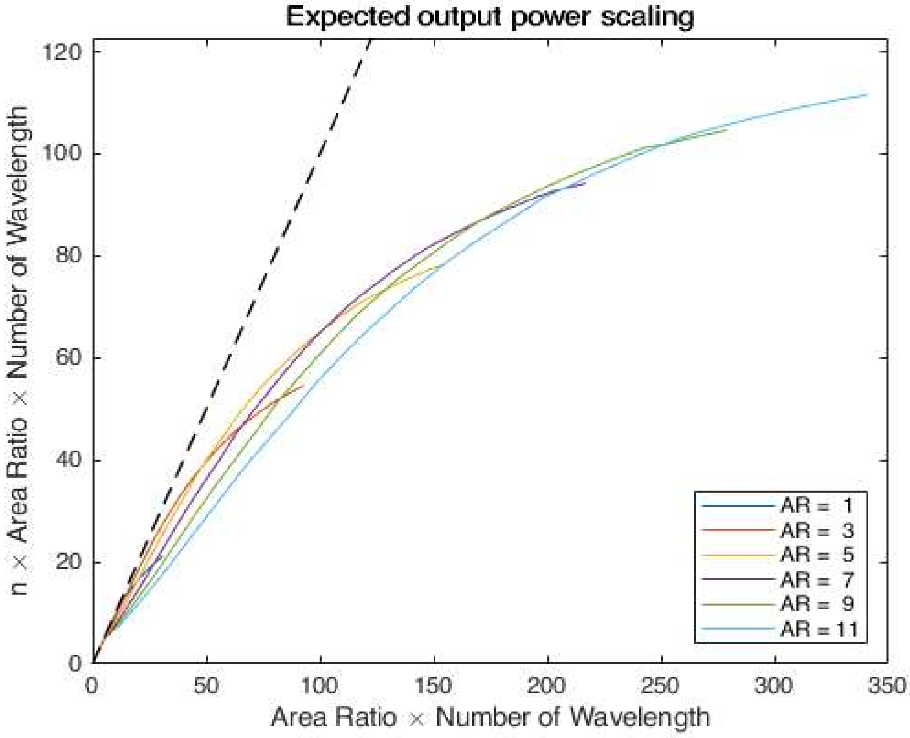
Expected output power scaling
n × Area Ratio × Number of Wavelength
Area Ratio × Number of Wavelength
AR = 1
AR = 3
AR = 5
AR = 7
AR = 9
AR = 11
0
20
40
60
80
100
120
0
50
100
150
200
250
300
350

(e)

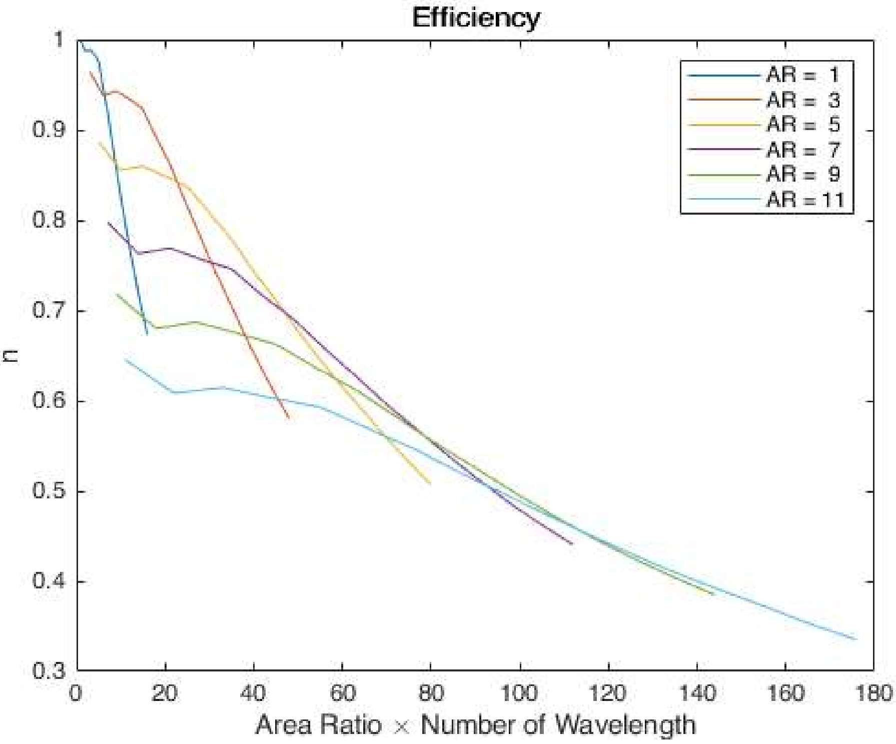
Efficiency
n
Area Ratio × Number of Wavelength
1
0.9
0.8
0.7
0.6
0.5
0.4
0.3
0
20
40
60
80
100
120
140
160
180
AR = 1
AR = 3
AR = 5
AR = 7
AR = 9
AR = 11

(f)

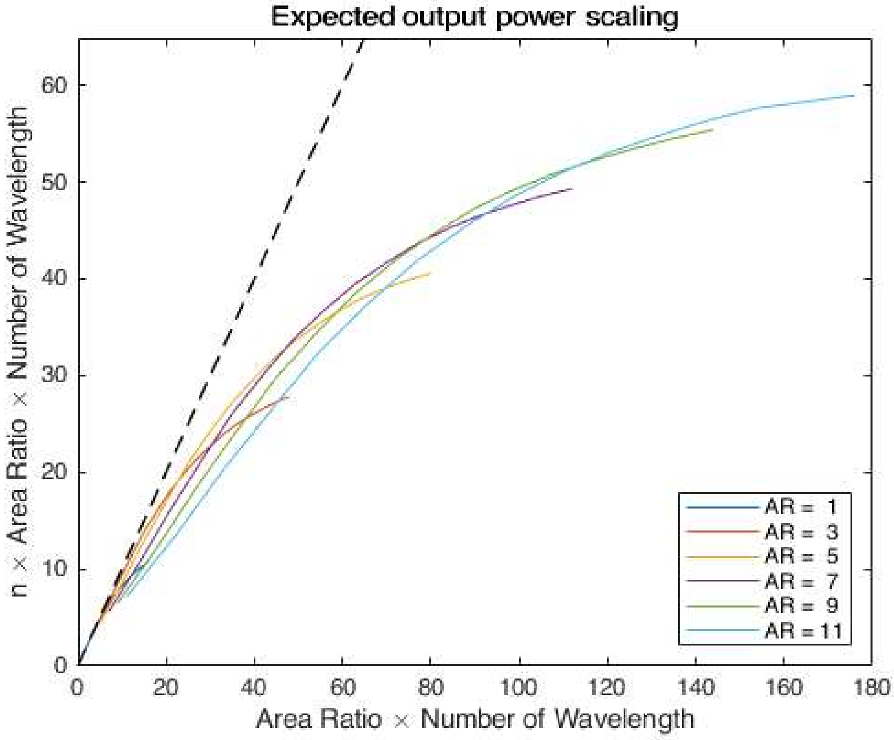
Expected output power scaling
n × Area Ratio × Number of Wavelength
Area Ratio × Number of Wavelength
60
50
40
30
20
10
0
0
20
40
60
80
100
120
140
160
180
AR = 1
AR = 3
AR = 5
AR = 7
AR = 9
AR = 11

(g)

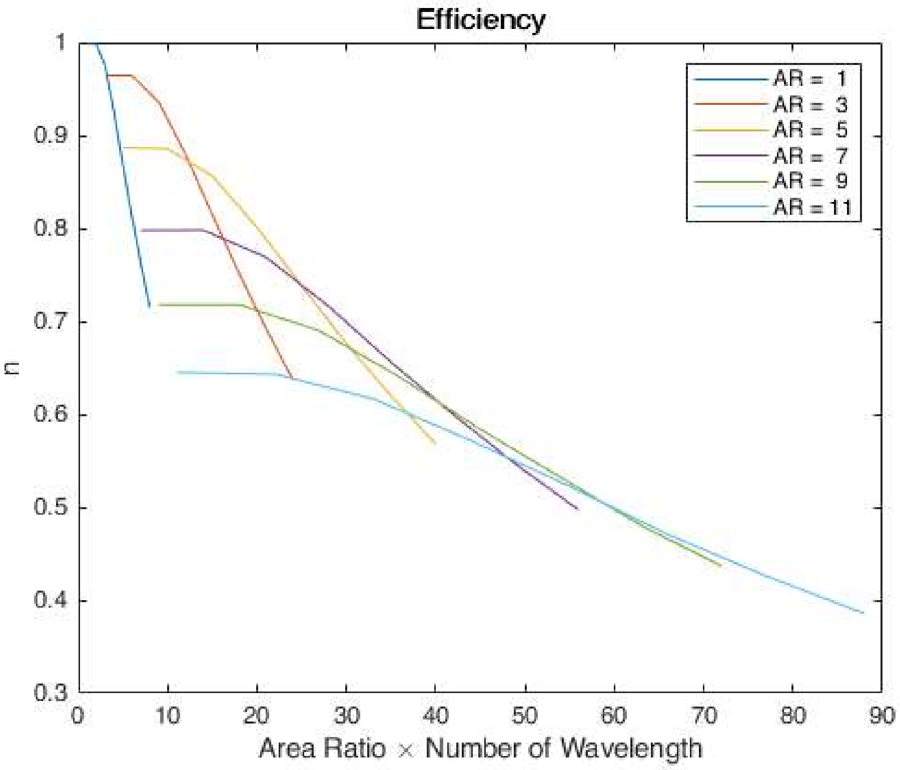

(h)

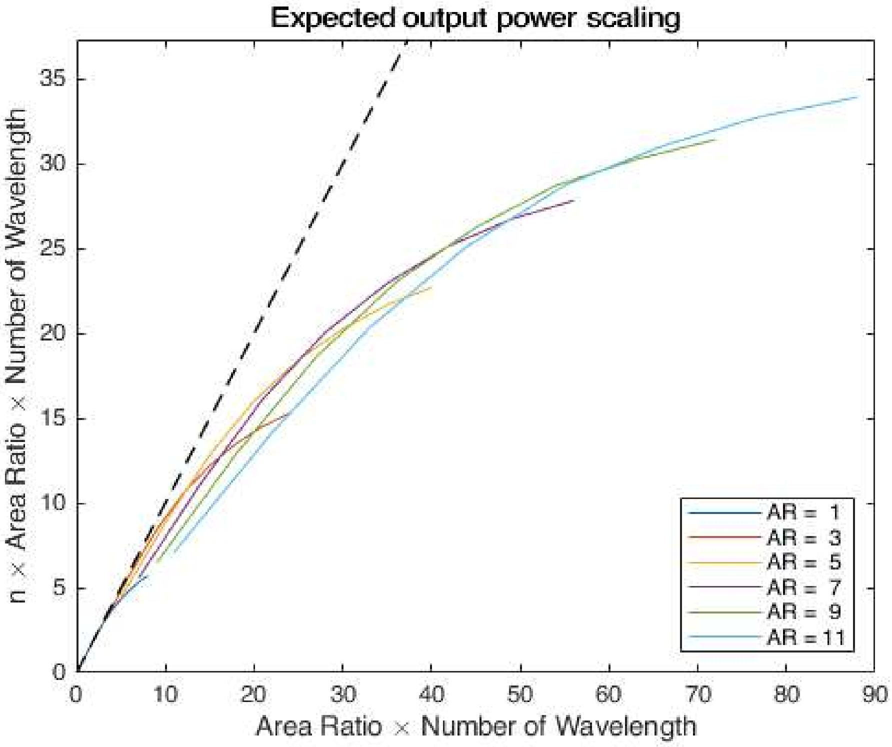

Figure 5.17 **(a, c, e, g)** Photon conversion efficiency and **(b, d, f, h)** and power scaling *vs.* AR times the number of pump wavelengths for the AR of 1, 3, … , 11 with the spacing of **(a, b)** 50, **(c, d)** 100, **(e, f)** 200, and **(g, h)** 400 cm^{-1}. The black dotted lines in **(b, d, f, h)** indicate a 100%-efficiency line.

the PM. This equals the output power divided by the unit pump power (the optically allowed power per one wavelength, per the area of core (when AR=1)). Therefore, it means how many times of the unit pump power the signal can reach with a given AR and number of pump wavelengths.

Although the increase of the AR reduces the overall efficiency, it is not always the unity AR that gives the best efficiency at a certain PM. Instead, an optimum pair of AR and number of wavelengths can be always found for a certain PM (e.g., the AR of 2 is better than other values of AR around a PM of 50 for 50-cm^{-1} spacing in **Figure 5.17(a)**).

The shape of the curves of the same spacings in **Figure 5.17** are similar to each other regardless of the AR. For sufficiently small spacings (except for 400 cm^{-1} in **Figure 5.17**), the efficiency drops sharply as the PM increases from its smallest value (equal to the AR, with a single pump wavelength). There is then a plateau before it gradually drops again, drawing something that looks like a shoulder. More importantly, it is found that the shoulders are formed around where the total span is 600-800 cm^{-1} regardless of AR and spacing within the range of interest (spacing < 570 cm^{-1}). Therefore, the number of pump wavelengths that leads to ~800 cm^{-1} of total span produces a good compromise between highest output power and efficiency for a given pump spacing for the considered ARs.

The scalability graphs (**Figure 5.17(b, d, f, h)**) give another view of the effect of increasing the AR. Increased AR, indeed, gives a higher output power though the increment by a higher PM becomes smaller for higher PM. The increment reduces further and eventually the output power does not grow at all beyond the AR of ~16 (not shown here). Overall, increasing the AR beyond ~7 appears to provide only marginal benefits as the efficiency drops quickly which is in line with ref.[2]. This is also shown **in Figure 5.18**.

Experimentally, around 50 W per diode laser at a wavelength could be launched into 50 – 60 μm diameter and 0.2-0.3 NA fibre in chapter 3 and chapter 4. This means the unit pump power is around 50 W for this configuration and the numbers in both axes in the scalability graphs in **Figure 5.17** can be multiplied by 50 W to convert the plots into power. For example, the output power can reach 2.7 kW pumped with 3 kW (conversion efficiency of 89%) when the AR is 3 and twenty pump wavelengths (150 W each) are equally spaced over ~100 nm for the given fibre specification (**Figure 5.17(a)** and **(b)**).

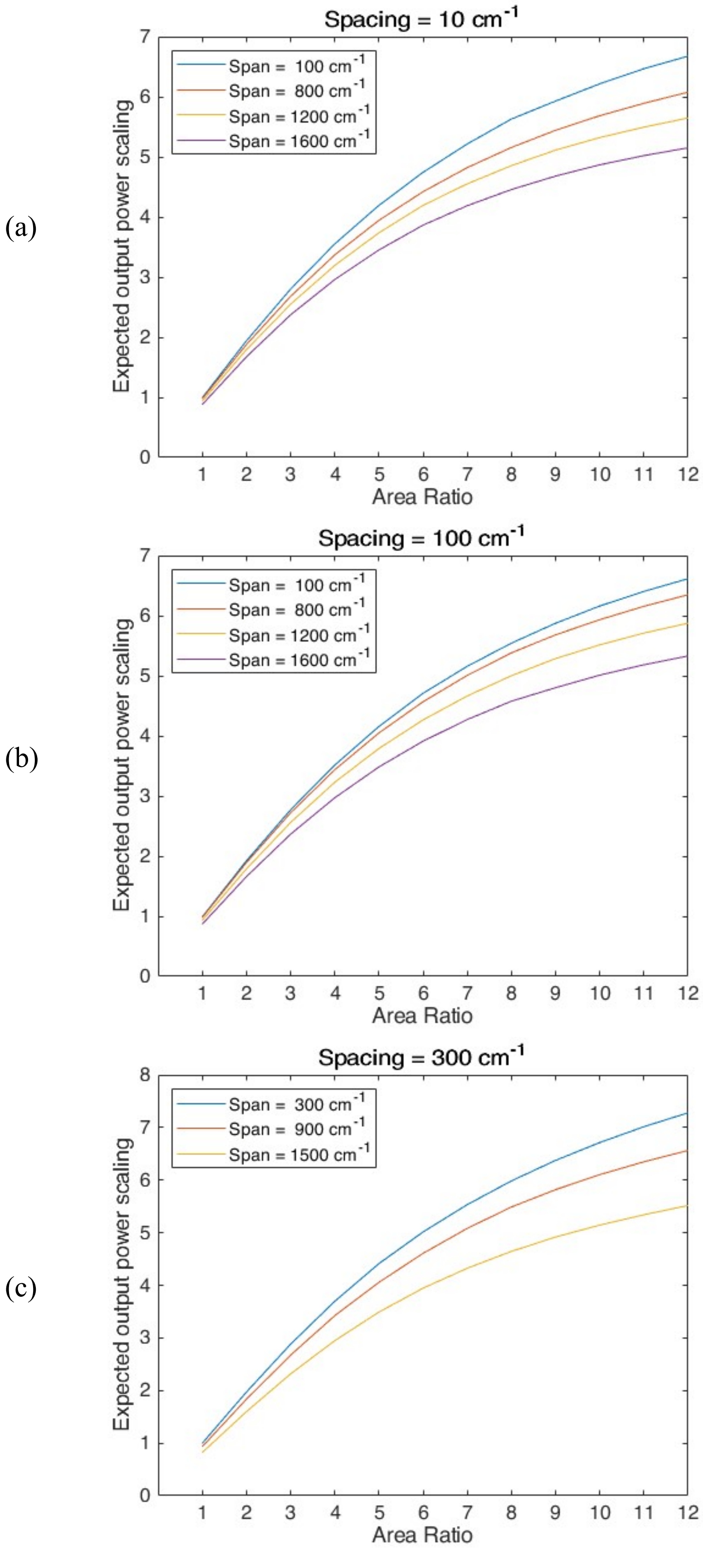

Figure 5.18 Expected output power scaling *vs.* area ratio when the total pump power is proportional to the area ratio for the cases of spacing of **(a)** 10, **(b)** 100, and **(c)** 300 cm^{-1} and total span as specified in legends.

5.3.3 The optimised length and lossy fibres

The analysis of the area ratio and the pump multiplier assumed that the loss is negligible. In reality, when loss is introduced, the total loss may be approximately proportional to the optimised fibre length calculated in the lossless cases. There is, however, a discrepancy which comes from the fact that the fibre loss impedes the growth of signal which changes the optimised length smaller value, which in turn reduces the total loss. I assume the change in optimum length is small and thus that the resulting discrepancy is much less than the estimation (the optimum length of fibre calculated in lossless cases × the background loss).

Figure 5.19 shows the optimised length, ζ_{opt} of lossless fibre *vs.* PM for the AR of 1, 3, … , 11 with the spacing of 50, 100, 200, and 400 cm^{-1} (same conditions as in **Figure 5.17**). The shoulders in **Figure 5.17** corresponds to bumps in **Figure 5.19**. The optimised length is smaller for larger efficiency within the same AR. For the single wavelength cases (the starting points of each curves), the optimised scaled length ζ_{opt} [J•s/m] differs by about 1 J•s/m for when the AR increases by 2. The gaps among the curves reduce as the span exceeds 800 cm^{-1} where the bumps (or the shoulders in **Figure 5.17**) end and the drop in the efficiency becomes steeper.

If the total pump power of 1.2 kW is launched into 50-μm-diameter core, the coefficient between ζ and z (*i.e.*, $h\mathbb{N}/A_{core}$, from **Eq. (5.6)**) becomes 1.75×10^{-3} J•s/m^2. In other words, 1 J•s/m of ζ converts to 572 m of actual length in this condition. Therefore, **Figure 5.19** suggests that the optimal fibre length is about 572 m for the AR of 1 and increases by 250 - 300 m per unit increase of AR within the span of 800 cm^{-1}. The loss of commercial fibre, such as the GRIN fibre in chapter 3 and chapter 4, is around 1.5 – 3 dB/km although it depends on wavelength and mode-excitation. Therefore, with the given total power input and fibre specification, the AR of 1 will see 0.8-1.6 dB of loss and 0.4-0.8 dB will be added, approximately, for a unity increase in AR.

(a)

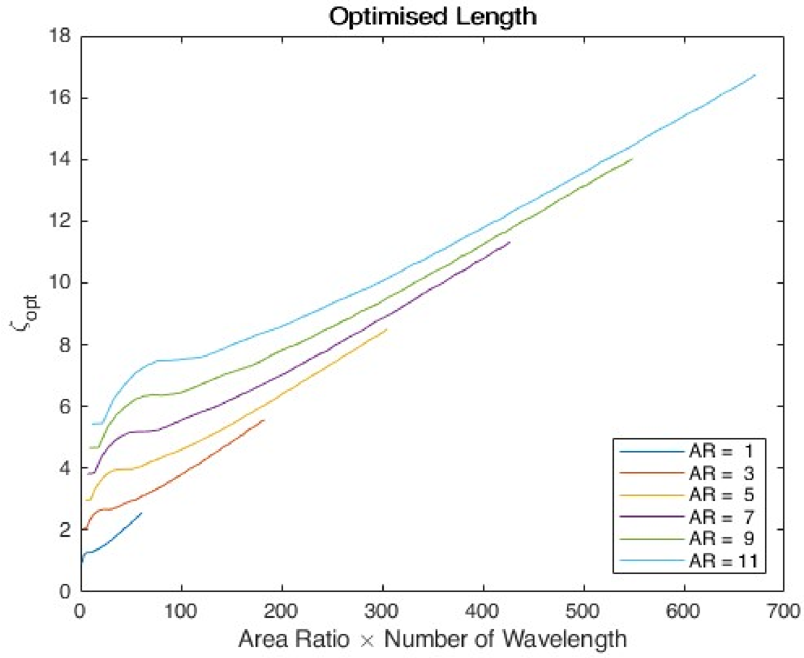
Optimised Length
ζ_{opt}
0
2
4
6
8
10
12
14
16
18
0
100
200
300
400
500
600
700
Area Ratio × Number of Wavelength
AR = 1
AR = 3
AR = 5
AR = 7
AR = 9
AR = 11

(b)

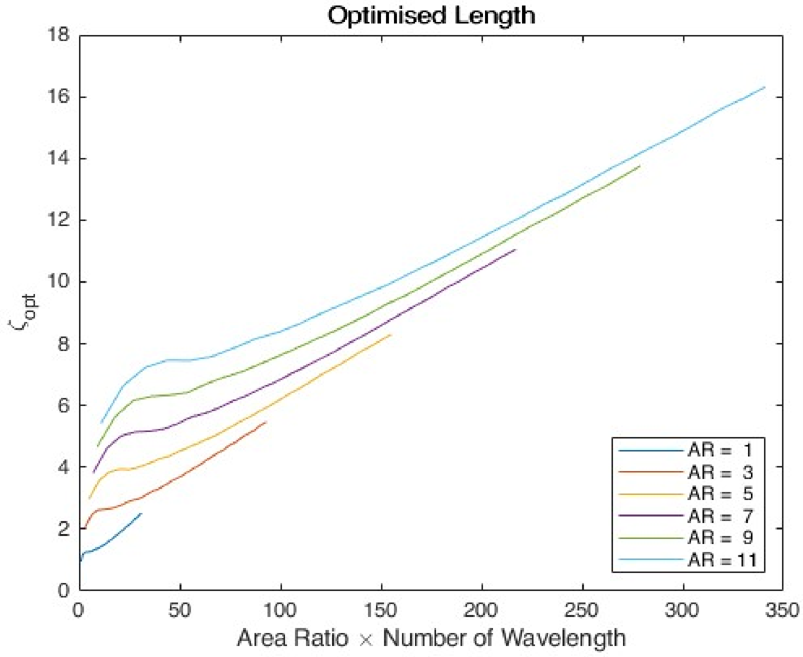
Optimised Length
ζ_{opt}
0
2
4
6
8
10
12
14
16
18
0
50
100
150
200
250
300
350
Area Ratio × Number of Wavelength
AR = 1
AR = 3
AR = 5
AR = 7
AR = 9
AR = 11

(c)

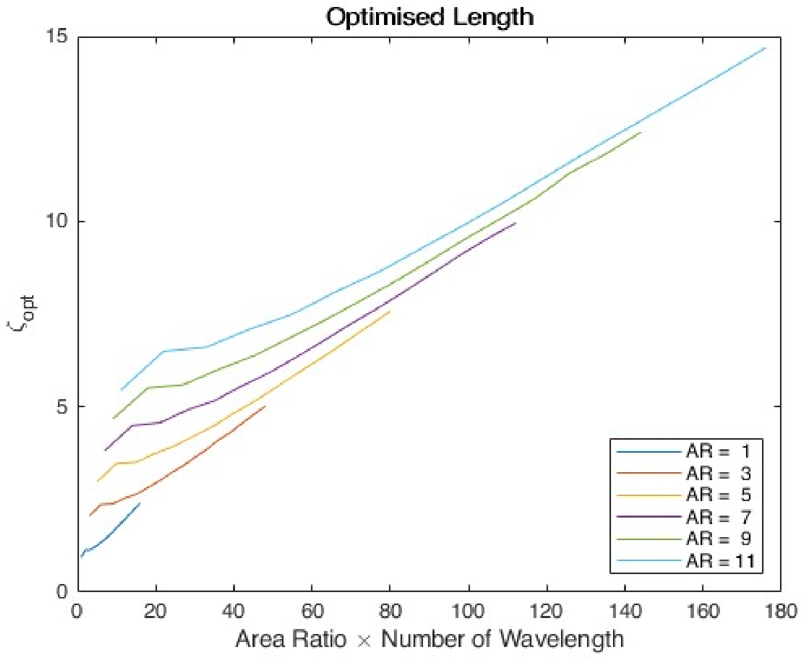

(d)

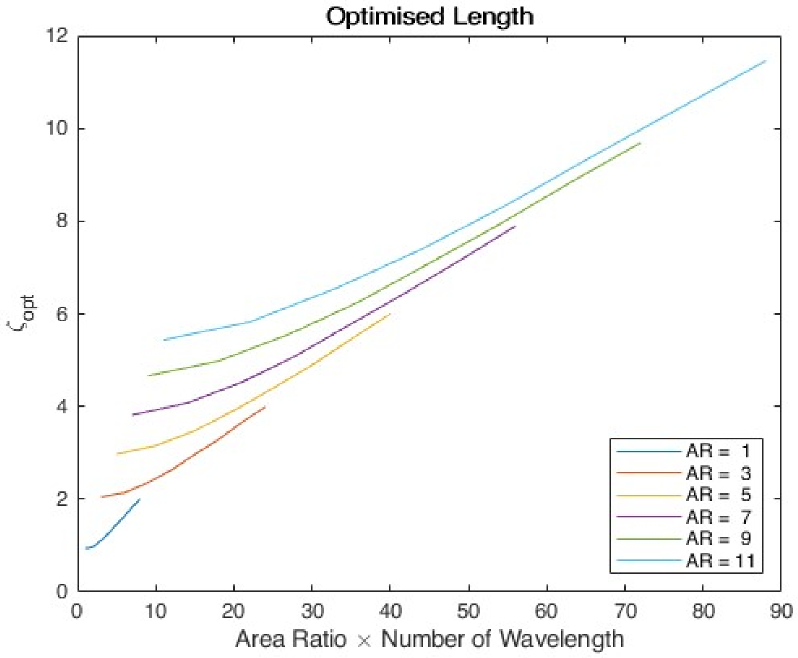

Figure 5.19 The optimised length of fibre *vs.* AR times the number of pump wavelengths for the AR of 1, 3, … , 11 with the spacing of **(a)** 50, **(b)** 100, **(c)** 200, and **(d)** 400 cm^{-1}.

5.4 Summary

Simulations on multi-wavelength pumping of double-clad FRA are conducted with two sets of assumptions. In the first set, up to ten diode lasers of various FoM at different wavelength pumped an FRA with the area ratio of eight. In the second set of assumptions, diode lasers of an infinite FoM (*i.e.*, a lossless fibre), whose wavelength spacings are fixed, pumped FRAs of different total spans and pump wavelength spacings as well as area ratio.

Both simulations suggest that efficient multi-wavelength pumped FRAs are possible with broad pump bandwidth up to ~1000 cm^{-1}. The efficiency improves for higher pump intensity through the reduction of the fibre length and thus the loss. In addition, the simulations with the first set of assumptions show that the optimisation of the wavelength-spacing can improve the efficiency by a few percent. Simulations with the second set of assumptions show that, although the maximum area ratio trades off against the pump bandwidth, up to the area ratio of seven still shows a good efficiency (above 70%) for up to ~800 cm^{-1} of the total pump bandwidth. This is not a big drop compared to the single-wavelength pumping case, where a limit of eight is often assumed for the area ratio.

This chapter established general guidelines and scaling laws for multi-wavelength pumping of fibre Raman amplifiers, including those that are cladding-pumped. The scaled parameters, e.g., in **Figure 5.17**, can be transformed to actual input and output powers in any step-index fibre cases. For example, if the unit pump power (the launchable pump power per wavelength, per core area) is around 50 W (this is true when the core size is around 50 μm and NA is around 0.3 as in experiments in **chapter 4**) the output power can reach 2.7 kW pumped with 3 kW (conversion efficiency of 89%) when the cladding-to-core area ratio (AR) is 3 and twenty pump wavelengths (150 W each) are equally spaced at 5 nm over ~100 nm. Likewise, output powers of multi-wavelength-pumped FRAs at other powers can be predicted with the graphs provided in this chapter.

5.5 References

[1] T. Yao, A. Harish, J. Sahu, and J. Nilsson, “High-Power Continuous-Wave Directly-Diode-Pumped Fiber Raman Lasers,” *Appl. Sci.*, vol. 5, no. 4, pp. 1323–1336, 2015, doi: 10.3390/app5041323.

[2] J. Ji, C. A. Codemard, and J. Nilsson, “Brightness enhancement limits in pulsed cladding-pumped fiber Raman amplifiers,” in *Proc. SPIE, Fiber Lasers VII: Technology, Systems, and Applications*, 2010, p. 75801L, doi: 10.1117/12.844919.

[3] S. Zhu *et al.*, “Multimode-pumped Raman amplification of a higher order mode in a large mode area fiber,” *Opt. Express*, vol. 26, no. 18, p. 23295, Sep. 2018, doi: 10.1364/OE.26.023295.

[4] J. Ji, “Cladding-pumped Raman fibre laser sources,”, University of Southampton, PhD thesis, 2011.

[5] E. A. Zlobina *et al.*, “Generating high-quality beam in a multimode LD-pumped all-fiber Raman laser,” *Opt. Express*, vol. 25, no. 11, p. 12581, 2017, doi: 10.1364/OE.25.012581.

[6] L. Zhang *et al.*, “Kilowatt Ytterbium-Raman fiber laser,” *Opt. Express*, vol. 22, no. 15, pp. 18483–18489, 2014, doi: 10.1364/OE.22.018483.

[7] H. Fritsche *et al.*, “Highly modular high-brightness diode laser system design for a wide application range,” in *Proceedings Volume 9348, High-Power Diode Laser Technology and Applications XIII*, Apr. 2015, p. 93480A, doi: 10.1117/12.2080123.

[8] J. Malchus, V. Krause, G. Rehmann, M. Leers, A. Koesters, and D. G. Matthews, “A 40kW fiber-coupled diode laser for material processing and pumping applications,” in *Proc. SPIE, High-Power Diode Laser Technology and Applications XIII*, 2015, p. 934803, doi: 10.1117/12.2083909.

[9] A. Sanchez-Rubio *et al.*, “Wavelength Beam Combining for Power and Brightness Scaling of Laser Systems,” *Lincoln Lab. J.*, vol. 20, no. 2, pp. 52–66, 2014.

[10] S. Aparanji, V. Balaswamy, S. Arun, and V. R. Supradeepa, “Simultaneous Power Combining and Wavelength Conversion of High Power Fiber Lasers,” in *Laser Congress*

2017 (ASSL, LAC), OSA Technical Digest (online) (Optical Society of America, 2017), 2017, vol. ATu3A.4.

[11] S. Hong, Y. Feng, and J. Nilsson, “Off-Peak Dual-Wavelength Multimode Diode-Laser-Pumped Fiber Raman Laser,” *IEEE Photonics Technol. Lett.*, vol. 30, no. 18, pp. 1625–1628, 2018, doi: 10.1109/LPT.2018.2863559.

[12] N. Zhao, S. Hong, A. V. Harish, Y. Feng, and J. Nilsson, “Simulations of multiwavelength cladding pumping of high-power fiber Raman amplifiers,” *Opt. Eng.*, vol. 58, no. 10, p. 1, 2019, doi: 10.1117/1.oe.58.10.102701.

[13] G. P. Agrawal, *Nonlinear Fiber Optics*, 4th ed. London: Elsevier, 2006.

[14] H. Kanamori *et al.*, “Transmission characteristics and reliability of pure-silica-core single-mode fibers,” *J. Light. Technol.*, vol. 4, no. 8, pp. 1144–1150, 1986, doi: 10.1109/JLT.1986.1074837.

[15] J. P. Koplow, D. A. V. Kliner, and L. Goldberg, “Single-mode operation of a coiled multimode fiber amplifier,” *Opt. Lett.*, vol. 25, no. 7, p. 442, Apr. 2000, doi: 10.1364/OL.25.000442.

[16] S. A. Babin, D. V. Churkin, A. E. Ismagulov, S. I. Kablukov, and E. V. Podivilov, “Four-wave-mixing-induced turbulent spectral broadening in a long Raman fiber laser,” *J. Opt. Soc. Am. B*, vol. 24, no. 8, p. 1729, 2007, doi: 10.1364/josab.24.001729.

[17] W. Liu, W. Kuang, M. Jiang, J. Xu, P. Zhou, and Z. Liu, “Modeling of the spectral evolution in a narrow-linewidth fiber amplifier,” *Laser Phys. Lett.*, vol. 13, no. 3, 2016, doi: 10.1088/1612-2011/13/3/035105.

[18] P. B. Hansen *et al.*, “Rayleigh scattering limitations in distributed Raman pre-amplifiers,” *IEEE Photonics Technol. Lett.*, vol. 10, no. 1, pp. 159–161, 1998, doi: 10.1109/68.651148.

[19] S. A. E. Lewis, S. V. Chernikov, and J. R. Taylor, “Characterization of Double Rayleigh Scatter Noise in Raman Amplifiers,” *IEEE Photonics Technol. Lett.*, vol. 12, no. 5, pp. 528–530, 2000, doi: 10.1109/68.841275.

[20] Bumki Min, Won Jae Lee, and Namkyoo Park, “Efficient formulation of Raman amplifier propagation equations with average power analysis,” *IEEE Photonics Technol. Lett.*, vol.

12, no. 11, pp. 1486–1488, 2002, doi: 10.1109/68.887702.

[21] J. Ji, C. A. Codemard, J. K. Sahu, and J. Nilsson, “Design, performance, and limitations of fibers for cladding-pumped Raman lasers,” *Opt. Fiber Technol.*, vol. 16, no. 6, pp. 428–441, Dec. 2010, doi: 10.1016/j.yofte.2010.09.011.

[22] R. Chang, R. Lehmberg, M. Duignan, and N. Djeu, “Raman beam cleanup of a severely aberrated pump laser,” *IEEE J. Quantum Electron.*, vol. 21, no. 5, pp. 477–487, May 1985, doi: 10.1109/JQE.1985.1072678.

[23] J. Reintjes, R. H. Lehmberg, R. S. F. Chang, M. T. Duignan, and G. Calame, “Beam cleanup with stimulated Raman scattering in the intensity-averaging regime,” *J. Opt. Soc. Am. B*, vol. 3, no. 10, pp. 1408–1427, 1986, doi: 10.1364/josab.3.001408.

[24] J. T. Murray, W. L. Austin, and R. C. Powell, “Intracavity Raman conversion and Raman beam cleanup,” *Opt. Mater. (Amst).*, vol. 11, no. 4, pp. 353–371, 1999, doi: 10.1016/S0925-3467(98)00033-0.

[25] T. Russell, “laser intensity scaling through stimulated scattering in optical fibers,” Air Force Institute of Technology Wright-Patterson, 2001.

[26] T. H. Russell, S. M. Willis, M. B. Crookston, and W. B. ROH, “Stimulated raman scattering in multi-mode fibers and its application to beam cleanup and combining,” *J. Nonlinear Opt. Phys. Mater.*, vol. 11, no. 03, pp. 303–316, Sep. 2002, doi: 10.1142/S0218863502001036.

Chapter 6: Conclusion and future work

6.1 Conclusion

The basic concept of the multi-wavelength-pumped FRL is newly suggested and established in this thesis. Although I could not exceed the highest output power reached by a single-wavelength diode laser pumped FRL reported by Glick *et al.* [1], it is clearly proven in this thesis that the concept of multi-wavelength pumping does work as expected and offers significant potential. For example, numerical simulations predict the possibility of an efficient multi-kW FRL pumped with spectrally combined diode laser sources.

The key findings from chapter 3-5 can be summarised as below.

Chapter 3 showed that the precise separation among pump wavelengths in multi-wavelength pumping is not crucial. A positive gain was achieved in an amplifier experiment and a FRL that did not reach threshold when pumped by a single diode at a single wavelength could reach threshold and generated 23 W of output power in a laser experiment.

Chapter 4 showed that high power FRL is possible with multi-wavelength pumping, as well as the benefit of germanium content. Three different fibres were tested and a fibre with a high-germanium core reached 100 W of the output power. The beneficial effect of germanium was discussed by comparing results from each fibre.

Chapter 5 showed through simulations that a wide-span (> 100 nm) pump can still pump an FRL efficiently (> 70%) for a clad-to-core area ratio of up to seven.

6.2 Future work

Some new questions have arisen that could not be fully answered in this thesis. What causes the temporal (sometimes periodic and sometimes seemingly stochastic) modulation in multi-wavelength FRL? What spatial modes are excited in multi-mode

FRL and how are they related to the beam quality and brightness enhancement (BE)? (*e.g.*, GRIN fibre's beam clean-up [2]) Is the modulation related to the mode content?

One thing I discovered about the first question is that it always appears with the 2nd order Stokes. Arguably, it will be more surprising if a multi-wavelength nonlinear system with abundant interactions and feedback does not show any temporal dynamics. The thing that triggers the modulation might turn out to be useful. For example, this can be used for generating giant pulses or random lasers. In addition to the factors mentioned in **Sect.4.7**, this might also be passive Q-switching [3]. In reference [3], the authors explain that the cause of Q-switching is related to Rayleigh scattering and stimulated Brillouin scattering form a random mirror but it is uncertain if that was what happened in my setup. To identify it, one may consider a similar multi-wavelength FRL setup but with a low-power single-mode fibres which will allow for better control of feedback. Note also that in a FRL cavity, energy only exists in the lightwaves, since the quasi-instantaneous response of SRS implies that there is no energy stored in the gain medium.

In regard to the second question, about spatial effects, an obvious thing to try is cladding-pumping, with which I can control the spatial mode of signal and pump separately. The cladding to core area ratio of seven or eight promises the BE factor of ~500 if the cladding-NA is about eight times that of the core [4]. For example, a cladding-NA of 0.46 and a core-NA of 0.06 satisfies the condition. This is not unrealistic, although it should be noted that with current fibre technology, an NA of 0.46 requires the use of low-index polymer which results in higher propagation loss. Therefore, the pump power densities must be high enough to allow for efficient SRS in relatively short fibres. Another thing that one can try is amplifying only a few high-order modes in multimode fibre. In our group, it is shown by Sheng *et al.* that a higher order mode or high-order Bessel mode in multi-mode fibre can be amplified and propagate over long distance, preserving the mode purity [5], [6]. Operating only few modes in a multi-mode fibre may dramatically improve the BE. This was still at low power, and a further question is to what extent nonlinear spatial mode instabilities ("TMI") may occur at high powers. This has been predicted [7]. It has also been observed in passive fibre with significant SRS [8]. However, the instability depended strongly on the pump, which was an YDFL producing a single- few-moded output. Such studies have yet to be undertaken with highly multimode diode-laser-pumping, including multi-wavelength pumping, of fibre Raman devices.

In addition, a different fibre material can be considered. The Raman shift of the phosphosilicate fibre is three times larger than that of silica [9]. This reduces the number of shifts towards the target wavelength through cascaded SRS, which simplifies the setup and also reduces the extra loss that occurs per shift [10]. If phosphosilicate fibre is used for multi-wavelength pumping, then the acceptable total pump bandwidth may become three times broader. Maybe, the high loss of fibre at shorter wavelength due to the Rayleigh scattering will be a problem if the signal wavelength is around 1 μm. In that case, one can simply choose a longer signal wavelength thanks to the wavelength agility of FRL. For a signal around 1.2 μm, the band of 900 nm to 1100 nm can efficiently pump an FRL. The only problem will be the commercial availability of higher power diode lasers at those wavelengths.

An ultimate goal is to reach kW-level output powers. The simulations in **Chapter 5** suggests that this is possible with multi-wavelength pumping. A master oscillator power amplifier (MOPA) system – *e.g.*, an oscillator that creates the signal of which the wavelength has the strongest Raman gain for the longest pump wavelength of amplifier, followed by an amplifier pumped by a spectrally combined beam made of tens of high-power diode lasers at different wavelength – can be a good design to achieve it. Maximising Raman gain for the amplifier is naturally achieved if the pump wavelength for the oscillator is same with the longest pump wavelength of the amplifier.

One problem is to find a high power diode array laser with good brightness. Commercially available kW-multi-wavelength diode array lasers has lower beam qualities (4-5 times higher M^2-value) than the diode lasers used in my thesis. That means it will need 16-25 times the core area with similar NA and length to achieve similar launch efficiency and conversion efficiency as the results of this thesis. Such a large core may not be economical to produce in case of high germanium-doping (germanium is expensive), but may be realistic in case of a silica core. Still, the beam quality of the generated output beam is not expected to be attractive from such fibre. Thus, another option is to build the combining setup on our own in the lab. Several diode lasers whose wavelengths are tuned to be closely spaced can be efficiently combined with VBGs as in [11]. The spacing is limited by the linewidth of wavelength-locked diode lasers, but 1 nm spacing may be realistic. Then, with 200-W diode lasers and a 100-nm pump span, 20 kW of pump power could be reached with BPP below 10 mm mrad. However, combining 100 lasers with VBGs is awkward. Alternatively, one can combine, e.g., five diode lasers into a single beam with 5 nm linewidth. Groups of such combined diodes with, e.g., 10 nm separation between groups can then be further combined with dichroic mirrors, thus, e.g., seven groups over a total span of 6 × 10 nm + 7 × 5 nm = 95 nm for a total power of 7 kW less losses. Alternatively, the diode lasers can perhaps be wavelength-combined with a conventional diffraction grating, although the finite diode-laser linewidth causes some dispersion and thus beam-quality degradation. Once such a bright pump source is secured, the required length of fibre and total background loss will reduce and, therefore, efficiency will improve. Chaotic temporal modulation is less likely happen as there will be no counter propagating beams in the power amplifier.

6.3 References

[1] Y. Glick, V. Fromzel, J. Zhang, N. Ter-Gabrielyan, and M. Dubinskii, “High-efficiency, 154 W CW, diode-pumped Raman fiber laser with brightness enhancement,” *Appl. Opt.*, vol. 56, no. 3, pp. B97–B102, 2017, doi: 10.1364/AO.56.000B97.

[2] K. Krupa *et al.*, “Spatial beam self-cleaning in multimode fiber,” *Nat. Photonics*, vol. 11, no. 4, pp. 3–8, 2016, doi: 10.1038/nphoton.2017.32.

[3] M. B. and P. M. G. Ravet, A.A. Fotiadi, “Passive Q-switching in all-fibre Raman laser with distributed Rayleigh feedback,” *Electron. Lett.*, vol. 40, no. 9, 2004, doi: 10.1049/el.

[4] J. Ji, “Cladding-pumped Raman fibre laser sources,”, University of Southampton, PhD thesis, 2011.

[5] S. Zhu *et al.*, “Multimode-pumped Raman amplification of a higher order mode in a large mode area fiber,” *Opt. Express*, vol. 26, no. 18, p. 23295, Sep. 2018, doi: 10.1364/OE.26.023295.

[6] S. Zhu, Y. Feng, P. Barua, and J. Nilsson, “Efficient low-brightness-pumped Raman amplification of a single high-order Bessel mode in 335-m of 70-µm-

diameter silica-core step-index fiber," *Opt. Lett.*, vol. 45, no. 21, p. 6018, 2020, doi: 10.1364/ol.404602.

[7] S. Naderi, I. Dajani, J. Grosek, and T. Madden, "Theoretical and numerical treatment of modal instability in high-power core and cladding-pumped Raman fiber amplifiers," Opt. Express, vol. 24, no. 15, p. 16550, 2016, doi: 10.1364/oe.24.016550.

[8] V. Distler, F. Möller, M. Strecker, T. Walbaum, T. Schreiber, and A. Tünnermann, "Transverse mode instability in passive fiber induced by stimulated raman scattering," Opt. InfoBase Conf. Pap., vol. 28, no. 15, pp. 22819–22828, 2020, doi: 10.1364/oe.398882.

[9] J. Z. Wang, Z. Q. Luo, Z. P. Cai, M. Zhou, C. C. Ye, and H. Y. Xu, "Theoretical and Experimental Optimization of O-Band Multiwavelength Mixed-Cascaded Phosphosilicate Raman Fiber Lasers," *IEEE Photonics J.*, vol. 3, no. 4, pp. 633–643, 2011, doi: 10.1109/JPHOT.2011.2159263.

[10] V. R. Supradeepa *et al.*, "Raman fiber lasers," *J. Opt.*, vol. 19, no. 2 (art. no. 023001), 2017, doi: 10.1088/2040-8986/19/2/023001.

[11] T. Yao, A. Harish, J. Sahu, and J. Nilsson, "High-Power Continuous-Wave Directly-Diode-Pumped Fiber Raman Lasers," *Appl. Sci.*, vol. 5, no. 4, pp. 1323–1336, 2015, doi: 10.3390/app5041323.

Appendix A Fibre parameters

Fibre name		GRIN(1.5km)	GRIN(0.5km)	Pure-silica core	High germanium
Manufacturer		OFS	OFS	Heraeus preform	Taihan
Loss at [dB/km] (my measurement)	[nm]				
	1020	1.45	3	1.07	-
	1016	-	-	-	2.98
	976	1.7	3.3	1.25	3.76
	969	1.75	-	1.28	4.55
	950	1.87	3.44	1.7	4.91
	940	1.93	-	1.9	5.14
	915	2.12	-	1.5	4.71
Core diameter [µm]		62.5 (1)	62.5 (1)	50 (2)	40 – 44 (1)
Clad diameter [µm]		125 (1)	125 (1)	345 (2)	141 – 145 (1)
Length [m]		1500 (2)	500 (2)	917 (2)	500 (1)
NA (core)		0.275 (1)	0.275 (1)	0.227 (2)	0.34 (1)
BPP [mm×mrad] (my calculation)		8.6	8.6	5.7	6.8

(1) From manufacturer

(2) Measured at ORC by me or a colleague

Table A.1 Parameters of the fibres used in the thesis

List of publications

- S. Hong, Y. Feng, and J. Nilsson, “Wide-Span Multi-Wavelength High-Power Diode-Laser Pumping of Fiber Raman Laser,” *IEEE Photonics Technol. Lett.*, vol. 31, no. 24, pp. 1995–1998, 2019, doi: 10.1109/LPT.2019.2953195.

- S. Hong, Y. Feng, and J. Nilsson, “Off-Peak Dual-Wavelength Multimode Diode-Laser- Pumped Fiber Raman Laser,” *IEEE Photonics Technol. Lett.*, vol. 30, no. 18, pp. 1625–1628, 2018, doi: 10.1109/LPT.2018.2863559.

- N. Zhao, S. Hong, A. V. Harish, Y. Feng, and J. Nilsson, “Simulations of multiwavelength cladding pumping of high-power fiber Raman amplifiers,” *Opt. Eng.*, vol. 58, no. 10, p. 1, 2019, doi: 10.1117/1.oe.58.10.102701.

- S. Hong, Y. Feng, and J. Nilsson, “Multi-Wavelength Diode-Pumping of Fiber Raman Laser,” in *Conference on Lasers and Electro-Optics*, 2018, p. SM1K.6.

- S. Hong, Y. Feng, and J. Nilsson, “Fiber Raman Laser Pumped by Five Wavelength-Combined Multimode Diode Lasers from 915 to 976 nm,” in *Laser Congress 2019 (ASSL, LAC, LS&C)*, 2019, p. ATu1A.1, doi: 10.1364/ASSL.2019.ATu1A.1.

- S. Zhu *et al.*, “Multimode-pumped Raman amplification of a higher order mode in a large mode area fiber,” *Opt. Express*, vol. 26, no. 18, p. 23295, Sep. 2018, doi: 10.1364/OE.26.023295.

- Y. Feng *et al.*, “Spatially gain-tailored fiber raman laser cladding- pumped by multimode disk laser at 1030 nm,” in *Optics InfoBase Conference Papers*, 2018, vol. Part F92-C, doi: 10.1364/CLEO_AT.2018.JTh2A.109.

- Y. Feng *et al.*, “Time Response Characteristics of Photodarkening-Induced Loss in Yb-Doped Fiber Amplifier,” in *2019 Conference on Lasers and Electro-Optics Europe & European Quantum Electronics Conference (CLEO/Europe-EQEC)*, Jun. 2019, pp. 1–1, doi: 10.1109/CLEOE-EQEC.2019.8872358.